

EVALUATION OF THEORIES
FOR THE INITIAL STAGES
OF PITTING CORROSION

by

Pierre G.R. Zaya, Ing. A&M, M.Sc.(Eng.), P.Eng.

A Thesis

Submitted to the School of Graduate Studies
in Partial Fulfilment of the Requirements
for the Degree of
Doctor of Philosophy

McMaster University

© October 1984

EVALUATION OF THEORIES FOR PITTING CORROSION

DOCTOR OF PHILOSOPHY (1984)

McMASTER UNIVERSITY

(Metallurgy)

Hamilton, Ontario

TITLE: EVALUATION OF THEORIES FOR THE INITIAL STAGES OF
PITTING CORROSION

AUTHOR: Pierre Gabriel Robert Zaya

Ingénieur Arts et Métiers (Paris, France)

M.Sc. (Eng.), (London, England)

SUPERVISOR: Professor M.B. Ives

NUMBER OF PAGES: xi, 217.

ABSTRACT

It is assumed in this study that the protection imparted by passive layers is dependent upon the balance between the breakdown of the protective film and the healing of the produced flaws. Therefore, the occurrence of a pit must coincide with a change in the local conditions in a flaw which did not heal.

Using this hypothesis, five proposed theories for pitting corrosion are compared using data published in the literature. The processes assumed to occur during pit nucleation are simulated. The solution compositions and potentials from reported experimental determinations of pitting potentials are used as initial conditions. The potential and concentrations at the base of the flaw are computed by using mass transport equations.

The values obtained are then used to compare the five models. For each theory, an expression depending on potential and concentrations at the metal surface was identified, so that where a theory is correct, this expression is smaller (or larger) than a parameter. This parameter, should be constant, and independent of the particular set of experimental conditions (e.g. pH, chloride concentration in

the bulk solution), as all the calculations are made for conditions corresponding to the pitting potential, i.e. conditions borderlining between pitting and passivity.

The particular case of iron in borate buffers is considered here. The computed results indicate that the most probable mechanism controlling pitting is the adsorption of the chloride ions at the metal surface. The repassivation by precipitation of ferrous hydroxide is always thermodynamically favoured, but apparently slow.

ACKNOWLEDGEMENTS

I wish to thank the following people for their help with this work:

Dr. M.B. Ives, my supervisor, for his support and understanding during the various stages of the project and for his generosity in facilitating encounters with specialists in the field.

Dr. J. Kirkaldy and Dr. W.K. Lu, the members of my Ph.D. Supervisory Committee, for their encouragement, critiques and focusing suggestions.

The staff of the McMaster Computer Centre, for their help in deciphering the "messages" of The Machine and for their suggestions which facilitated and expedited its operation.

Drs. R.C. Alkire, M. Janik-Czachor, B. MacDougall and H.H. Strehblow who, at various times during the development of this work, have patiently listened to my ideas and came forward with valuable suggestions and counter-arguments. This thesis would have been very different without their help.

Angela Bull and Gail MacLean, for their skill in typing
and their patience with the countless revisions.

And Phyllis Gordon and Claire Zaya for their love and
understanding during all those evenings.

We dance around in a ring and suppose,
But the Secret sits in the middle and knows.

Robert Frost

TABLE OF CONTENTS

I INTRODUCTION

II CHARACTERISTICS AND THEORIES OF PITTING CORROSION

- 2-1 Stages of Pit Development
- 2-2 Characteristics of Pitting Corrosion
- 2-3 Defects in the Passive Film
- 2-4 Dissolution of the Passive Layer
- 2-5 Film Breaking
- 2-6 Breakdown and Repair
- 2-7 Competitive Adsorption
- 2-8 Ion Penetration
- 2-9 Local Changes in the Environment
 - 2-9-1 Critical Concentration
 - 2-9-2 Localized Acidification
 - 2-9-3 Resistance Polarization
- 2-10 Salt Film
- 2-11 Concluding Remarks

III METHODS OF INVESTIGATION OF PITTING CORROSION

- 3-1 Electrochemical Methods
- 3-2 Surface Analysis Techniques

3-3 Probabilistic Approach

3-3-1 Time Distribution (stochastic approach)

3-3-2 Spatial Distribution

3-4 Mass Transfer Calculations

IV MECHANISMS OF IRON DISSOLUTION

4-1 Mechanisms Involving Only OH^-

4-2 Mechanisms in the Presence of Cl^-

4-3 Mechanisms on Scratched Electrodes

4-4 Mechanisms Relevant to Pitting Corrosion

V PROPOSED MODEL FOR PIT INITIATION

5-1 Definition of the Problem

5-2 Chemical System

5-3 Transport Equations

5-4 Boundary Conditions

5-5 Computation of Current

5-6 Charge of the Electrical Double Layer

5-7 Numerical Values of the Parameters

5-7-1 Anodic Dissolution of Iron

5-7-2 Other Parameters

5-8 Numerical Solution of the Equations

5-9 Possible Criteria for Pitting

5-9-1 Repassivation

5-9-2 Salt Film Precipitation

5-9-3 Adsorption

5-9-4 Critical Chloride Concentration

VII RESULTS

6-1 General Results

6-2 Sensitivity of the Results to the Input Values

6-3 Precision

6-4 Stability

6-5 Testing of the Program

6-6 Pitting in NaOH-NaCl Solutions

6-7 Pitting in NaOH-NaCl-B(OH)₃ Solutions

6-7-1 Sources of Data

6-7-2 Analysis of the Results

VIII DISCUSSION

7-1 Ideal Solution

7-2 One Dimensional Diffusion

7-3 Inert Film

7-4 No Convection

7-5 No Precipitation

7-6 Supporting Electrolyte

7-7 Chemical Reactions

7-8 Steady State

7-9 Breakdown and Repair

7-10 Temperature

- 7-11 Fixed Geometry
- 7-12 Cathodic Reaction
- 7-13 Comparison of Criteria

VIII CONCLUSIONS

IX FUTURE WORK

X REFERENCES

APPENDIX A: DESCRIPTION OF THE COMPUTER PROGRAM

- A-1 Program MAIN
- A-2 Subroutine DRIVER
- A-3 Subroutine CALC
- A-4 Subroutine RIN
- A-5 Subroutine DERIV
- A-6 Subroutine INTEG
- A-7 Subroutine CONC
- A-8 Subroutine DCDT

APPENDIX B: LIST OF SYMBOLS

CHAPTER I

INTRODUCTION

It has been estimated that the cost of corrosion in the United States is approximately 70 billion dollars a year, or 4.2% of the Gross National Product (Payer, Boyd, Dippold and Fisher, 1980). Comparable percentages of the GNP have been obtained in other countries where evaluations have been undertaken (Behrens, 1975; Hoar, 1971; Rene and Uhlig, 1974). Pitting corrosion is certainly responsible for a respectable fraction of this cost, as judged by its impact on certain sectors, such as the pulp and paper industry. One chemical manufacturer found that over a four-year period, pitting corrosion was responsible for about 8% of all failures of the metallic piping and equipment (Collins and Monack, 1973).

Pitting can be defined as a form of corrosion "in which only small areas of the metal surface are attacked whilst the remainder is largely unaffected" (Shreir, 1976a). This can occur on many common metals such as iron, nickel, titanium, aluminum, zinc, and their alloys. The danger of this type of attack is that it is impossible to monitor its

progress by visual inspection until the metallic part has been completely perforated.

The study of pitting corrosion has received great impetus from the development of commercial potentiostats and their systematic use in experimental electrochemistry since the early 1960's (Macdonald, 1977). These instruments, by controlling the potential between the sample under study and a reference electrode in the solution of interest, can rapidly indicate some of the conditions necessary for the occurrence of pitting corrosion. Numerous experimental results have been obtained: Shreir (1976b) gives a list of 269 articles published on the subject between 1960 and 1974.

The present work is motivated by a desire to gain theoretical insights by using the already accumulated experimental data. Starting with the assumption that pitting proceeds through processes of breakdown and repair, the elemental physico-chemical processes are simulated, using contemporary numerical techniques. These permit the solution of the relevant differential equations with a minimum of restrictive assumptions. By simulating the behaviour of a passive metal during a potentiostatic experiment, it is possible to use the experimental pitting potentials and the solutions in which they were determined to compute local electrochemical conditions. These results in turn allow the quantitative evaluation of five different theories

attempting to explain pitting corrosion.

After a short description of the characteristics of corrosion pits, the different theoretical models which have been proposed to elucidate this phenomenon are discussed. The main approaches of current research are then reviewed in order to situate the methodology used here. As iron is the metal which has been selected for the application of the proposed methodology, the concluding section of the literature review discusses the most important theories of iron dissolution.

CHAPTER II

CHARACTERISTICS AND THEORIES OF PITTING CORROSION

As individual theories of pitting corrosion usually emphasize only one step in the development of a pit, it is useful to firstly distinguish the various stages in this development as described in the literature. Before considering the theoretical aspects of pitting corrosion, generally accepted characteristics of pitting corrosion will be listed, these facts being the basis to which all theories should conform.

2-1 Stages of Pit Development

The initiation and growth of corrosion pits has been, for the purpose of this discussion, divided into 4 steps which separate the 5 stages described (Figure 1).

Stage 0 represents an unattacked metallic surface, still covered with its passive film, itself in contact with the corrosive solution. Step 1 involves the rupture of the passive layer. At stage 1, the substrate is still protected but for a small patch whose dimensions are smaller or comparable to the thickness of the passive film. The solution has just entered into contact with the metal.

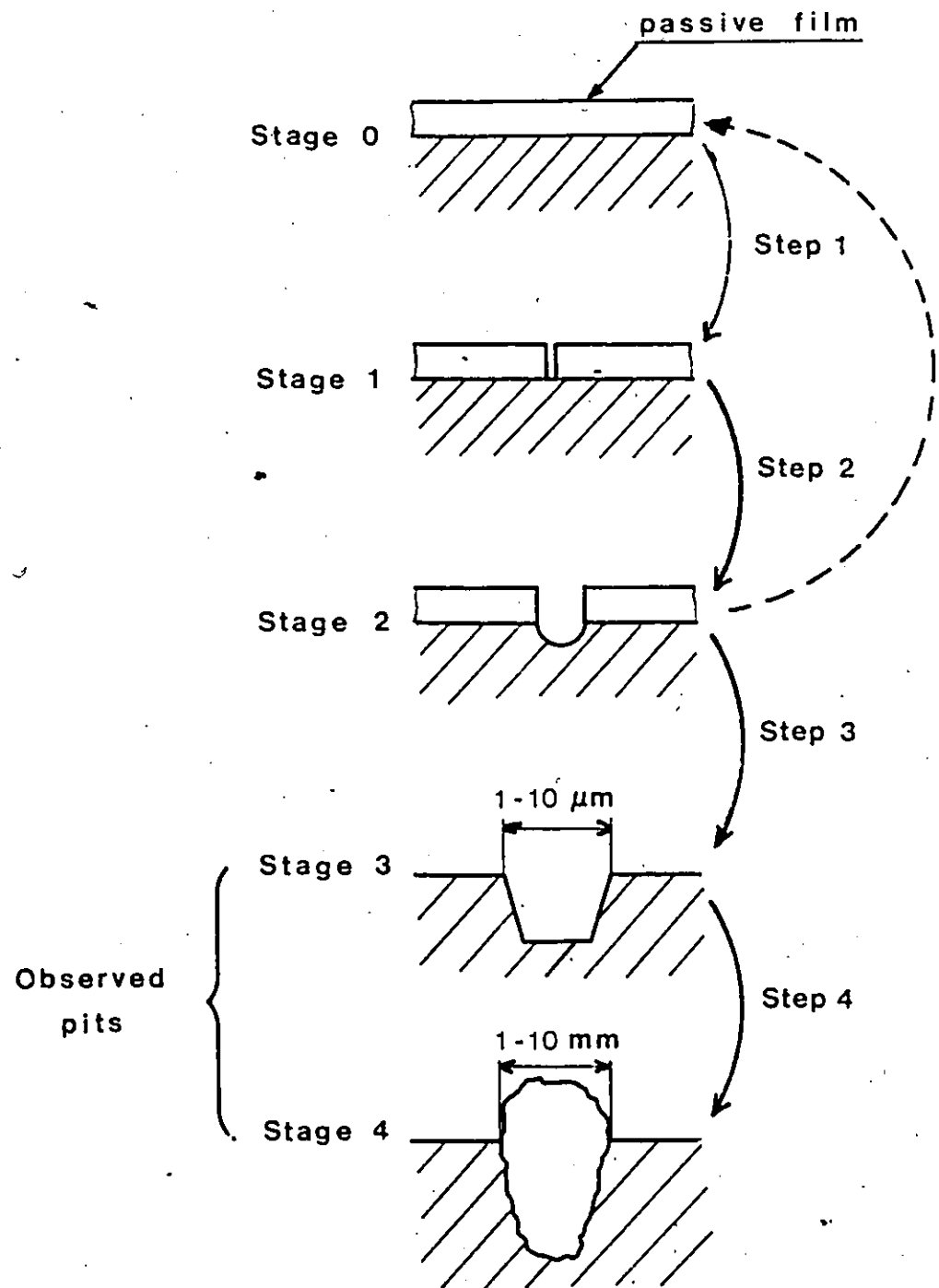


Figure 1 - Stages of Pit Development

During step 2, some dissolution of the substrate occurs as a result of the interaction of the solution with the metal, but some flaws still do repassivate and therefore come back to stage 0. Stage 2 is reached when the conditions for pit growth are met and repassivation cannot occur any more. The size of the pit at this stage depends on the external conditions (potential, concentrations, etc...).

Step 3 involves further dissolution of the substrate such that at stage 3, the pit is about 1 to 10 μm and can be seen under the optical microscope. Pits have then the shape of a hemisphere or of a polyhedron.

Finally, stage 4 is reached when the pit can be seen with the naked eye. The cavity has then an irregular shape and is partially filled with solid corrosion products which also deposit around and over the mouth of the pit. It is usually at this stage that corrosion pits become a source of concern in practice.

2-2 Characteristics of Pitting Corrosion

The following properties have been selected because they have been extensively observed in association with the pitting of many metal-solution combinations. A comprehensive theory of pitting corrosion should therefore be able to explain all these facts.

* The potential of the metal must exceed a certain threshold. This is true in general terms, although the

definition and determination of this threshold is complex (see 3-1).

* Some aggressive anion must be present. These ions correspond to strong acids (Hoar, 1947), and they tend to form complex and very soluble salts with the metal they attack (Foley, 1975; Augustynski, Dalard and Sohm, 1972). Galvele (1978) has compiled an extensive list of relevant metal-ion pairs.

* Some other ions inhibit the effect of the aggressive ion as pitting agent. The relation between the potential necessary for pitting and the concentrations of aggressive and inhibiting ions is generally of the type:

$$E = E_0 - a \cdot \log [\text{Agg.}] + b \cdot \log [\text{Inh.}]$$

Some numerical values are quoted by Szklarska-Smialowska (1971), Vetter and Strehblow (1974) and Galvele (1978).

* There is a delay, called induction time, between the fulfillment of the necessary conditions for pitting and the detection of the first pit. Because of instrumental limitation, this detection does not take place until the pit has reached stage 3. This induction time varies with the concentration of the corrodent and of the other components of the solution and it decreases when the potential increases. Its lack of reproducibility in many cases has led to statistical studies of its distribution as a source

of information (see 3-3-1).

* The corrosive attack is highly localized on a metal surface otherwise still passive. The precise location of a pit is unpredictable, but the probability of occurrence is higher at grain boundaries, inclusions, and other surface discontinuities.

* Inside the pit, the aggressive ions reach concentrations much higher than in the bulk of the solution. This is accompanied by changes in the concentrations of the other components of the solution, notably a usual drop in pH (for instance: Suzuki, Yamabe and Kitamura, 1973).

2-3 Defects in the Passive Film

Various workers, starting with Evans, Bannister and Britton (1931), and more recently Wood and coworkers (Richardson and Wood, 1970, 1973; Wood, Sutton, Richardson, Riley and Malherbe, 1974; Wood, Richardson, Abd Rabbo, Mapa and Sutton, 1978) claim that there are always local weak spots or defects in the passive film. Therefore, stage 0 never exists and immediately after immersion, the process starts at stage 1, i.e. metal and solution are in contact. The induction period only corresponds to the time necessary for the corrosion to be detectable, for instance by the pitting current becoming large enough to be registered.

Aside from the experiments reported by Wood et al in the references already mentioned, there are numerous other

observations showing that pits do nucleate preferentially at surface defects, beginning with the early experiments of Britton and Evans (1930). Szklarska-Smialowska, Szummer and Janik-Czachor (1970) and Wranglen (1969, 1974) show that the boundary between the metal matrix and non-metallic inclusions or second^aphase particles is more susceptible to pit nucleation. This fact can be explained either by the establishment of a local cell between metal and inclusion, the cathodic reaction being hydrogen reduction, or by preferential dissolution of the inclusion (Wranglen, 1969).

Brooksbank and Andrews (1969, 1971) also argue that non-metallic inclusions exhibit different expansion coefficients and elastic constants from those of the metal matrix. For instance, sulphides have a higher expansion coefficient than steel and will shrink on cooling and form a crevice between inclusion and matrix (Smialowski, Szklarska-Smialowska, Rychcik and Szummer, 1969).

These arguments, therefore, reduce the nucleation of pits to a particular case of crevice corrosion.

2-4 Dissolution of the Passive Layer

Heusler and Fischer (1976) propose another mechanism by which the induction time corresponds to the dissolution of the passive layer. They show experimentally using a ring-disc electrode system, that the presence of chloride in the solution catalyzes the dissolution of $\gamma\text{-Fe}_2\text{O}_3$, the

passivating compound on iron in borate buffer. Thus some iron passes into solution as Fe^{3+} , which is detected in the ring electrode. When pitting corrosion occurs, it generates Fe^{2+} ions which can also be detected. This difference between the origin of the two types of ions has been noticed by Uhlig and Wulff (1939) and confirmed by Engell and Stolice (1959), Weil and Manzel (1959) and Kabanov and Kashcheev (1963). According to Heusler and Fischer, the dissolution of the passive layer proceeds until a new steady state is established, corresponding to a thinner oxide layer. However, because of some unevenness of the layer, the solution may come in contact with the metal and form a pit. At the same time, these authors also suggest that this unevenness is accentuated by the formation of chemisorbed chloride islands on the oxide-solution interface. They advance as proof that the experimental relation they found between the induction time and the potential is analogous to the relation governing the mean time of formation of 2-dimensional nuclei as a function of overvoltage.

Strehblow and Lochel (1983) and Lochel and Strehblow (1983) use XPS to measure the thickness of the passive layer on iron and nickel. They find that fluoride ions cause a thinning of the barrier-type oxide protecting the metal, and interpret this as a model for the effect of the other halides.

This theory thus offers an explanation for steps 1

and 2 in that it states that when metal and solution come into contact, chlorides have already agglomerated on the active areas, and the pit is ready to grow.

There is evidence contradicting this theory. McBee and Kruger (1974) find, in the same system, not only that the induction time increases with the film thickness as measured by ellipsometry, but also that the film thickness increases with the chloride concentration. Also Wood et al (1978) show that this mechanism does not apply to aluminum: chromate and phosphate solutions are much more aggressive than chlorides in accelerating the dissolution of Al_2O_3 , and yet act as corrosion inhibitors for aluminum.

2-5 Film Breaking

A film breaking theory has been originally proposed by Hoar (1967) and later extended by Sato (1971) to explain step 1. Hoar postulates that the adsorption of the damaging ions on the surface of the passive film, producing mutual repulsion, lowers the interfacial surface tension. When the repulsive forces are sufficient, the passive film cracks.

Sato also takes into account in his calculations the work of the electrostatic forces, and shows that high electric fields could lead to mechanical rupture of the films by pressures exceeding the compressive strength. One of the remarkable features of this theory is that it explains easily the formation on aluminum of a duplex layer structure

of the oxide film, consisting of an inner barrier-type layer and an outer porous layer with regularly aligned pores in a close-packed pattern (Edwards and Keller, 1944; Keller, Hunter and Robinson, 1953). The porous layer would be formed by plastic flow (extrusion) of the thin barrier layer, which would maintain itself at a constant thickness by anodic oxidation of the substrate. The hexagonal pattern would be the most stable form for stress relief.

But this type of cracking of the passive film offers, no explanation for the induction period, unless some other phenomenon, like creep, is introduced. Also, it does not justify the special role of the aggressive ion as compared with other ions of similar adsorption properties, such as O^{2-} (Kruger, 1976).

2-6 Breakdown and Repair

The key concept of a continuous process of breakdown and repair of the passive film appears through the work of Novakovski and Sorokina (1966), Richardson and Wood (1970) and Okamoto (1973). In the words of Okamoto: "The process during the induction of pit formation is considered to be a dynamical process, in which the film breaking reaction and the film formation reaction are in a delicate balance to keep a steady state of the film". The presence of chloride ions influences the repassivation process. The breakdown process can take place through natural flaws and defects

(Richardson and Wood²), film breaking or any of the other possible modes. Ambrose and Kruger (1974) put forward a model which involves the penetration of chloride ions into the film, forming pockets of corrosion products. As these pockets expand, the stress on the film increases and results in a fracture. MacDougall (1979) favours, in the case of nickel, a local film breakdown by dissolution, this process being enhanced by a local enrichment in chloride and an increase in pH. Lochel and Strehblow (1980) find that the mechanism of breakdown and repair is also consistent with their measurements of Fe^{2+} concentrations after positive or negative potentials jumps.

The advantage of this mechanism is that it gives a coherent image of what may happen from stage 0 to stage 2, and back to stage 0 in the case of repassivation, or passing to stage 3 in case of pit propagation. The specific role of the aggressive ion is in this case to prevent repassivation. The role of the potential can be seen as influencing either the adsorption of aggressive ions or the repassivation kinetics. The induction period may correspond to the time necessary for the penetration through the film.

The main justification for a process of breakdown and repair is found in the observation of violent jumps in the corrosion current (or potential, depending on the method) before the appearance of the first pit, i.e. during the induction period (Lotlikar and Davies, 1966; Bond and

Lizlovs, 1968; Forchhammer and Engell, 1969; Richardson and Wood, 1970). This has led to the study of the electronic noise itself and its relationship to the electrochemical conditions. Iverson (1968) notices that the addition of an inhibitor decreases markedly the intensity of the fluctuations. Okamoto, Tachibana, Nishiyama and Sugita (1976) find that the noise spectrum changes with time during the induction period, and that noise intensity increases in the presence of chloride ions. Bertocci (1980, 1981) notices an increase in the noise current greater than two orders of magnitude above the pitting potential.

Another argument in favour of a "live" passive film in dynamical balance between breakdown and repair can be found in the recent results provided by the study of pitting as a stochastic process. Shibata and Takeyama (1981) explain the distribution of induction times in the potentiostatic pitting of ferritic stainless steels, through the introduction of two parameters. One is associated with the probability of breakdown of a passive sample, the other with the probability of repassivation of a pitted sample. These two parameters behave in a remarkably independent manner. The breakdown parameter varies with potential and with the addition of titanium (probably through a modification of the inclusions) and changes very little when molybdenum is added. The repassivation parameter is independent of the potential and titanium concentration, but varies with the,

addition of molybdenum.

A related concept is put forward by Hisamatsu (1976) to the effect that current "bursts" or fluctuations seem to occur in a potential band below the conventional pitting potential but above a potential called E_z by Forchhammer and Engell (1969). These fluctuations are associated with the appearance on the surface of depressions, presumably the repassivated flaws. Hisamatsu, Yoshii and Matsumura (1974) find that the diameter of these "pre-pits" is of the order of 30 μm which would then be the approximate size of the defect at stage 2 in these particular conditions. The implications of these ideas is that there would be a potential E_z , associated with steps 1 and 2, and another potential, E_b , or conventional pitting potential, more noble than the first one, associated with stage 3 and the propagation of the pit.

2-7 Competitive Adsorption

This theory is germane to the one which sees an absorbed oxygen film as the primary source of passivity. Uhlig (1946, 1967) proposes that such a film forms on the transition metals because of the ability of their uncoupled d electrons to create a stable bond with oxygen. The effect of the adsorbed oxygen is to reduce the kinetics of metal dissolution. Consequently, the pitting process starts by the adsorption of the aggressive ion on the metal surface,

and simultaneous displacement at local sites of the adsorbed passivating ions (oxygen and possible inhibitors) (Uhlig, 1950; Kolotyrkin, 1961). Once the aggressive ions are adsorbed on the surface, the current density for metal dissolution increases and breakdown commences. The aggressive ions are ions with a large polarizability, like the halogens, and they have the tendency to form numerous complexes with metals (Foley, 1975). The pitting potential represents that minimum electrode potential value, at which the aggressive anions become capable of producing a reversible displacement of the passivating ions from the metal surface.

This model has been modified and the phenomenon of adsorption incorporated into other theories, mainly to take into account the unquestionable presence of a tri-dimensional oxide film on passive surfaces during many experiments. As already mentioned (2-4), Heusler and Fischer (1976) introduce in their mechanism two-dimensional islands of adsorbed chlorides. They see the induction time as the time necessary to build up these islands. Dissolution of the oxide begins ~~only~~ after the formation of the islands.

Induction times confirming this theory are reported by Janik-Czachor (1979). Evidence is also found by Janik-Czachor, Szummer and Sklarska-Smialowska (1975) of pit "pre-nuclei" at potentials lower than the pitting potential. Using an electron microprobe, they find "salt islands" between 60 and 800 Å thick. Similar results are reported

for Br on titanium by Petit, Kondo and Dabosi (1980) and on iron by Weil and Menzel (1959) using autoradiography.

Another interpretation which can be considered as falling under the same heading is that described by Hoar, Mears and Rothwell (1965) and Hoar and Jacob (1967) for the pitting of stainless steel. In this model the joint adsorption of aggressive ions (3 or 4) is taking place on the surface of the oxide film, around a lattice cation. The probability of formation of such a complex is low and thus requires a high activation energy for formation, and a delay corresponding to the induction period. Once the complex is formed, however, the aggressive ions will readily remove the cation from the passive lattice. The film is thus made thinner at the site where the complex first formed and the stronger anodic field at the thinned site will rapidly pull another cation through. The process will then repeat itself at an accelerating pace, as the electrostatic field increases. However, this model does not appear to be applicable to all systems, as Hoar himself (Hoar and Foster, 1970) and Ambrose and Kruger (1972) found that it does not hold for iron.

Strehblow (1976) uses adsorption of the aggressive ion on the passive layer in a manner similar to Hoar's, as a precursor to the salt film formation. Strehblow and Titze (1977) explain the logarithmic relationship between aggressive ion, inhibitor and potential (see 2-2) by assuming that

Langmuir adsorption takes place on the metal surface, and that a critical surface coverage by the aggressive anions is necessary for pitting. Uhlig and coworkers (Matsuda and Uhlig, 1964; Uhlig and Gilman, 1964; Leckie and Uhlig, 1966; Bohni and Uhlig, 1969) obtain results which can be fitted to the same relationship, which they explain using the Freundlich adsorption isotherm. Videm (1974) also uses adsorption of the chlorides on the passive film as a first step in his breakdown and repair model of aluminum pitting.

An important confirmation of the adsorption theory is given by the experiments of Rosenfeld and Maximtschuk (1960) on the adsorption of chloride on chromium, using radioactive chlorine. They find that more chloride adsorbs as the potential increases and that increases in hydroxyl and sulfate ion concentrations decrease the chloride adsorption until it is negligible.

However, the opponents of these models point out that they cannot satisfactorily account for the influence on the induction time of the thickness or the heat treatment of the passive film (McBee and Kruger, 1974).

2-8 Ion Penetration

Various models involve the migration of the damaging ions through the lattice of the passive film, via defects or some sort of ion exchange, the breakdown process being complete when the anion reaches the metal/film interface.

Hoar, Mears and Rothwell (1965) assume anion entry without exchange to produce "contaminated" passive films. This would produce an induced ionic conductivity in the film, which, then becomes able to sustain local high current densities. Heine, Keir and Pryor (1965) and Pryor (1974) suggest that chloride ions enter the film by a substitution process and that therefore cation vacancies are created. McBee and Kruger (1974) propose a scheme whereby the aggressive ion is exchanged with oxygen or hydroxyl ions. The role of the potential in all these mechanisms is that of controlling the adsorption of aggressive ions at the film/solution interface; the induction period corresponds to the time necessary for penetration to the metal/film interface.

Recently, Chao, Lin and Macdonald (1981, 1982) and Lin, Chao and Macdonald (1981) have proposed a new theory for pit initiation based on the movement of point defects in the electrostatic field of the film. For them, the rate controlling step for film growth is the diffusion-migration of oxygen vacancies through the film. Breakdown is due to the collapse of voids resulting from the coalescence of metal vacancies at the metal/film interface. The model is found to be in reasonable quantitative agreement with experimental data for the dependence of the pitting potential of iron and nickel on the halide ion concentration and for the dependence of the induction time on the potential (data of Heusler and Fischer, 1976).

Experimental tests of these theories try to detect permanent changes induced in the passive film by the presence of chlorides. McBee and Kruger (1971) find, through ellipsometric studies on iron, that chloride ions produce reversible changes in the properties of the oxide film. Another of their results (McBee and Kruger, 1974) is that the thicker the passive film, the longer the time to breakdown. Ambrose and Kruger (1972) interpret as evidence for the penetration theories that the time for breakdown was shortened by dissolving part of the passive layer by cathodic reduction and regrowing it in the presence of chlorides. The same authors show that the induction time is increased over 100-fold by annealing the passive film at 65°C, which they explain by the removal of the defects used for penetration.

But the results of this type of experiments are still contradictory. Okamoto (1973) finds that annealing shortens the induction time for stainless steel. Vetter and Strehblow (1970, 1974) report the pitting potential to be independent of film thickness on iron, as do Bohni and Uhlig (1969) and Foroulis and Thubrikar (1975) for aluminum. However these last authors find the induction time to be nearly proportional to the film thickness.

Davydov, Mirzoev, Kamkin and Roshchina (1978) and Davydov and Kamkin (1978) take an interesting approach which provides a way to reconcile the contradictory results found

in the literature. Using a glass capillary, they measure the pitting potential of aluminum in a NaCl solution on a very small surface (100 measurements/cm²), and obtain therefrom a distribution of potentials for each sample (200 measurements). The mode of this distribution is seen to depend strongly on the thickness of the passive film, but the tail of the distribution at lower potential is always present. This is taken to mean that most of the surface is covered with a sound passive film for which breakdown by penetration is strongly dependent on the thickness. However, at a few points, the film is defective, and the pitting potential at these points drops to a value independent of the thickness. Since pitting on a "normal" sample (1 to 100 cm²) occurs at the weakest link, the pitting potential recorded during a usual experiment will be the lowest value. The same line of reasoning is used in the stochastic studies of pit nucleation (see 3-3-1).

An argument often presented against the theories involving penetration is their inability to explain the presence of electrochemical noise (see 2-6) preceding the initiation of a pit (Wood et al, 1978). The current bursts start much too soon after the establishment of the pitting conditions (less than 0.1 s according to Videm, quoted by Davydov and Kamkin, 1978) to be explained in terms of gradual transport of the halide ions through the film.

Another argument pointed out by Vetter and Strehblow

(1970, 1974) is that penetration of polyatomic aggressive anions such as SO_4^{2-} , ClO_4^- , or SCN^- , through a solid layer is improbable as a consequence of their large dimensions, although they do cause pitting with short induction times. A counter-argument might be that these ions, once in close contact with (or inside) the passive film, decompose to S^{2-} and Cl^- , which are known pitting agents themselves. This is apparently the case for ClO_4^- on aluminum (Augustynski, 1978).

A third criticism of the models of Pryor, and McBee and Kruger, is that they suppose that the O^{2-} ions can migrate against the huge electric field necessary for transporting the metal and chloride ions through the passive layer (Vetter, 1974).

Evidence from surface analysis techniques is contradictory. For aluminum, Augustynski and coworkers report the incorporation of chlorides into the film, as measured by x-ray electron spectroscopy (ESCA) (Painot and Augustynski, 1975 and 1976; Koudelkova, Augustynski and Berthou, 1977; Augustynski, 1978; Koudelkova and Augustynski, 1979), as did Maitra and Verink (quoted by Galvele, 1978) using Auger electron spectroscopy (AES). On the other hand, Videm (1974) finds no sign of chloride by autoradiography, and Wood and coworkers (Abd Rabbo, Wood, Richardson and Jackson, 1974; Abd Rabbo, Richardson and Wood, 1976; Wood et al, 1978) report that using secondary ion mass spectroscopy

(SIMS), chlorides are found only on the outside surface, even if there are signs of penetration of other anions (chromates and phosphates). For iron, chloride is detected only on or near the oxide-solution interface using AES (Janik-Czachor, 1980) or ESCA and AES (Szkłarska-Smiałowska, Viefhaus and Janik-Czachor, 1976). The same is true for stainless steel by AES (Lumsden and Staehle, 1973). The results of MacDougall (1982) using AES and SIMS on nickel seem to indicate only a slight penetration (2 atomic layers).

2-9. Local Changes in the Environment

Three sets of theories which claim that the self-perpetuation of local conditions during step 2 is the cause of pitting corrosion have been grouped under this heading.

2-9-1 Critical Concentration

As discussed earlier (2-2), it has been noticed for a long time that the environment inside a pit differs widely from the bulk of the solution (Boylis, 1925; Schwenk, 1964; Mankowski and Szkłarska-Smiałowska, 1977; Suzuki et al, 1973). In particular, when halides are the aggressive anions, they are found to migrate inside the pit under the influence of the electric field (Greene and Fontana, 1959), thereby increasing the aggressiveness of the solution.

Kolotyarkin and coworkers (Kolotyarkin, 1961, 1963;

Kolotyrkin and Gilman, 1961) and Wilde (1976) propose that pits develop once a critical concentration of activating ions is locally exceeded. This is caused originally by the nonuniformity of the metal surface and its passive layer, which generates variations in local current density, and in anion adsorption.

This theory has been modified (Freiman, LeMin and Raskin, 1973) to also take into account the build-up of corrosion products. Similarly, Hisamatsu (1976) considers that the critical quantity is the difference between the sum of all the concentrations inside the pit and the sum of all the concentrations outside.

2-9-2 Localized Acidification

It is generally recognized that the low pH in occluded cells is due to the hydrolysis of the metal ions (Suzuki et al, 1973; Jones and Wilde, 1978). According to the localized acidification theory, pitting is the result of this low pH of the solution in contact with the metal surface, these local acid conditions preventing the repassivation and reformation of the passive film. This idea was originated by Hoar (1947, 1949) and has been developed by Greene and Fontana (1959), Schwenk (1963) and Galvele (1976b, 1978, 1981). The arguments put forward in favour of this theory are based on the thermodynamic stability of the passivating compound (oxide, hydroxide, etc.) and are

illustrated by the corresponding Pourbaix diagram (Van Muylder, Pourbaix and Van Laer, 1965).

2-9-3 Resistance Polarization

Other researchers (Franck, 1960, 1961; Brauns and Schwenk, 1961; Herbsleb and Engell, 1961) point to the high voltage drop inside the pit to explain why there could be, on a passive metal surface, some obviously active regions. Franck (1960) considers that, on the pit surface, conditions similar to electrobrightening are obtained and the surface is covered with a viscous supersaturated solution of high ohmic resistance.

Pickering and Frankenthal (1972) find evidence of a high potential drop inside the pit by actual measurements with a microprobe. They also observe the presence and evolution of hydrogen in all their experiments, and conclude that a hydrogen bubble provides the necessary constriction and voltage drop to maintain the bottom of the pit in the active zone. The evolution of hydrogen from the pit also explains the sudden variation in current obtained by other workers.

Ateya and Pickering (1975, 1977) also find that dissolution can take place at a crack tip during hydrogen charging of a metal. Bargerion and Benson (1980) analyze the gases evolving from aluminum pits and find that their composition varies with the composition of the solution, hydrogen

evolving in chloride and sulfocyanide solutions.

These three families of theories can explain easily the induction time as the time necessary for the establishment of their respective necessary condition after breakdown of the passive film.

Alkire, Ernsberger and Damon (1976) show that the variation of conductivity within a pit can contribute significantly to the acceleration of the corrosion process.

Jones and Wilde (1978) find that, during the localized corrosion of stainless steels, the active state in concentrated and acid chloride solutions is much more noble than the active state in the dilute solutions used for testing. Therefore, the need for a potential difference, between passive surface and pit bottom disappears, as they can both be stable at the same potential because of the difference in solutions.

Vetter (1974) and Vetter and Strehblow (1970, 1974) claim that, in the small pits they have observed, the changes caused to the pit environment are not sufficient to justify the theories presently under discussion: for iron in a chloride solution, they calculated that the maximum enrichment in Fe^{2+} is 0.13 M (well below saturation), the maximum difference in pH is 0.8 and the maximum potential difference is 40 mV.

2-10 Salt Film

This theory, although it shares many characteristics with the models previously discussed in 2-9, will be described separately due to recent developments and the bearing it has on the assumptions made in the model presented here. The salt film theory assumes that step 2 is the critical step, during which conditions may or may not be established for the further growth of the pit.

According to Vetter (1965, 1974) and Vetter and Strehblow (1970, 1974), pitting has its origin in the stability at the bottom of the pit of an anhydrous salt layer similar to the passive layer. This layer is a thin non porous film formed by the aggressive anions and the metal cations. It is in contact with a nonsaturated solution in the pit and therefore dissolves fast. When steady state is reached, the disappearance of the salt by dissolution is compensated by the growth of the film at the metal/film interface. This high growth rate is made possible by the ionic current flowing through the film under the high electric field.

The thickness of the salt film layer is calculated to be about 40 Å, which agrees with the results of Strehblow, Vetter and Willgallis (1971) obtained with the electron microprobe.

This view is also supported by the experiments of Beck (1973) on titanium. Alkire, Ernsberger and Beck (1978)

and Beck (1982) even propose that the formation of a salt film layer is a preliminary condition for repassivation, at least for titanium and iron in the media investigated. Beck and Alkire (1979) conclude from their calculations that the salt layer thickness could be between 40 and 190 Å and that, at pit nucleation, current densities between 10^3 and 10^6 A/cm² might be reached, leading to salt film precipitation within 10^{-8} to 10^{-4} s of the breakdown of the passive layer. It may be worth noting here that, although these current densities are much higher than the highest values reported during a pitting experiment (100 A/cm²; Strehblow and Wanners, 1975), Tajima and Ogata (1968) obtain an estimated current density of 2,400 A/cm² at the tip of a dendrite during Ni plating, and Hills, Pour and Scharifker (1983) report current densities between 10^3 and $3 \cdot 10^4$ A/cm² for metal plating on microscopic electrodes.

Isaacs (1973) studies the layer formed on AISI 304 stainless steel in various chloride solutions and concludes that it is approximately 100 Å thick, its resistivity is about 10^8 Ω.cm and the conduction mechanism is ohmic.

Since one of the factors controlling pit growth is the dissolution of a salt layer, this model explains the fact that only anions giving high solubility salts produce pitting (Foley, 1975). It also explains the instability and the oscillations generated when other anions are present. Galvele (1978) mentions the possibility that pitting

inhibitors, like molybdate ions, could act by adsorbing on the salt layer and thereby prevent its dissolution.

2-11 Concluding Remarks

It can be seen that many models have been proposed to explain pitting corrosion. Although some of them do not claim to be universally applicable, most are mutually exclusive. It is the purpose of this work firstly to formulate quantitatively some of the models, which lend themselves to this exercise, and secondly to use the obtained criteria to compare the merits of the different theories which explain experimental data.

CHAPTER III

METHODS OF INVESTIGATION OF PITTING CORROSION

The following review of the methods used in recent years to investigate pitting corrosion does not attempt to be exhaustive, but rather emphasizes the methods relevant to the work presented here.

3-1 Electrochemical Methods

Brennert (1937) was apparently the first to realize that a critical potential is associated with localized corrosion. At the present time, the breakdown potential, E_b , is usually defined as that potential above which pits can nucleate, and below which they are unable to nucleate but can nevertheless propagate. E_b can be determined by fixing the current in the system (galvanostatically), by shifting the potential at a constant speed from the cathodic region (potentiodynamically) or by fixing the potential and waiting for the occurrence of a pit (potentiostatically). This last method is considered the most precise. Its drawback, however, comes from the fact that above the pitting potential, the closer the potential is to E_b , the larger the induction time. This makes the pitting potential a function of the

patience of the investigator.

Pourbaix et al (1963) introduce another potential, the protection potential or repassivation potential, E_r , considered as another characteristic feature of pitting corrosion. This is the potential below which a pit cannot propagate. Since it is lower than E_b , pits cannot initiate either. Above E_r , a pit already formed may be able to propagate. The determination of E_r implies a potentiodynamic shift toward negative values from a value where some pits have already grown. Yoshii and Hisamatsu (1972) show that the value of E_r obtained depends on the potential sweep rate. Wilde and Williams (1971) and Suzuki and Kitamura (1972) find that the repassivation potential also depends on the extent of pit growth before shifting the potential toward negative values.

Bond (1972) notes that for stainless steels, the results obtained in the electrochemical studies of pitting can depend upon the surface preparation and the gas used for purging the solution (probably through traces of oxygen). Pessal and Liu (1971) propose that the pitting potential could be determined by scratching the surface at a fixed potential. If the current subsequently decreases continuously, the potential is considered below the pitting potential. Conversely, it is above the pitting potential when the scratch does not repassivate, but pitting takes place instead. This method gives results which are reproducible

and less dependent on extraneous variables, such as surface preparation and potential sweep rate.

It must also be mentioned that various authors believe that, when properly determined, the breakdown potential and the repassivation potential are identical, at least in some cases (Broli and Holtan, 1973; Broli, Holtan and Prestrud, 1974; Strehblow and Titze, 1977; Petit et al, 1980).

Extensive development in two electrochemical methods used in the study of corrosion have occurred in the last few years.

First, the analysis of the "noise" or small fluctuations in current or potential, is being used to investigate the breakdown and repair of the passive layer, and its relation with the potential and the concentrations of aggressive ions (see section 2-6).

Secondly, AC impedance techniques are used more and more to obtain a fast estimate of the polarization resistance of an electrode and from it, its uniform corrosion rate (Mansfeld, 1981). But this method can also detect localized corrosion by measurement of the Warburg impedance (Mansfeld, Kendig and Tsai, 1982). It has also been extensively used by electrochemists to investigate surface phenomena in general and corrosion processes in particular (Macdonald, 1977; Epelboin, Gabrielli, Keddam and Takenouti, 1975).

3-2 Surface Analysis Techniques

These modern methods of surface analysis are increasingly being used to detect and quantify elements present inside the passive layer (Evans, 1977). Only the techniques mentioned in this thesis (mainly in 2-8) will be reviewed here.

During Auger electron spectrometry (AES), the sample is bombarded with 1 to 10 keV electrons and the instrument analyzes the emitted Auger electrons. The depth of material sampled is about 10 Å and on some instruments, some lateral resolution (of the order of 10 µm) is possible. The sensitivity to individual elements is about 0.1%, but the accuracy of the results is fairly poor.

X-ray photo-electron spectroscopy (XPS or ESCA) consists of subjecting a specimen to X-ray photons and analyzing the ejected electrons. The main advantage of this technique is that the energy of these electrons varies with the chemical state of the sample element. The depth sampled is approximately the same as for AES (10 Å), as is the sensitivity (0.1%). The main disadvantage is the poor lateral resolution obtained, due to the absence of focussing of the incoming energy.

Secondary Ion Mass Spectrometry (SIMS) is performed in the following way: the sample is bombarded with 1 to 30 keV ions and the secondary ejected ions are analyzed. The impact of the ion beam gives a simultaneous sputtering

of the target material. The depth analyzed is also about 10 Å, and some lateral resolution is possible whereby an area of about 10 µm can be analyzed. It is the most sensitive method (100 ppm to 10 ppb, depending on the atomic weight of the target species), but quantitative analysis is difficult due to large matrix effects.

Usually, these techniques are associated with ion sputtering to allow for in-depth analysis of the sample. But sputtering has various disadvantages: it destroys the chemical bonding which may have been present on the surface, as well as the original fine topography; it may form craters when the sputtering is uneven; and some elements sputter more slowly than others, creating a new distribution in the sample and a bias in the estimate of the rate of material removal.

An additional drawback common to all the surface analysis methods described is the necessity of introducing the sample in a high vacuum, which is a very different environment from the aqueous solutions where passive films are grown. As well, it is known that passive films do contain water and some authors believe that water plays a major role in the corrosion protection mechanism (Saito, Shibata and Okamoto, 1979). The water contained in the passive film will disappear or at least will be affected by the high vacuum. The passive film may also be affected by possible contaminants in the system and/or the high temperature

induced by the ion or electron beam.

3-3 Probabilistic Approach

Pitting has long been known to be a particularly fickle and unpredictable process (Evans, 1930; Mears and Evans, 1935). More precisely, it is impossible to forecast when a pit will initiate and where this is going to take place (assuming, of course, that conditions make pit initiation possible). Therefore, researchers have tried to extract information from the distributions in time, and in space, of pit nucleation events.

3-3-1 Time Distribution (Stochastic Approach)

Shibata and Takeyama (1976) postulate that the nucleation of a pit is a statistical process similar to the development of a crack in a brittle material. They assume that the pit generation process has the Markov property, i.e. that the future probability of pit nucleation is uniquely determined once the state of the system at the present stage is given. The pitting process is characterized by the pit generation rate λ , the pit repassivation rate, μ , and the incubation time t_0 , during which no pits occur. λ is such that the probability of nucleation one pit between t and $t + dt$ is $\lambda(t) \cdot dt$. Similarly, the probability of repassivating one pit is $\mu(t) dt$ (Shibata and Takeyama, 1981). A theoretical expression is then derived for $P(t)$,

the probability of having a non-pitted specimen at time t , as a function of λ , μ and t_0 ; $P(t)$ is evaluated experimentally as the proportion of non-pitted specimens, and from these values, λ , μ and t_0 are obtained.

As can be expected, these three parameters may vary with all the factors influencing pitting corrosion, such as potential, environment and alloy compositions. The application of this technique by Shibata and Takeyama (1981) has already been mentioned in 2-6.

It may be worth pointing out that this methodology makes few assumptions other than the ones outlined here, and does not deny the influence of factors such as surface defects on pit nucleation, as argued by Janik-Czachor (1981). On the contrary, the latest results of Shibata and Takeyama (1981) imply that inclusions do affect pit nucleation. This dependence was likely anticipated even in their first report, as they had developed their methodology from the one used for the analysis of brittle fracture of glass, where the distribution of defect sizes are paramount. Thus, the stochastic approach can be fruitful precisely because 'there is always a "spectrum" of the induction period for pit nucleation, τ , suggesting a "spectrum" of susceptibility for different sites on the surface' (Janik-Czachor and Ives, 1978; Janik-Czachor, 1981).

3-3-2 Spatial Distribution

This problem has been studied by Mears and Brown (1937) who find that after free pitting of many identical samples, the probability of having 1, 2 ... etc. pits on the sample does not exactly follow a Poisson distribution, as has been expected. The distribution is modified in the following way:

a) The maximum of the distribution is shifted towards low pit numbers. Mears and Brown explain this by the cathodic protection effect that a pit would provide to the metal zone surrounding it.

b) At high pit numbers the probability is higher than expected, possibly because the corrosion products generated by a few pits are fostering the nucleation of new ones.

These same arguments have been repeated in the last forty years in the technical literature, but few experiments have been conducted to confirm them.

Aziz (1956) assumes an exponential distribution of the pit depth to calculate the maximum depth by the statistics of extreme values. These are also used in the oil industry to estimate maximum pit depth (Eldredge, 1957; Finley and Toncre, 1964; Finley, 1967).

Janik-Czachor and Ives (1978) show the possibility to extract information about the pitting process from pit size distributions. They indicate that, with suitable

assumptions, the distribution depends on two functions: the nucleation rate and the growth rate.

Masuko (1974) proposes a method to quantify the tendency of corrosion pits to spread on the surface or to group in clusters, through the use of an homogeneity function. A similar method is used by Heimann, Ives and Zaya (1982) to show the presence of a small, regular population of etch pits on silicon, attributable to the presence of dislocations in the surface film.

3-4 Mass Transfer Calculations

The difficulty of evaluation of the electrochemical conditions within pits has led to the development of various theoretical models. The purpose of these models is ultimately to predict concentrations and potential at the bottom of the pit and to deduce from these the external conditions (solution composition, potential) leading to pitting.

One of the first applications of mass transfer to pitting corrosion was in a model developed by Kaesche (1962) of a hemispherical pit on aluminum. The same principles have also been applied to the modelling of other localized corrosion phenomena, for example by Hines (1961) and Beck and Grens (1969) to stress corrosion cracking, by Vermilyea and Tedmon (1970) and Shuck and Swedlow (1974) to crevice corrosion and by Turnbull (1980) and Turnbull and Thomas (1982) to corrosion fatigue.

5

Pickering and Frankenthal (1972) and Ateya and Pickering (1978) consider a cylindrical pit in which one-dimensional mass transfer was taking place. It is assumed that no reaction (hydrolysis, complexing) is taking place and that the electrolyte is a completely dissociated supporting electrolyte. This model explains the logarithmic type of relationship between aggressive ions and inhibitor ions necessary to prevent pitting (2-2). It also predicts the inhibitive action of divalent anions in the presence of aggressive monovalent anions.

This model has been modified by Galvele (1976a, 1976b, 1978, 1981) by introducing the hydrolysis of the metal ions, causing a drop in the pH of the solution near the bottom of the pit, more in line with experimental observations. The last modification of this model (Galvele, 1981) also takes into account the actual precipitation of hydroxide in the pit. The critical parameter found for the existence of a pit is the product of the depth and the current density.

Tester and Isaacs (1975) develop a model of a pit using both cylindrical and hemispherical geometries. Their prediction of a linear relationship between time and the inverse squared current density is corroborated by their experiments.

Hisamatsu (1976), through a slightly different model, reaches the conclusion that the critical quantity is

the concentration difference of total salts between the inside and the outside of the pit. Through diffusion calculations Alkire et al (1976) show that changes in the conductivity of the solution inside the pit can lead to an autoacceleration of the dissolution rate.

Vetter and Strehblow (1970, 1974) use a hemisphere as a model for a dissolving pit and compute the changes in concentrations and the potential drop between the bulk of the solution and the bottom of a 1 μm pit. These are shown to be too small to explain the presence of an active surface (the pit) on a passive sample.

Epelboin et al (1975), Epelboin and Keddam (1977) and Gabrielli (1973) have demonstrated that by assuming a coupling between dissolution and passivation reactions, and the diffusion of the species intervening in the passivation reaction (OH^-), it is possible to obtain a theoretical polarization curve similar to the one obtained with the negative resistance potentiostat they have used.

Epelboin and Keddam (1977) conclude that "any condition which impedes diffusion during metal dissolution will favour the occurrence of an active state of the metal at potentials which correspond to passive state". This could therefore be a general process, applicable not only to the stabilization of the pitting process, but also to its initiation.

One of the most detailed and exhaustive models

published so far has been developed by Popov, Alekseev and Kolotyrkin (1978, 1979). These authors use concentrated solution equations, while all the other models assume that dilute solution approximations are still valid. They also take into account the effect of convection induced by the high density of the solution inside the pit. One of the major conclusions of this work concerns the loss of water taking place at the bottom of the pit, leading to the formation of hydrated metal chloride. Unfortunately, the drastic assumptions made by the authors to solve the equations obtained reduce the generality and interest of the actual numerical results.

CHAPTER IV

MECHANISMS OF IRON DISSOLUTION

Although the dissolution of iron in aqueous solution always takes place according to the global reaction:



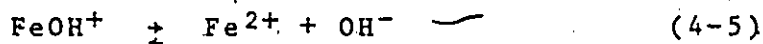
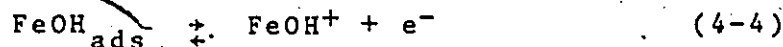
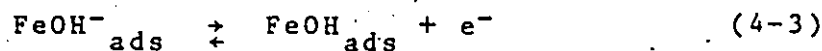
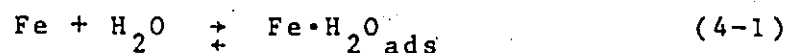
various mechanisms must be invoked to explain the details of the experimental results obtained. As the anions present may have a large influence on the mechanisms of dissolution, we shall consider the different mechanisms operating for different types of solution.

4-1 Mechanisms Involving Only OH⁻

In aqueous solutions containing only ions, such as perchlorates, which have little tendency to adsorb, the dissolution of iron depends strongly on the concentration of OH⁻ ions, the rate of dissolution increasing with [OH⁻]. This was first advanced by Bonhoeffer and Heusler (1957) to explain the fact that, at the same potential, iron dissolves more slowly in acid solutions than in basic solutions. For this reason, all the mechanisms involved in this case

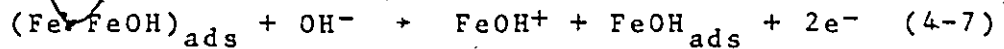
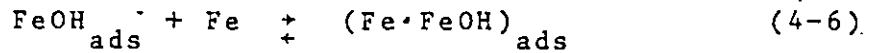
include the OH^- ion in the dissolution process. In acid solutions, these ions are presumably formed by the decomposition of adsorbed water molecules.

Two mechanisms have been proposed for the dissolution of iron when only OH^- are involved. The first one, known as the Bockris mechanism or noncatalyzed mechanism (Bockris, Drazic and Despic, 1961; Kelly, 1965), takes place as follows:



where step (4-4); the desorption of FeOH^+ with loss of one electron, is the rate determining step.

The second one, known as the Heusler mechanism or catalyzed mechanism (Bonhoeffer and Heusler, 1956, 1957; Heusler, 1958), involves steps (4-1) to (4-3) and (4-5) as above, but step (4-4) is replaced by:



where step (4-7) is the rate determining step.

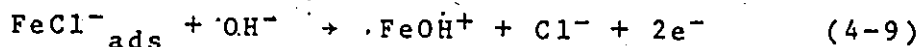
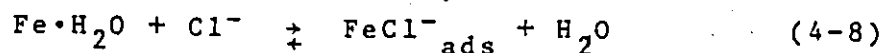
The occurrence of two different mechanisms for the same reaction has been explained (Lorenz and Eichkorn, 1965; Eichkorn, Lorenz, Albert and Fisher, 1968; Hilbert, Miyoshi, Eichkorn and Lorenz, 1971) by postulating that the reaction will be influenced by the state of the surface. If the surface contains a high density of active sites (grain and sub-grain boundaries, dislocations), equilibrium (4-6) will be shifted to the right-hand side and the Heusler mechanism will be favoured. On the other hand, if the material has a low density of defects, the Bockris mechanism is valid. Lorenz and Eichkorn (1965) were able to encounter the two mechanisms on two specimens of the same material after different thermo-mechanical treatments.

4-2 Mechanisms in the Presence of Cl^-

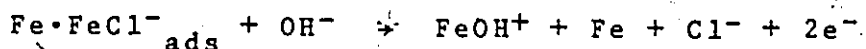
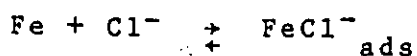
In the case where chloride ions are present, they will tend to adsorb preferentially on the iron surface, and therefore displace the OH^- ions and modify the mechanism of dissolution. This tendency will be accentuated in solutions of low pH and high chloride concentration. Kolotyrkin

(1961) finds that Cl, as well as the other halides, participates directly in the processes of anodic dissolution. However, the effect of the presence of Cl can vary with its concentration and the concentration of the other ions. At low concentration, the presence of Cl⁻ ions can have an inhibiting effect, while at higher concentrations, it increases the corrosion rate (Golovina, Florianovich and Kolotyarkin, 1965; Lorenz, 1965).

For solutions of pH < 2, a mechanism has been proposed by Lorenz, Yamaoka and Fisher (1963), where the Cl⁻ displaces the adsorbed water and catalyzes the reaction with OH⁻:

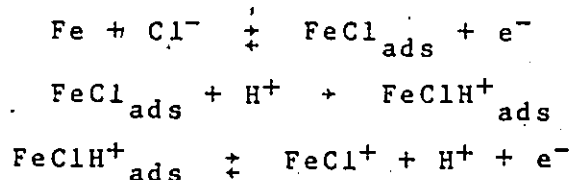


Lorenz (1965) proposes a similar mechanism to explain results of dissolution in sulphuric acid, introducing a complex similar to the one introduced by the Heusler mechanism:

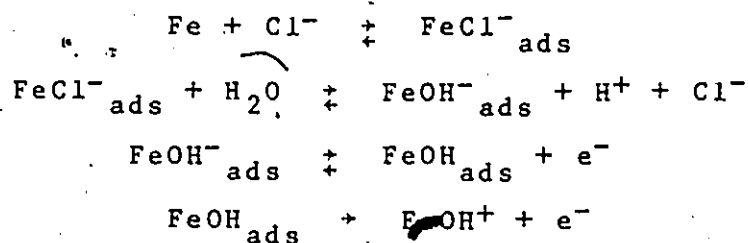


Darwish, Hilbert, Lorenz and Rosswag (1973) propose

another mechanism to account for results obtained at high concentrations of chloride ($> 1 \text{ M}$) and hydrogen ions ($> 1 \text{ M}$):

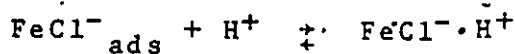


Arvia and Podesta (1968) introduce into the mechanism an equilibrium between the adsorbed Cl^- and OH^- :



the last two steps being the same as for the Bockris mechanism.

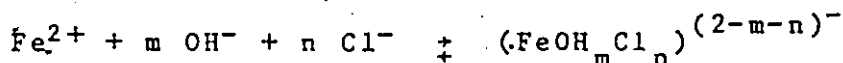
McCafferty and Hackerman (1972) find that when both $[\text{Cl}^-]$ and $[\text{H}^+]$ are high (larger than 6 N and 1 N, respectively), there is a synergism between the effects of the two ions. After reviewing the other possible reaction sequences, they propose a new mechanism, in which the hydrogen ions participate directly:



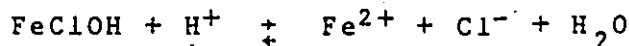
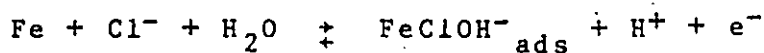


The justification for this mechanism is that, when the concentration of chloride ions is very high, they adsorb continuously on the surface and therefore attract the positively charged hydrogen ions to form the $\text{FeCl}^- \cdot \text{H}^+$ complex.

For neutral and basic solutions, Asakura and Nobe (1971) find that the data obtained can be explained through the introduction of another complex formed with Cl^- and OH^- :



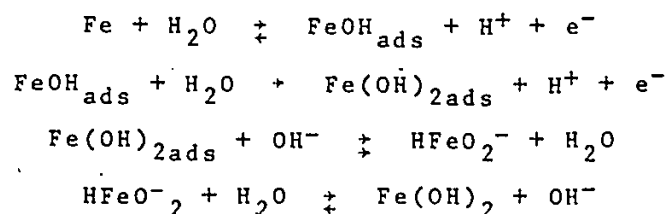
Chin and Nobe (1972) use a very similar model in acid solutions:



The same mechanism is used by Kuo and Nobe (1978), who claim that, when the pH is larger than about 1.1, iron dissolution occurs through the parallel paths of a Cl^- -accelerated mechanism (above) and a OH^- -accelerated mechanism, the Bockris mechanism. For more acid solutions, they find, as

do McCafferty and Hackerman (1972), that another mechanism is necessary. In their case, the data were consistent with the mechanism proposed by Darwish et al (1973).

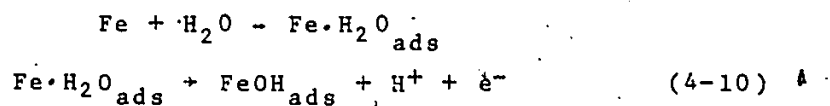
Drazic and Hao (1982) propose in the case of alkaline solutions the following process:



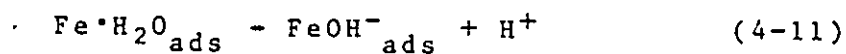
4-3 Mechanisms on scratched electrodes

Most of the results already reviewed are obtained by gathering data when the iron electrode had reached the steady state. By contrast, Burstein and Davies (1980, 1981) have performed a series of polarization experiments on scratched iron surfaces. They conclude that in borate and chloride solutions, the dissolution of iron is assisted by OH^- and Cl^- .

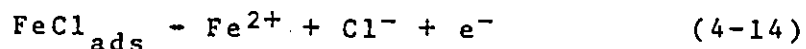
The mechanism involving OH^- is (Burstein and Davies, 1981):



or:



When Cl^- is present, the dissolution mechanism becomes (Burstein and Davies, 1980):



4-4 Mechanisms Relevant to Pitting Corrosion

In the case of the experiments considered here, the pH is slightly basic (7 to 9), all the solutions contain chloride ions and the electrochemical reactions involve freshly generated metallic surfaces. It is this last characteristic which was decisive in selecting the results of Burstein and Davies to determine the numerical values of the parameters. Their experimental results yield values of the current densities several orders of magnitude larger than the steady state values obtained by the other authors.

CHAPTER V

PROPOSED MODEL FOR PIT INITIATION

The review of pitting corrosion theories indicates that the crucial events leading to pitting nucleation occur on a scale of a few nm (thickness of the passive layer) and within a few ms or less (approximate lifetime of current burst). Electron microscopy and allied surface analysis methods, the only experimental techniques capable of dealing with such microscopic sizes, require working in a vacuum on the withered remains of a once "alive" passive film, resulting in the loss of any information respecting the chronology of events. On the other hand, electrochemical methods such as AC impedance, are quite sensitive with respect to the relevant time scale, but provide no information about where events take place.

It is therefore suggested that the surest way of understanding the phenomena involved would be to simulate the process assumed to occur during pit nucleation and to compare these results with reported experimental results.

The present undertaking is inspired by the mass transfer models of Pickering and Frankenthal (1972) and Galvele (1976b). By using a computer to solve the system of

partial differential equations, it has been possible to discard some of the simplifying hypotheses present in the previous models and to amplify these models by introducing additional features in an effort to more accurately simulate the phenomena involved.

5-1 Definition of the Problem

The following description of pitting corrosion and definition of the problem studied makes reference to the steps of pitting development defined in 2-1.

The model assumes that pitting corrosion occurs as a result of a breakdown and repair mechanism and that step 1, the breakdown of the passive layer has already occurred. This study concentrates on the phenomena causing step 2 to result in pitting or repassivation.

The initial conditions (stage 1) are shown in figure 2. At this point, a sample is polarized at constant potential. A cylindrical hole has just opened into the passive film, and has been filled with the bulk solution. The passive film is assumed to be inert and does not intervene in the processes to be described. At the bottom of the pore, the metal is in contact with the solution and will begin dissolving.

It is expected that this small area of bare metal will be subjected to very high current densities during a very short time before being covered by an adsorbed layer or

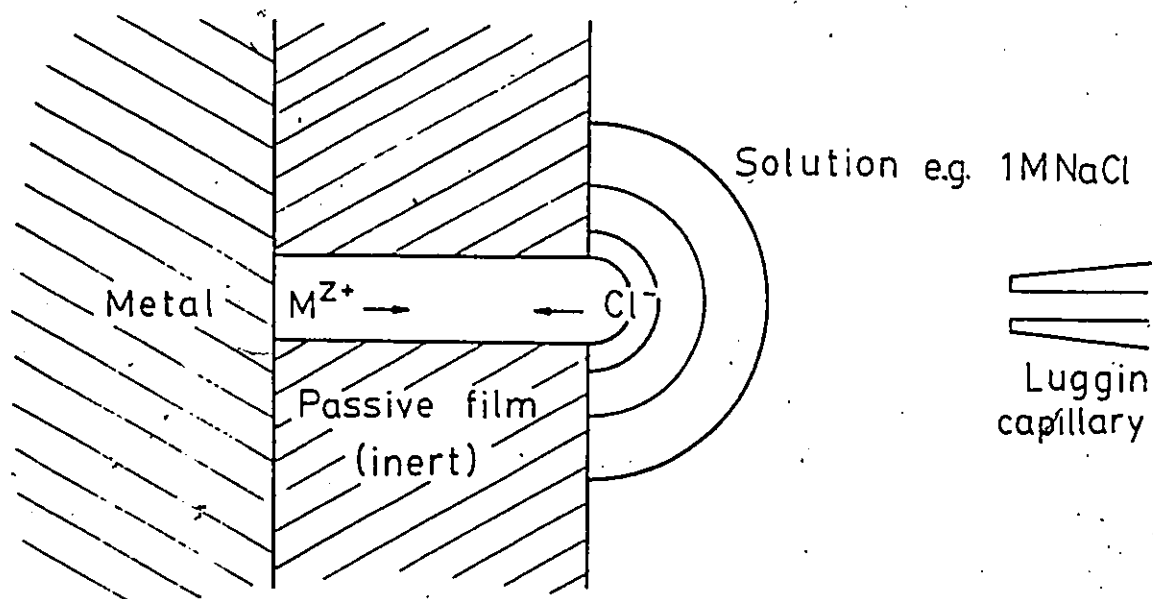


Figure 2 - Geometry of the model

by a tri-dimensional film, as pointed out in 2-10. It must be realized that the increase in current will be too small and too brief to be recorded adequately. On the other hand, all the experimental polarization data have been obtained after this initial period. The currents involved in the processes considered in this study are much smaller than the anodic and cathodic currents establishing the corrosion potential. Therefore, the conclusions of the present work can be extended, at least qualitatively, to the free corrosion case.

Five pitting theories are compared in the following manner. The solution compositions and potentials from reported experimental determinations of pitting potential are used as initial conditions and the situation at the bottom of the pore is evaluated at pseudo steady-state. The notion of breakdown and repair of a passive film implies that when the potential is lower than the pitting potential, the pore will repassivate, while if it is higher, dissolution will proceed and a pit will be created. For each theory, an expression depending on potential and concentrations at the metal surface was identified, such that, if the theory is correct, then this expression is smaller (or larger) than a parameter. This parameter should be constant and independent of the particular set of experimental conditions (e.g. pH, chloride concentration in the bulk solution), since all the calculations are made for conditions corresponding to

the pitting potential, that is for conditions borderline between pitting and passivity.

For these calculations, the phenomena taken into account are the metal dissolution, the metal hydrolysis, the metal complexing with the chloride ion and any other chemical equilibria present. In spite of metal dissolution, the geometry of the model is fixed and no deepening of the pore is considered.

5-2 Chemical System

The species present are H^+ , OH^- (H_2O is assumed to be in excess and present always and everywhere with an activity of 1), Cl^- , the metallic ion and its complexes with OH^- and Cl^- , plus some other non-complexing anions and cations. It is assumed that all reactions are at equilibrium and that all activity coefficients are equal to 1.

To compute the concentrations, use is made of the equilibrium constants of the metallic complexes and of the principle of electroneutrality:

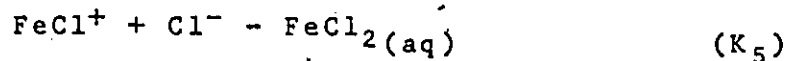
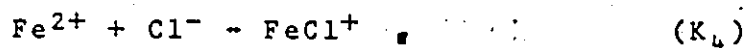
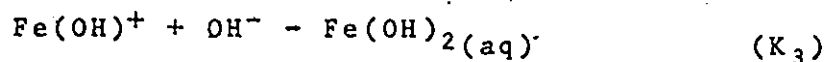
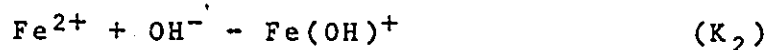
$$\sum_{i=1}^n z_i c_i = 0 \quad (5-1)$$

where c_i is the concentration of species i ,

z_i its charge and,

n is the number of species considered.

For instance in the case of iron dissolving in a NaCl solution, the 9 species considered are Fe^{2+} , H^+ , OH^- , Na^+ , Cl^- , $\text{Fe}(\text{OH})^+$, $\text{Fe}(\text{OH})_2(\text{aq})$, FeCl^+ and $\text{FeCl}_2(\text{aq})$. The 5 equilibria considered are:



Taking into account the equations corresponding to these 5 equilibria and to the electroneutrality, there are 6 relations. Therefore, only 3 concentrations out of the 9 are independent and are computed using mass transfer equations.

5-3 Transport Equations

Assuming the dilute solution approximation, the flux

of species 1 is equal to the diffusion flux plus the migration flux (the convection flux is neglected):

$$\vec{N}_1 = -z_1 u_1 F c_1 \vec{\nabla} \phi - D_1 \vec{\nabla} c_1 \quad (5-2)$$

for $i = 1$ to n .

where

\vec{N}_1 : flux of species 1 (out of n species),

\bar{c}_1 : activity of species 1 (assumed equal to the concentration),

z_1 : charge number of species 1,

u_1 : mobility of species 1,

D_1 : diffusion coefficient of species 1,

F : the Faraday (96,487 C/equiv.)

ϕ : electrochemical potential at the point of the solution considered.

It will be assumed that the diffusion coefficients are independent of the concentrations and that mobilities and diffusion coefficients are related by the Nernst-Einstein equation:

$$D_1 = RTu_1$$

for $i = 1$ to n

where R : gas constant (8.316 J/mole.K)

T : temperature.

A second equation expresses that the current is due to the motion of the charged species:

$$\vec{j} = F \sum_{i=1}^n z_i \vec{N}_i \quad (5-3)$$

for $i = 1$ to n .

where \vec{j} : current density:

A third equation states the material balance. The accumulation of species i is equal to the input of i by mass transport, plus the amount produced by chemical reaction:

$$\frac{\partial c_i}{\partial t} = -\vec{\nabla} \cdot \vec{N}_i + R_i \quad (5-4)$$

for $i = 1$ to n ,

where R_i : production rate of species i by chemical reaction.

The fourth equation used expresses the electro-neutrality (equation 5-1), as already mentioned in 5- 2.

Proceeding exactly as Newman (1973) and introducing (5-2) in (5-3), using (5-1) and rearranging, the potential gradient in the solutions is obtained:

$$\vec{\nabla} \phi = - \frac{\vec{j}}{K} - \frac{F}{K} \sum_{i=1}^n z_i D_i \vec{\nabla} c_i \quad (5-5)$$

where K : conductivity of the solution, equal by definition

to:

$$F^2 \sum_{i=1}^n \frac{z_i^2 u_i c_i}{z_i}$$

Equation (5-5) is then used to eliminate the potential from (5-2) and, after elimination of one of the n equations using (5-1) and replacement in (5-4), the following is obtained:

$$\begin{aligned} \frac{\partial c_1}{\partial t} = & D_1 \nabla^2 c_1 - \frac{\vec{\nabla} \cdot (t_1 \vec{j})}{z_1 F} \\ & - \sum_{k=2}^n \frac{z_k}{z_1} (D_k - D_1) \vec{\nabla} \cdot (t_1 \vec{\nabla} c_k) \\ & + R_1 \end{aligned} \quad (5-6)$$

for $i = 1$ to n ,

where t_1 : transport number of species 1, defined as:

$$\sum_{k=1}^n \frac{z_1^2 u_1 c_1}{z_k^2 u_k c_k}$$

Equation (5-6) is slightly different from Newman's equation 74-4 in that he uses $\vec{j} \cdot \vec{\nabla} t_1$ rather than $\vec{\nabla} \cdot (t_1 \vec{j})$. The notation adopted here is more general, as it does not assume that the current density is independent of the spatial coordinates.

The first two lines of the right-hand side of equation (5-6) will be referred to as T_1 ; thus:

$$\frac{\partial c_1}{\partial t} = T_1 + R_1 \quad (5-6')$$

for $i = 1$ to n .

It can be seen that if we know the values of c_i , its derivatives, D_i and z_i for $i=1$ to n and if we also know the values of \bar{J} , then T_i can be computed.

Where m is the number of equilibria considered, it has been indicated in 5-2 that only $n-m-1$ concentrations are independent. The $n-m-1$ independent components have been called the main components. The equations (5-6') are used to compute them after eliminating the R_i 's by expressing the conservation of the elements in each equilibrium. For example, using the system described in 5-2, we find:

conservation of Cl:

$$R_{Cl^-} + R_{FeCl^+} + 2 R_{FeCl_2} = 0$$

conservation of Fe:

$$R_{Fe^{2+}} + R_{Fe(OH)^+} + R_{Fe(OH)_2} + R_{FeCl^+} + R_{FeCl_2} = 0$$

conservation of H:

$$R_{H^+} = R_{OH^-} + R_{Fe(OH)^+} + 2 R_{Fe(OH)_2}$$

These relations combined with (5-6') become:

$$\frac{\partial}{\partial T} ([Cl^-] + [FeCl^+] + 2[FeCl_2]) = T_{Cl^-} + T_{FeCl^+} + 2 T_{FeCl_2} \quad (5-7A)$$

$$\frac{\partial}{\partial T} ([Fe^{2+}] + [Fe(OH)^+] + [Fe(OH)_2] + [FeCl^+] + [FeCl_2]) = T_{Fe^{2+}} + T_{Fe(OH)^+} + T_{Fe(OH)_2} + T_{FeCl^+} + T_{FeCl_2} \quad (5-7B)$$

$$\frac{\partial}{\partial t}([H^+] - [OH^-] - [FeOH^+] - 2[Fe(OH)_2]) = T_{H^+} - T_{OH^-} - T_{FeOH^+} - 2T_{Fe(OH)_2} \quad (5-7C)$$

The $n-m-1$ equations of this type are simplified using the m equilibria considered in 5-2; for example, the decomposition of water:

$$[H^+] \cdot [OH^-] = K_w$$

gives:

$$\frac{\frac{\partial [H^+]}{\partial t}}{[H^+]} = - \frac{\frac{\partial [OH^-]}{\partial t}}{[OH^-]}$$

An example of these calculations is shown in more detail in A-8.

Finally, a system of $n-m-1$ equations is obtained, where the left-hand side provides the time derivatives of the $n-m-1$ main components; for example:

$$\begin{aligned} \frac{\partial [Na^+]}{\partial t} = & -2 T_{Fe^{2+}} - T_{H^+} + T_{OH^-} - T_{FeOH^+} \\ & + T_{B(OH)_4} + T_{Cl^-} \end{aligned} \quad (5-8)$$

5-4 Boundary Conditions

The system of partial differential equations to be solved is parabolic and the problem is an initial value problem in time, and a boundary value problem in space.

The initial conditions are that the concentrations are everywhere equal to the bulk concentrations.

At a sufficiently great distance from the pore into the solution, the concentrations of all species are equal to the bulk concentrations at all time.

On the metal surface, the flux of metal ions is given by Faraday's law and the fluxes of all the other species are null:

$$\begin{aligned}\vec{N}_1 &= \frac{j}{z_1 F} \\ \vec{N}_i &= 0\end{aligned}$$

for $i = 2$ to n .

Combining equations (5-2), (5-5) and (5-1) as above, we obtain in the case of a one-dimensional transport problem:

$$N_1 = \frac{j}{z_1 F} - D_1 \frac{\partial c_1}{\partial x} + \frac{t_1}{z_1} \sum_{k=2}^n z_k (D_k - D_1) \frac{\partial c_k}{\partial x}$$

By inserting the values of N_1 into this system and simplifying, we obtain as the final expression of the boundary condition:

$$\frac{\partial c_1}{\partial x} = \frac{j}{FD_1} \cdot \frac{z_1 c_1}{\sum_k z_k^2 c_k} - \frac{j}{z_1 D_1 F}$$

$$\frac{\partial c_i}{\partial x} = \frac{j}{FD_1} \cdot \frac{z_i c_i}{\sum_k z_k^2 c_k} \text{ for } i = 2 \text{ to } n.$$

5-5 Computation of the Current

It is assumed that the only electrochemical reaction taking place is the anodic dissolution of the metal at the bottom of the pore. It is further assumed that the overpotential is sufficiently large that we may neglect the reverse reaction. Thus:

$$j = j_0 \cdot \exp \left(\frac{E}{b_a} \right) \quad (5-9)$$

where E is the potential at the metal surface (at the outer Helmholtz plane), b_a the experimental anodic Tafel slope and j_0 a coefficient determined experimentally (see 5-7).

E is equal to the applied potential E_0 minus:

- (1) The ohmic drop in the bulk, that is, between the Luggin capillary and that point considered as the "infinite" boundary for the purpose of mass transport.

$$\Delta V_1 = R_B j$$

where the resistance R_B is calculated according to the method of Kasper (1940):

- (2) The ohmic drop in that part of the solution where there is a variation in composition. This is computed by numerically integrating the first term of equation (5-5):

$$\Delta V_2 = \int \vec{j} \cdot \frac{dx}{K} = j \int \frac{dx}{K} \quad (\text{planar})$$

$$\text{OR} \quad j \cdot \frac{r_o^2}{2} \int \frac{dx}{r^2 K} \quad (\text{spherical})$$

where r_o is the radius of the pore.

- (3) The potential difference due to the concentration gradient, obtained by integrating the second term of equation (5-5):

$$\Delta V_3 = F \int \frac{z_i (D_i - D_1) \partial c_i / \partial r}{K} dr$$

5-6 Charging of the Electrical Double Layer

At the beginning of the process, the surge in current necessary to charge the double layer should be taken into account. The hypothesis is that the system behaves in a manner similar to that of the electrical circuit of figure 3. The two ohmic drops mentioned previously are represented by R . At the surface, the circuit is equivalent to a capacitor C in parallel with the faradaic dissolution process (noted F) described by equation (5-9). j_c is the total current density flowing from the surface.

As the differential equation relating E and j cannot be solved exactly, it is therefore solved numerically together with the main system of differential equations of type (5-8). If E is known, j , the faradaic current density, can be calculated by equation (5-9). Then the total current density is calculated as follows:

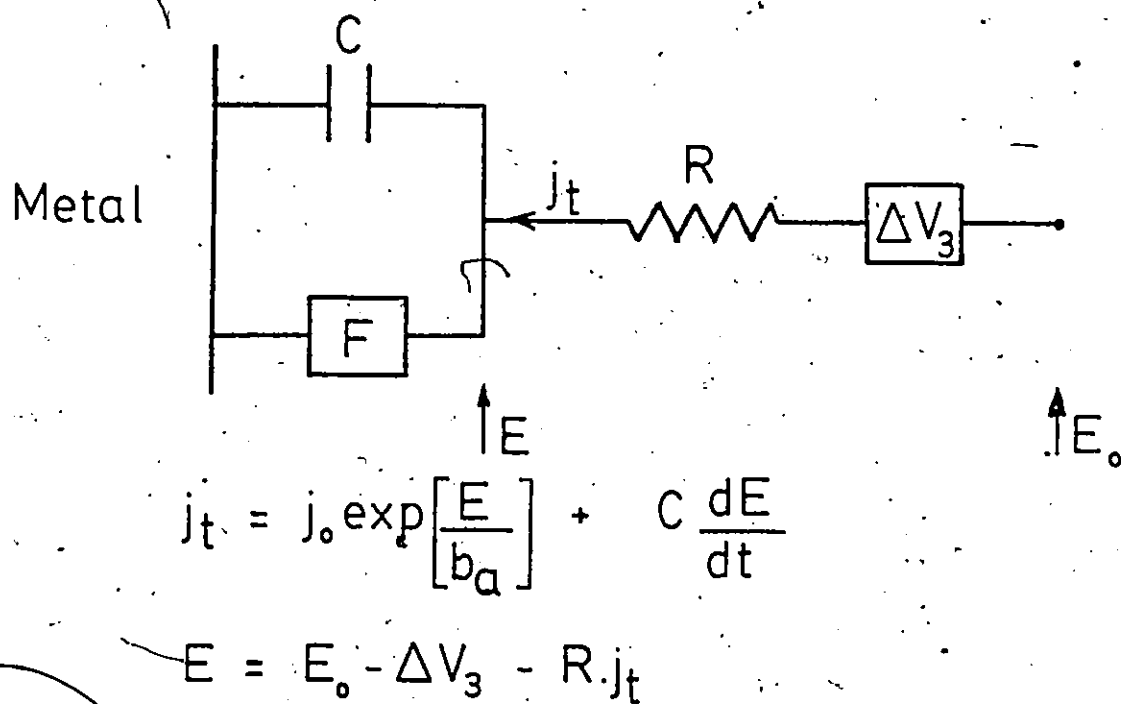


Figure 3 - Charging of the electrical double layer

$$j_t = \frac{E_0 - E - \Delta V}{R}$$

and finally:

$$\frac{dE}{dt} = \frac{j_t - j}{C}$$

It is assumed that initially, when the solution comes into contact with the metal, the capacitor is discharged and the potential E is equal to the potential of zero charge (Bockris and Reddy, 1970, p. 706).

5-7 Numerical Values of the Parameters

Two factors led to the decision to use iron in order to test the present model. First, under the conditions considered, the chemistry of iron is relatively simple. Secondly, the electrochemistry and the pitting corrosion of iron are fairly well covered in the literature.

5-7-1 Anodic Dissolution of Iron

The experimental results of Burstein and Davies (1980, 1981) were used to determine the relation between current and potential at the bottom of the pore (j_0 and b_a in equation 5-9). Although numerous other studies have been published on the subject of iron dissolution (see Chapter 4), Burstein and Davies are the only investigators measuring the current density on scratched metal. It is felt that this method reproduces the conditions at the metal/solution

interface more accurately than do the conventional steady state experiments which use an electrode covered with an adsorbed or tri-dimensional film.

At low pH, (4-10) occurs, giving:

$$j = F \cdot k_{10} \exp\left(\frac{\beta FE}{RT}\right)$$

Otherwise, (4-12) is the rate determining step, giving:

$$j = \frac{F k_{12} K_{11}}{[H^+] + K_{11}} \exp\left(\frac{\beta FE}{RT}\right)$$

When chloride ions are present, (4-13) is the rate determining step, and occurs at a rate given by:

$$j = F k_{13} [Cl^-] \exp\left(\frac{\beta FE}{RT}\right)$$

With this information, the following formula is used to compute the current density (5-9):

$$j = \left(m_1 + \frac{m_2}{m_3 + [H^+]} + m_4 [Cl^-] \right) \exp(C_1 E) \quad (5-10)$$

where $C_1 = \beta F/RT = 19.8 \text{ V}^{-1}$ for $\beta=0.5$ (equivalent to a Tafel slope of 116 mV/decade) and m_1 , m_2 , m_3 and m_4 are empirical coefficients determined by non linear regression to the data

of Burstein and Davies involving inert anions and Cl^- (9 points). The numerical values obtained are (concentrations in mol/l and current density in A/cm^2):

$$m_1 = 76.7$$

$$m_2 = 1.15 \cdot 10^{-5}$$

$$m_3 = 3.87 \cdot 10^{-12}$$

$$m_4 = 4.57 \cdot 10^4$$

5-7-2 Other Parameters

The depth of the pore, which is also the thickness of the film, is taken to be equal to 5 nm, although it is somewhat greater than to the range of 1 to 3 nm measured by Nagayama and Cohen (1962).

In the absence of any data, the radius of the pore is taken to be equal to 1 nm, as surface diffusion on the pore surface could be significant for a pore of smaller radius. Furthermore, the radius of the pore only intervenes as a boundary of the region of spherical mass transfer (see 5-8) and it is shown a posteriori (see 6-2) that it has little influence on the results.

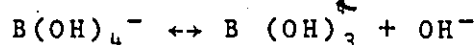
The values of the following equilibrium constants (see 5-2) are taken from the compilation of Baes and Mesmer (1976):

$$[\text{H}^+] \cdot [\text{OH}^-] = K_1 = 1.78 \cdot 10^{-14}$$

$$\frac{[\text{Fe}(\text{OH})^+]}{[\text{Fe}^{2+}] \cdot [\text{OH}^-]} = K_2 = 2 \cdot 10^4$$

$$\frac{[\text{Fe}(\text{OH})_2(\text{aq})]}{[\text{Fe}^{2+}] \cdot [\text{OH}^-]} = K_3 = 1.3 \cdot 10^3$$

as well as the buffering reaction



$$\frac{[\text{B}(\text{OH})_4^-]}{[\text{B}(\text{OH})_3] \cdot [\text{OH}^-]} = K_6 = 8.93 \cdot 10^4$$

The constants corresponding to the complexes of Fe^{2+} and Cl^- have been reported with widely different values:

$$\frac{[\text{FeCl}^+]}{[\text{Fe}^{2+}] \cdot [\text{Cl}^-]} = K_4 = 2.3 \text{ (Butler, 1964)}$$

$$< 0.5 \text{ (Sillen and Martell, 1964)}$$

$$= 3.2 \text{ (Faita et al, 1974)}$$

$$\frac{[\text{FeCl}_2(\text{aq})]}{[\text{FeCl}^+] \cdot [\text{Cl}^-]} = K_5 = 1.1 \text{ (Butler, 1964)}$$

To follow qualitatively the variation of these two complexes while keeping their concentrations at a negligible level, these two constants are set equal to 10^{-2} .

The values of the diffusion coefficients of the following ions are taken from Parsons (1959):

$$\text{Fe}^{2+} : 0.7 \cdot 10^{-9} \text{ m}^2/\text{s}$$

$$\text{H}^+ : 9.5 \cdot 10^{-9} \text{ m}^2/\text{s}$$

$$\text{Cl}^- : 2.0 \cdot 10^{-9} \text{ m}^2/\text{s}$$

$$\text{OH}^- : 5.3 \cdot 10^{-9} \text{ m}^2/\text{s}$$

$$\text{Na}^+ : 1.3 \cdot 10^{-9} \text{ m}^2/\text{s}$$

In the absence of published data, the following values have been chosen by comparison with the values for similar ions published in the literature (Parsons, 1959; Newman, 1973):

$$\text{Fe(OH)}^+ : 1.5 \cdot 10^{-9} \text{ m}^2/\text{s}$$

$$\text{Fe(OH)}_2(\text{aq}) : 1.0 \cdot 10^{-9} \text{ m}^2/\text{s}$$

$$\text{FeCl}^+ : 1.2 \cdot 10^{-9} \text{ m}^2/\text{s}$$

$$\text{FeCl}_2(\text{aq}) : 1.0 \cdot 10^{-9} \text{ m}^2/\text{s}$$

$$\text{B(OH)}_3 : 1.0 \cdot 10^{-9} \text{ m}^2/\text{s}$$

$$\text{B(OH)}_4^- : 1.5 \cdot 10^{-9} \text{ m}^2/\text{s}$$

The capacity of the double layer is considered equal to $40 \mu\text{F}/\text{cm}^2$, in the range given by Macdonald (1977). The potential of zero charge is considered equal to -370 mV (West, 1965).

Using the solubility of Fe(OH)_2 from Baes and Mesmer (1976), we can determine the concentration of $\text{Fe(OH)}_2(\text{aq})$ at saturation:

$$[\text{Fe(OH)}_2(\text{aq})] = 2 \cdot 10^{-8} \text{ mol/l}$$

Using a solubility of 4.25 mol/l for FeCl_2 (Kuo and Landolt, 1975) and the equilibrium constants selected for FeCl^+ and $\text{FeCl}_2(\text{aq})$, we obtain at saturation:

$$[\text{FeCl}_2(\text{aq})] = 2.6 \cdot 10^{-2} \text{ mol/l}$$

5-8 Numerical Solution of the Equations

To solve the system of partial differential equations of type (5-8), T_1 , as defined in (5-6) and (5-6') must be evaluated as must the spatial derivatives of the concentrations. This is done by the method of finite difference as follows.

The space studied is divided into 3 regions:

1 - The cylindrical hole, between the metal surface and the plane of the film/solution interface. The mass transport equation (5-6) is uni-dimensional and planar. The derivatives are computed with a net of NN_1 equidistant nodes with formulae of the type:

$$\frac{\partial c_1}{\partial x} = DC(I, N) = \frac{C(I, N+1) - C(I, N-1)}{2 \times DX}$$

$$\frac{\partial^2 c_1}{\partial x^2} = DDC(I, N) = \frac{C(I, N+1) - 2 \times C(I, N) + C(I, N-1)}{DX^2}$$

where $DC(I, N)$ and $DDC(I, N)$ are the first and second spatial derivatives, respectively, of the concentration $C(I, N)$ of species I at node N and DX is the distance between nodes.

2 - The region bounded by the plane of film/solution interface, by an hemisphere whose large circle is the pore mouth and by another concentric hemisphere of sufficiently

large radius, where the concentration is not affected by the pore opening. In this region, the mass transport equations are spherical and the derivatives are computed using a net of points equidistant on a logarithmic scale. This permits a large reduction in the number of net points and therefore in the amount of necessary calculation (Newman, Hanson and Vetter, 1977). The derivatives are:

$$\frac{\partial c_i}{\partial r} = DC(I, N) = \frac{C(I, N+1) - C(I, N-1)}{2 \times R(N) \times DLR}$$

$$\frac{\partial^2 c_i}{\partial r^2} = DDC(I, N) = \frac{1}{R(N)^2} \left[\frac{C(I, N+1) - 2 \times C(I, N) + C(I, N-1)}{DLR^2} - \frac{C(I, N+1) - C(I, N-1)}{2 \times DLR} \right]$$

where $R(N)$ is the radius at node N ,

RR is the ratio of the radii at two successive points: $RR = R(N)/R(N-1)$ and

$$DLR = \ln(RR).$$

3 - The transition region situated at the pore mouth, between the two regions already mentioned. Here, the mass transport geometry is assumed to be spherical, the nodes are equidistant and the formulae for the computation of the derivatives are identical to the ones used in the first region.

Once the T_i have been computed, the right-hand side

of the system of $n-m-1$ equations of type (5-8) is calculated. If NN is the total number of nodes used on all three regions, the number of unknowns is $(n-m-1) \times NN$ and the system of partial differential equations is now reduced to a system of ordinary differential equations.

This latter system is solved using the Livermore Solver for Ordinary Differential Equations (LSODE) package, obtained through the National Energy Software Center. This group of routines was specially designed to automatically integrate systems of ordinary differential equations of the type generated here, known as stiff differential equations. It is based on an original algorithm by Gear (1971).

A listing of the computer program which has been written and used in this study is included in Appendix A.

5-9 Possible Criteria for Pitting Initiation

The results of the integration of the mass transport equations are used to compute the numerical values of the following parameters which correspond to different theories of pitting corrosion. Here, the concentrations and potential mentioned in the equations are calculated values at the bottom of the pore.

5-9-1 Repassivation

According to the localized acidification theory (see 2-9-2), a pit will form if the local conditions are such

that no passivating species is insoluble (Galvele, 1981). In the conditions encountered in this study, magnetite should be the thermodynamically stable species in the passive range (Pourbaix, 1974). But a recent recalculation of the Pourbaix diagram by Silverman (1982), using more recent data, shows that ferrous hydroxide is stable between the iron-metal and the magnetite regions. It is also unlikely that magnetite would precipitate from solution. Rather, it may form by oxidation and dehydration of ferrous hydroxide. For these reasons, $\text{Fe}(\text{OH})_2(\text{s})$ has been chosen as the most probable passivating species, following Galvele (1976b, 1981). The criterion for pitting is:

$$\frac{[\text{Fe}(\text{OH})_2(\text{aq})]}{S_1} \equiv K_{rp} < K_{rp}^0$$

where S_1 : concentration of $\text{Fe}(\text{OH})_2(\text{aq})$ at saturation,
 K_{rp} : supersaturation ratio,
 K_{rp}^0 : the pitting criterion parameter for this mechanism.

5-9-2 Salt film precipitation

Vetter (1965) originally proposed that pits are characterized by the presence of a salt film on the metal/solution interface (see 2-10). Therefore, the precipitation of FeCl_2 was taken as another possible criterion for the occurrence of pitting:

$$\frac{[\text{FeCl}_2(\text{aq})]}{S_2} \equiv K_{sf} > K_{sf}^0$$

where S_2 : concentration of FeCl_2 at saturation,
 K_{sf} : supersaturation ratio,
 K_{sf}^0 : the pitting criterion parameter for this mechanism.

It must be noted however that this mode of formation of the salt layer is different from Vetter's model in that he proposes that the salt film growth from the metal surface is a solid state process and that the salt film is in contact with an undersaturated solution. Thus the present criterion is closer to the mechanisms involving precipitation considered by Engell (1977) and Beck and Alkire (1979).

5-9-3 Adsorption

As mentioned in 2-7, theories have been proposed which see the adsorption of the aggressive ion as the critical step in the pitting process. As the dissolution model of Burstein and Davies has been adopted to compute the current density on the metal surface (5-7-1), a criterion for the onset of pitting consistent with the adsorption theory is that a pit will form if the coverage of FeCl_{ads} exceeds a critical value. Assuming that equation (4-14) holds:

$$E = E_{14} - \frac{RT}{F} \log \left(\frac{[Fe^{2+}][Cl^-]}{\theta_1} \right)$$

where E_{14} : standard potential of (4-14) and

θ_1 : coverage of $FeCl_{ads}$

The criterion for pitting in this case would thus be:

$$\theta_1 = [Fe^{2+}][Cl^-] \exp \left(\frac{(E - E_{14}) F}{RT} \right) > \theta_{c1}$$

$$\begin{aligned} \text{or: } [Fe^{2+}][Cl^-] \exp \left(\frac{EF}{RT} \right) &= \theta_1 \exp \left(\frac{E_{14} F}{RT} \right) = \\ &\equiv K_{ad1} > K^0_{ad1} = \theta_{c1} \exp \left(\frac{E_{14} F}{RT} \right) \end{aligned}$$

where θ_{c1} : critical coverage of $FeCl_{ads}$,

K_{ad1} : variable representing the product mentioned,

K^0_{ad1} : the pitting criterion parameter for this mechanism.

Another possible criterion consistent with the adsorption mechanism considers the adsorption equilibrium of Cl^- on the iron surface (Strehblow and Titze, 1977):



giving the relation:

$$\theta_2 = [Cl^-] \exp \left(\frac{(E - E_{11}) \gamma_A F}{RT} \right) \quad (5-12)$$

where θ_{2c} is the coverage of Cl_{ads} ,
 E_{11} is the standard potential for (5-11), and
 γ_A is the electrosorption valency (assumed equal to 1).

If pitting is triggered by a critical coverage of Cl_{ads} , then:

$$[Cl^-] \exp\left(\frac{EF}{RT}\right) = \theta_{2c} \exp\left(\frac{E_{11}F}{RT}\right) \\ \equiv K_{ad2} \rightarrow K_{ad2}^0 = \theta_{c2} \exp\left(\frac{E_{11}F}{RT}\right)$$

where θ_{c2} : critical coverage of Cl_{ads} ,
 K_{ad2} : variable representing the product mentioned,
 K_{ad2}^0 : the pitting criterion parameter for this mechanism.

5-9-4 Critical chloride concentration

It has been assumed that pitting is initiated by a critical concentration of aggressive ion at the metal surface (Wilde, 1976), as discussed in 2-9-1. Pitting will occur then if:

$$[Cl^-] > K_{cc}^0$$

where K_{cc}^0 : the pitting criterion parameter for the mechanism.

CHAPTER VI

RESULTS6-1 General Results

The computations are performed at equal time intervals on a logarithmic scale usually starting at 10^{-11} s, as in, for example, 10^{-11} s, $3.16 \cdot 10^{-11}$ s, 10^{-10} s, $3.16 \cdot 10^{-10}$ s, etc. The program stops when a pseudo steady-state is reached, that is, when the concentrations in the pore are not varying appreciably. This is deemed to be obtained when all the following conditions are satisfied on two successive computations:

- * $[H^+]$ at the metal surface varies by less than 0.5%,
- * $[Fe^{2+}]$ at the metal surface varies by less than 0.5%,
- * $[Fe^{2+}]$ at the pore mid-length varies by less than 0.5%,
- * The slope of $\log [Fe^{2+}]$ vs $\log [t]$ at the metal surface is less than 0.01.

When these conditions cannot be obtained, an extrapolation method is used (see 6-4).

Figures 4 to 7 show typical curves obtained for the concentrations of the main components. Each of the four

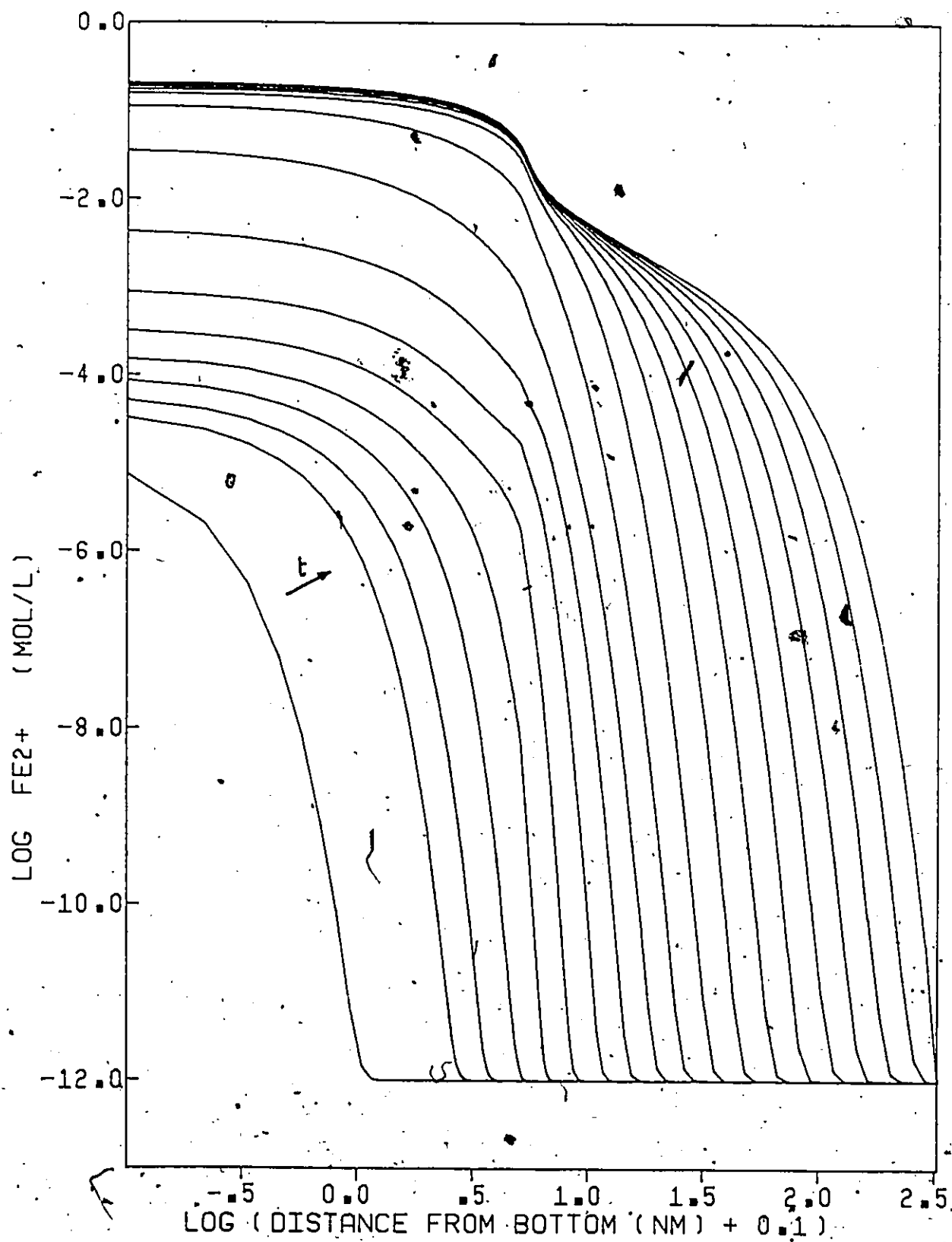


Figure 4 - Example of variation of $\text{Log [Fe}^{2+}]$ with distance at different times

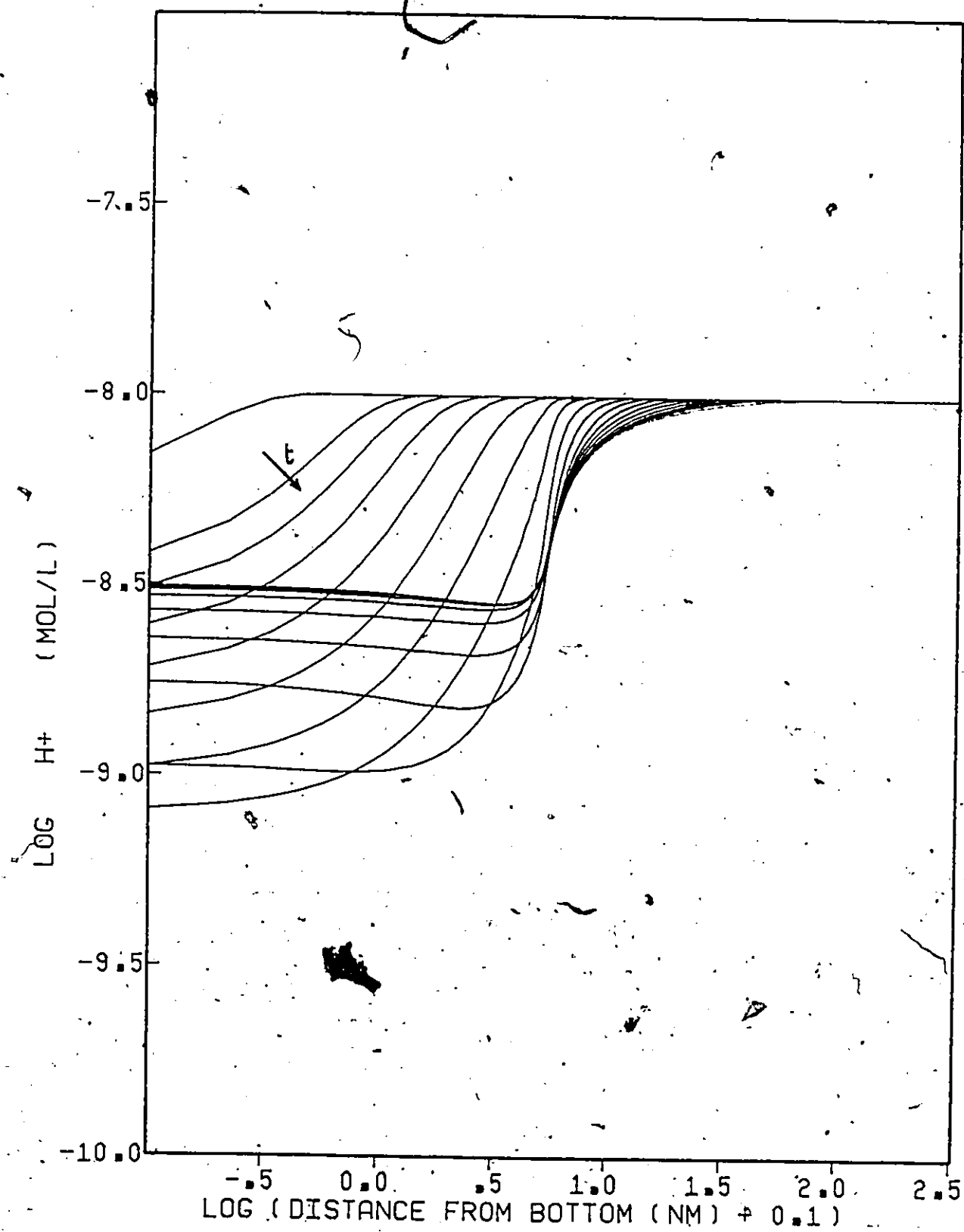


Figure 5 - Example of variation of $\text{Log } [H^+]$ with distance at different times

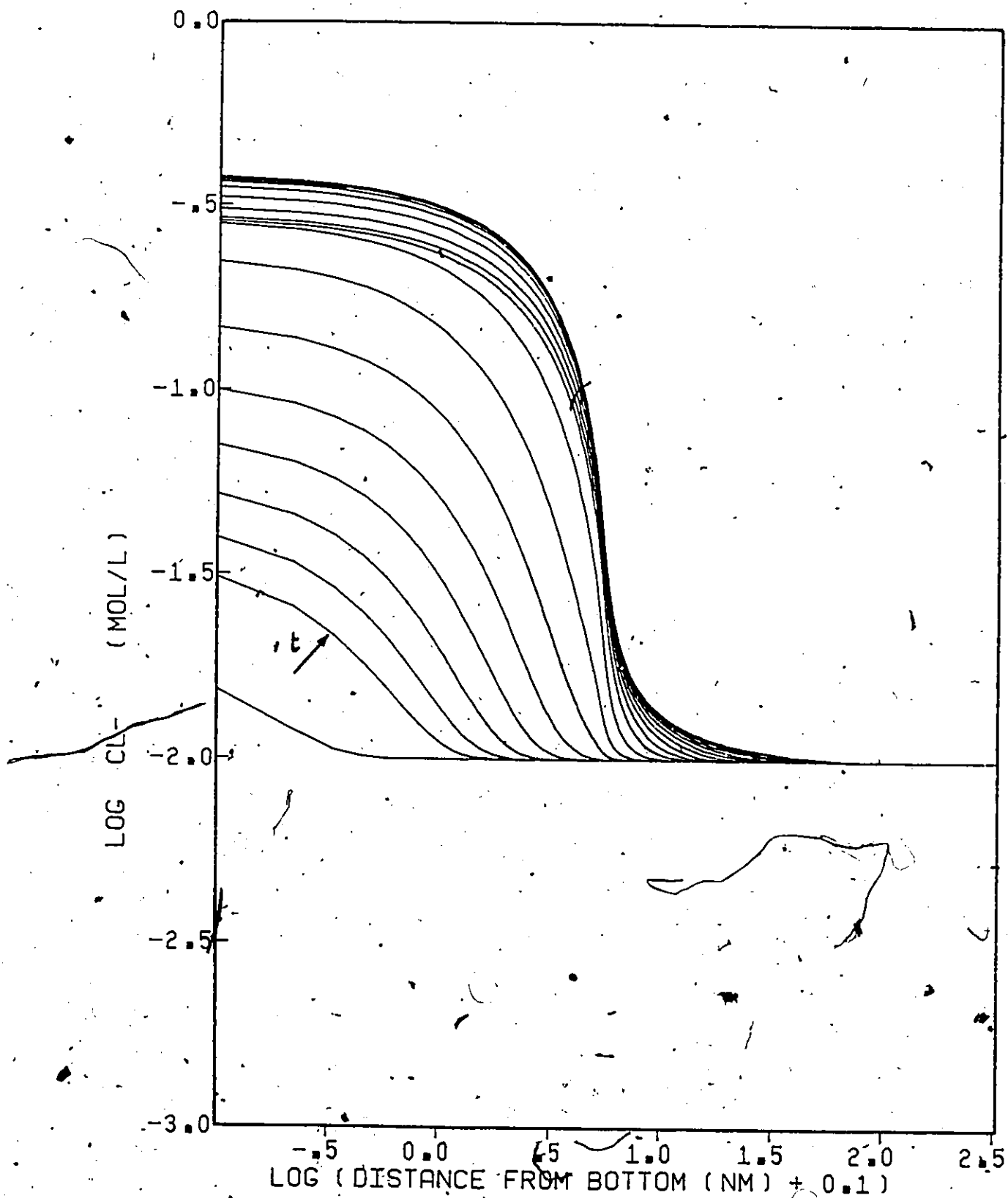


Figure 6 - Example of variation of $\text{Log } [\text{Cl}^-]$ with distance at different times

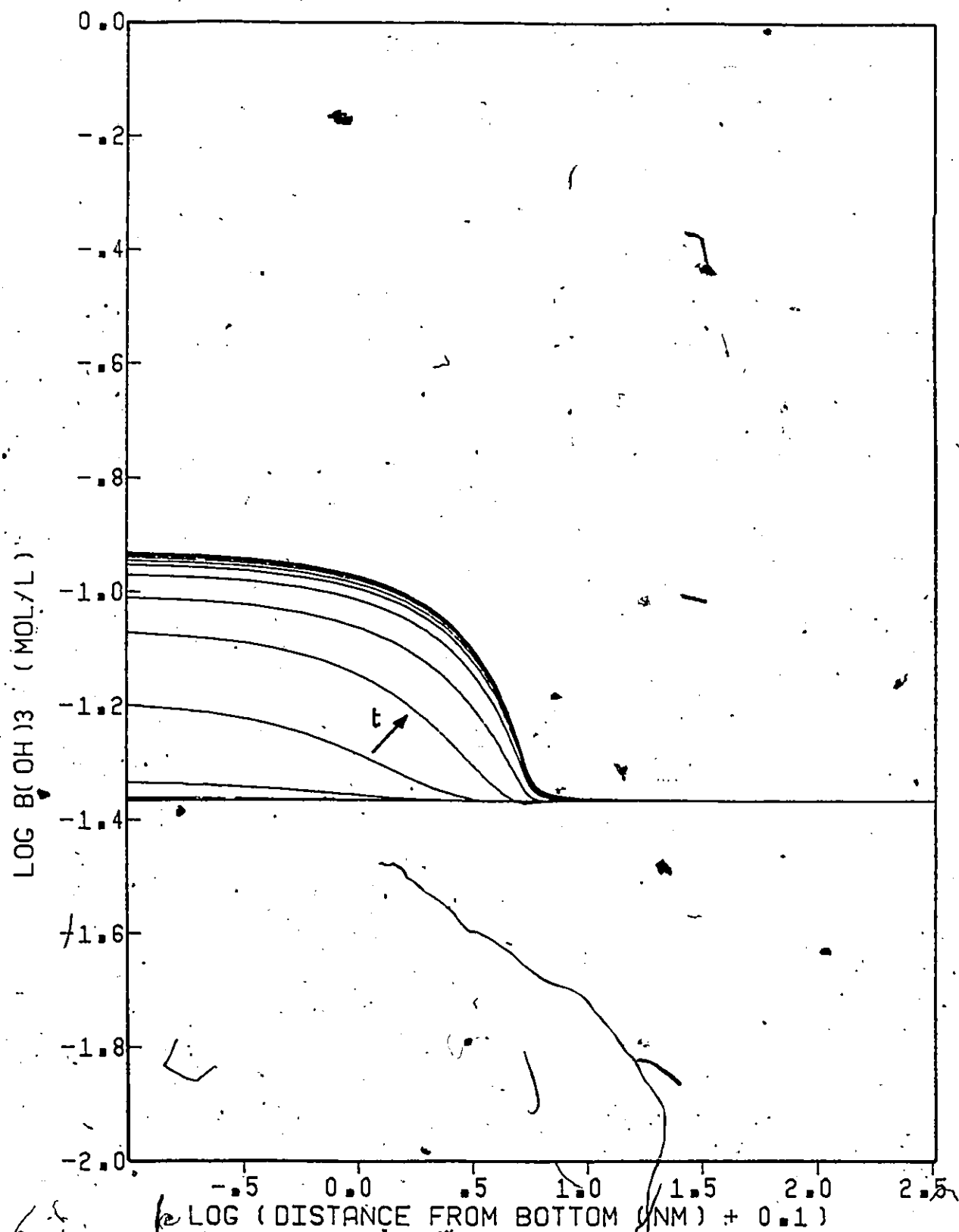


Figure 7 - Example of variation of Log. $[B(OH)_3]$ with distance at different times

curves illustrates the same computation where the iron electrode is polarized at -19 mV vs SHE in a pH 8 borate buffer with $[Cl^-] = 0.01$ M. Each line corresponds to a computation at the time intervals mentioned above.

The iron concentration (Figure 4) rises monotonically from the arbitrarily small level of the bulk solution (10^{-12} M) to its final value at the pseudo steady-state. The kink in the curves close to the pseudo steady-state marks the transition between the region of planar diffusion (the pore) and the region of spherical diffusion. Figure 8 (corresponding to another simulation) illustrates that when the pseudo steady-state is reached, the diffusion gradient for $[Fe^{2+}]$ is nearly constant within the pore. In the region of spherical diffusion, this concentration will keep on increasing far away from the pore, but with a minimal effect on the values close to the pore mouth.

The variations of pH (Figure 5) are small in the case of a buffered solution and are within about 1 unit of pH in this particular case. It may be noted that the pH is higher in the pore than in the bulk, contrary to what would be expected. By contrast, Figure 9 shows the variation of pH in a non-buffered solution (1 M NaCl, pH 9, polarized at -80 mV vs SHE) where the pH drops by more than 4 pH units.

This conforms to those experimental results on ferrous alloys which report that the solution in occluded cells is definitely acidified.

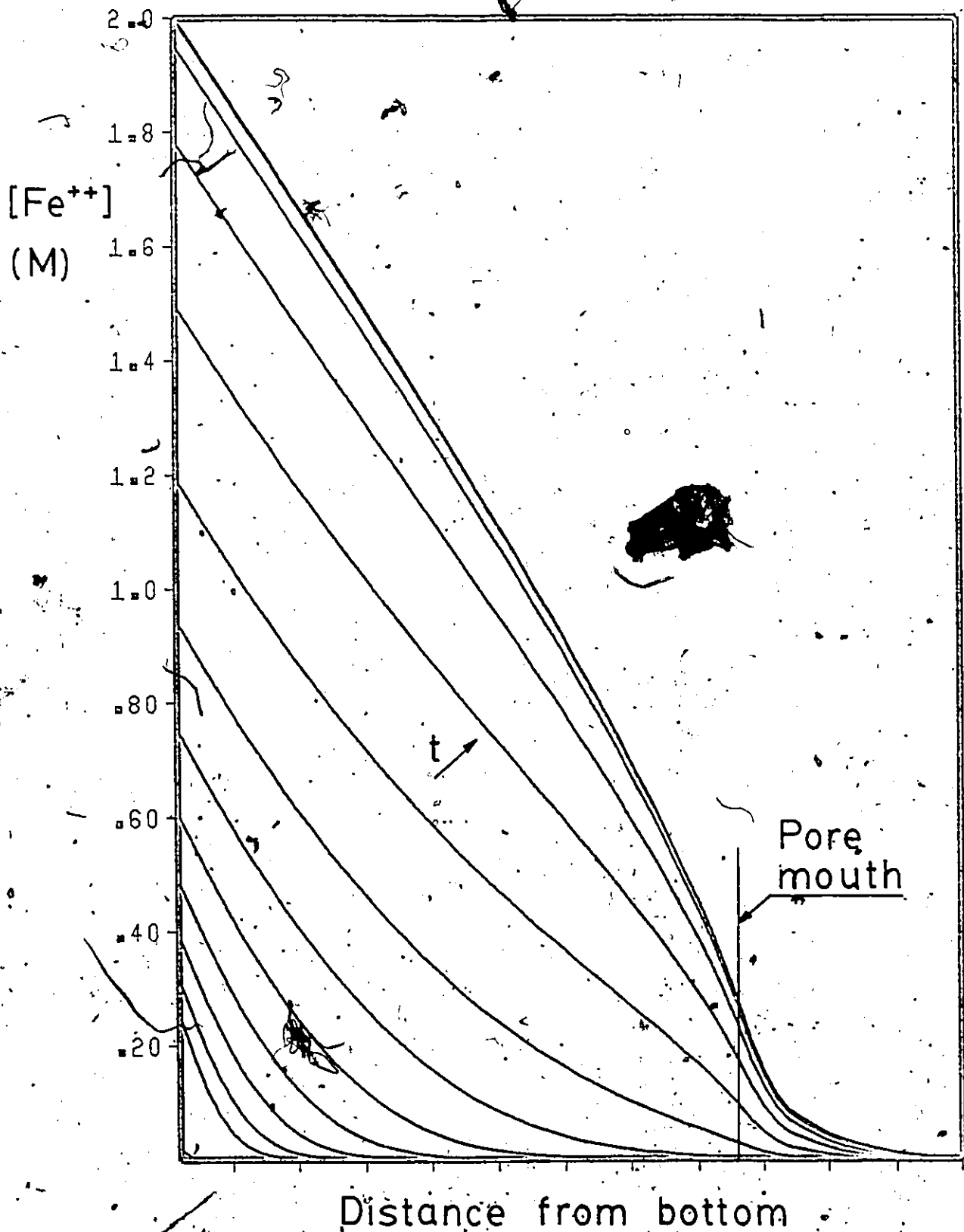


Figure 8 - Example of variation of $[\text{Fe}^{2+}]$ with distance (linear coordinates)

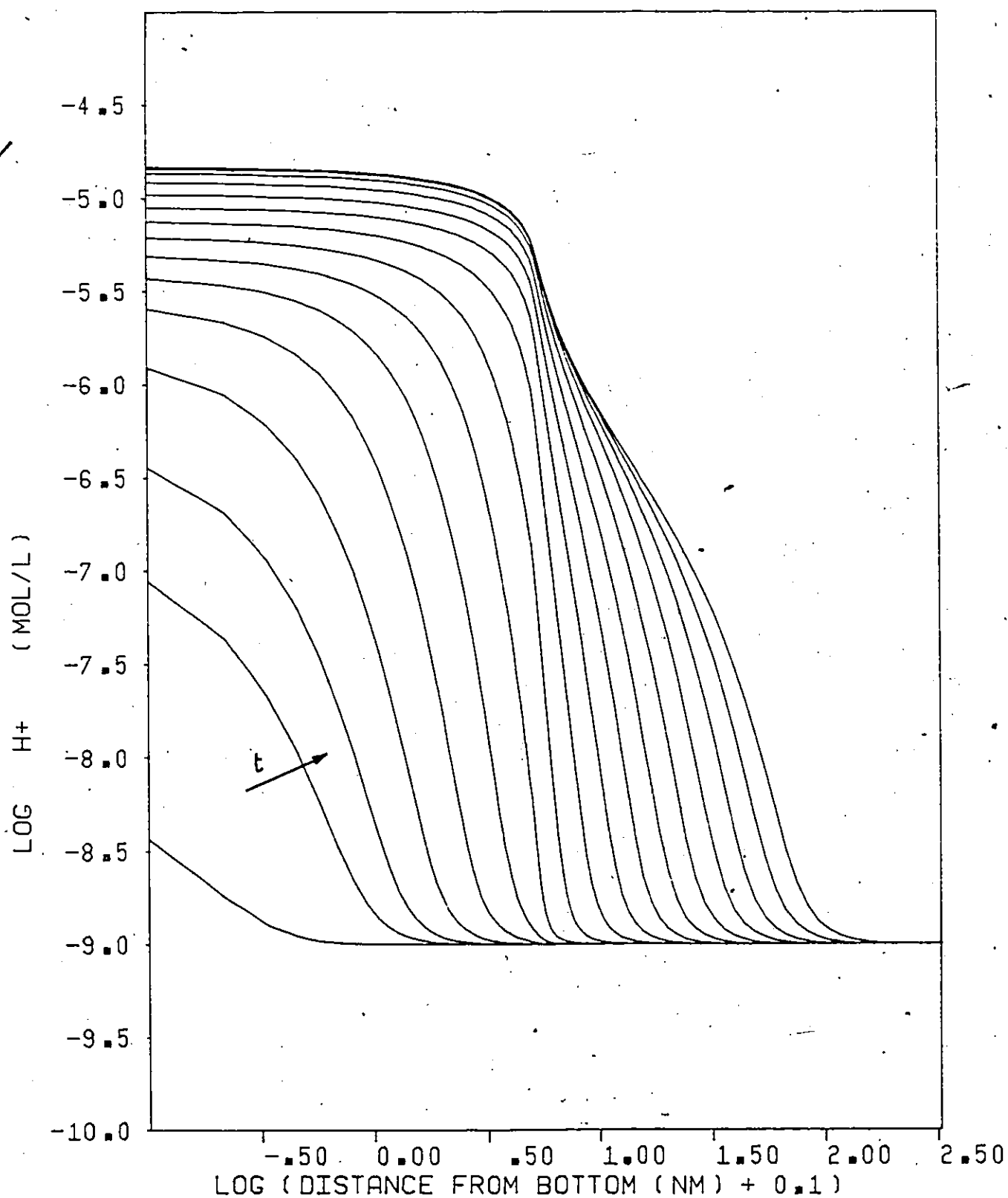


Figure 9 - Variation of pH with distance at different times (1M NaCl, pH 9)

Figure 6 shows that the concentration of chloride increases in the pore by migration to maintain electroneutrality, as does the concentration of borate (Figure 7).

The variation of all the concentrations with distance at pseudo steady-state can be followed on Figure 10. The sodium concentration in the pore becomes very low, so that the solution in the pore really becomes a concentrated solution of ferrous chloride.

The parameters corresponding to the hydroxide precipitation K_{rp} , and to the chloride precipitation K_{sf} , vary generally in a manner similar to $[Fe^{2+}]$. They increase monotonically with time and decrease monotonically with the distance from the bottom of the pore. However, in some instances, K_{rp} behaves differently (Figure 11). A maximum appears early in the process and moves away from the metal surface while keeping an approximately constant height. The value of K_{rp} at the metal surface eventually reaches a pseudo steady-state value lower than the maximum. It is this lower, pseudo steady-state value which has been selected as representative in the computation, since if precipitation is going to take place, it will be more likely by heterogeneous nucleation.

Figure 12 summarizes the variation with time of 3 concentrations (Fe^{2+} , H^+ and Cl^-), K_{rp} and K_{sf} at the surface, as well as the faradaic current density for the same

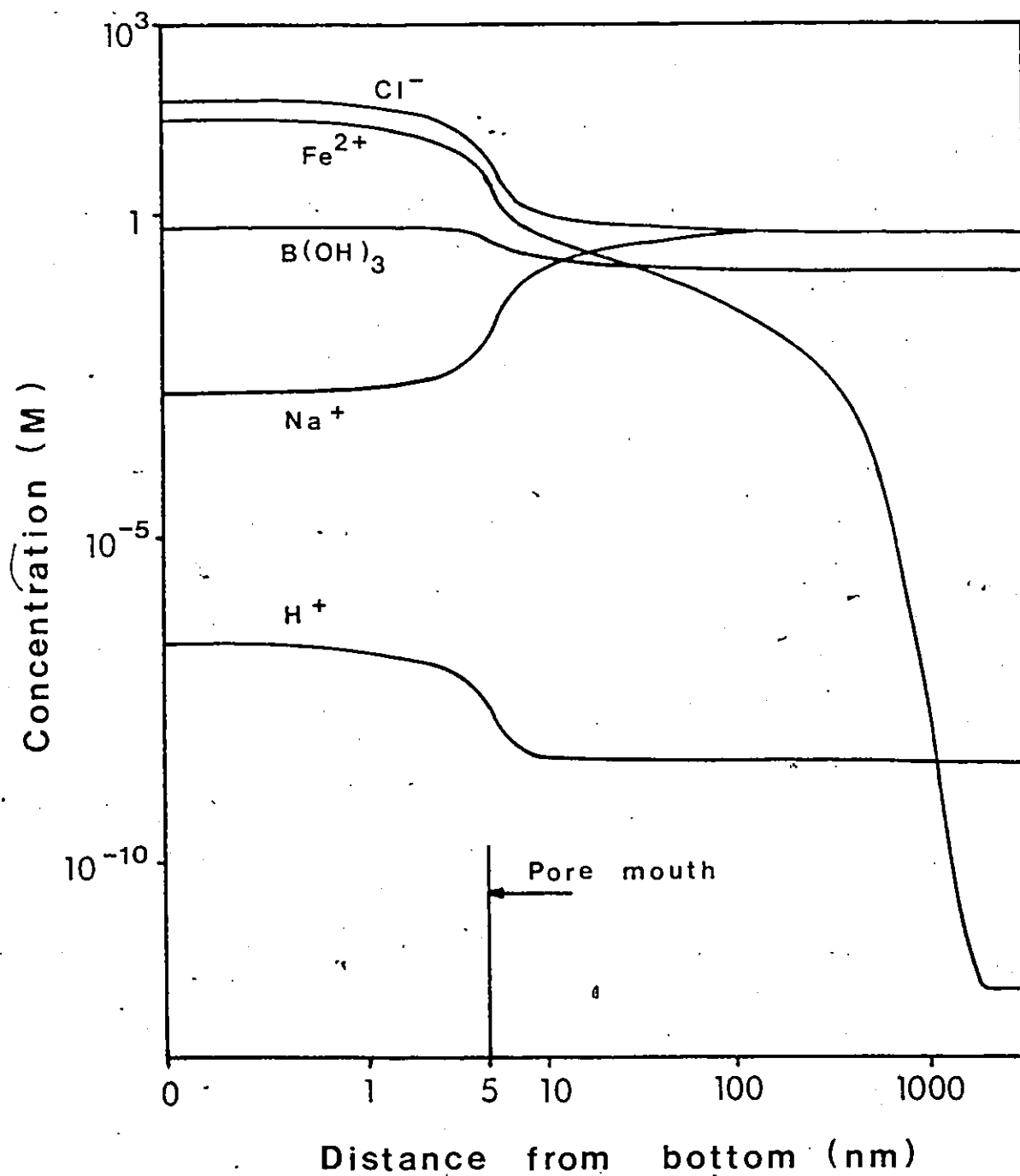


Figure 10 - Variation of all the concentrations with distance at pseudo-steady state.

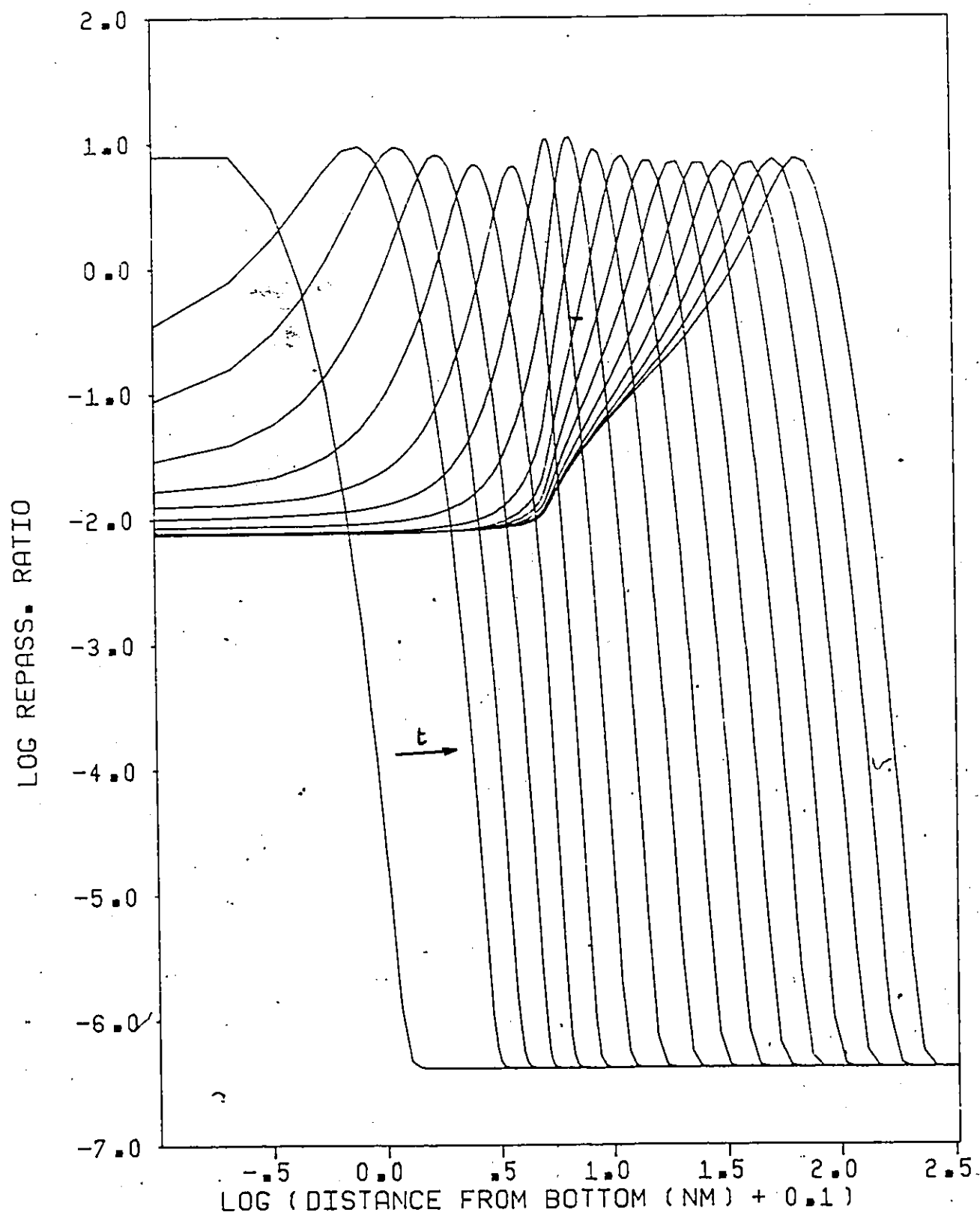


Figure 11 - Variation of K_{rp} with distance at different times

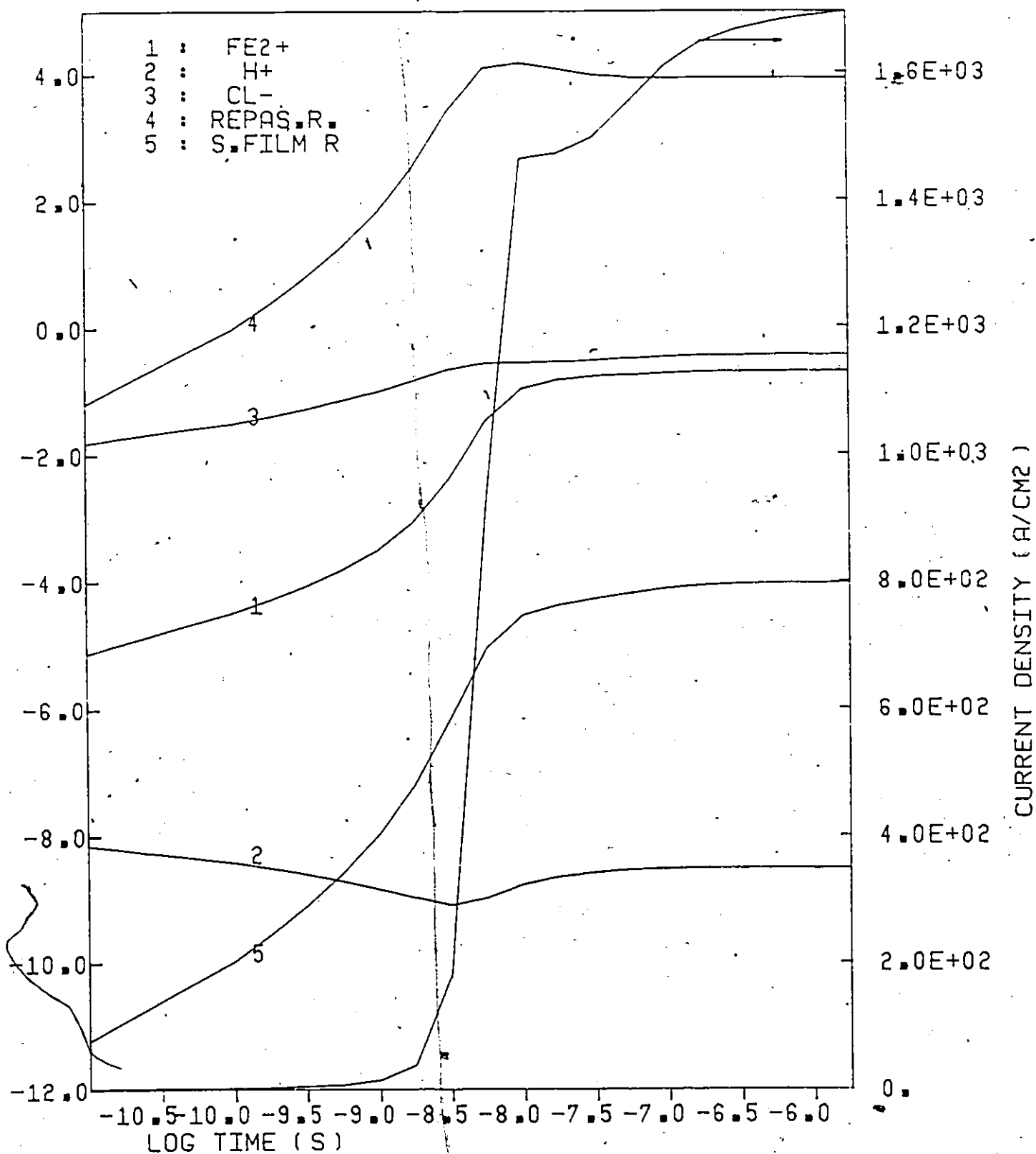


Figure 12 - Variation with time of the current density, $[\text{Fe}^{2+}]$, $[\text{H}^+]$, $[\text{Cl}^-]$, K_{rp} and K_{sf} at the metal surface

simulations as Figures 4 to 7. It can be seen that the pseudo steady-state is typically reached at about 10^{-6} s. The double layer is essentially charged at about $5 \cdot 10^{-9}$ s, at which time a steep rise occurs in the faradaic current density.

6-2 Sensitivity of the Result to the Input Values

It is important to assess the relative influence of all the input parameters on the results, and more particularly, to evaluate the importance of the lack of precision on many of the values used for these parameters. For this purpose, the uncertainty on each of the 27 input parameters is estimated by choosing an alternative value from another source than the one used in 5-7. When this is not possible, the alternative value is estimated in the same way as the original value. Calculations are made varying each input parameter, one at a time, by an amount equal to the estimate of the uncertainty. The results are compared to a reference calculation in which all the parameters have the values selected in 5-7, simulating the dissolution of iron in a NaCl-NaOH solution with $[Cl^-] = 1$ M, pH 9 and polarized at -80 mV vs SHE.

The estimates of the original and alternative values of the input parameters are given in Table 1, together with the corresponding source. Whenever an altered input parameter is used to compute another parameter, all the necessary

Table 1

Alternative Values of the Input Parameters

<u>Parameter</u>	<u>Original</u> <u>Value</u>	<u>Alternative</u> <u>Value</u>	<u>Source</u>
Depth	5 nm	8 nm	
Radius	1 nm	0.5 nm	
Solub. $\text{Fe}(\text{OH})_2$	$2.0 \cdot 10^{-8} \text{ M}$	$3.2 \cdot 10^{-8} \text{ M}$	(1)
Solub. FeCl_2	$2.6 \cdot 10^{-2} \text{ M}$	$2.9 \cdot 10^{-2} \text{ M}$	(2)
(4-7-2) $\left\{ \begin{array}{l} K_1 \\ K_2 \\ K_3 \\ K_4 \\ K_5 \end{array} \right.$	$1.78 \cdot 10^{-14}$	$6.82 \cdot 10^{-15}$	(3)
	$2 \cdot 10^4$	$4 \cdot 10^7$	(1)
	$1.3 \cdot 10^3$	$2 \cdot 10^3$	(1)
	10^{-2}	3.16	(2)
	10^{-2}	1.1	(4)
Tafel slope (+)	116 mV/dec	136 mV/dec	(5)
Tafel slope (-)		108 mV/dec	(5)
Cap. 2ble layer	$40 \mu\text{F}/\text{cm}^2$	$20 \mu\text{F}/\text{cm}^2$	(6)
Pot. 0 charge	-370 mV	-300 mV	
(4-7-1) $\left\{ \begin{array}{l} m_1 \\ m_2 \\ m_3 \\ m_4 \end{array} \right.$	76.7	30	(7)
	$1.15 \cdot 10^{-5}$	$5 \cdot 10^{-6}$	(7)
	$3.87 \cdot 10^{-12}$	10^{-12}	(7)
	$4.57 \cdot 10^4$	$2 \cdot 10^4$	(7)

- Sources:
- (1) - Baes and Mesmer (1976)
 - (2) - Falta et al (1974)
 - (3) - Harned and Robinson (1940)
 - (4) - Butler (1964)
 - (5) - Burstein and Davies (1980)

Table 1 (cont'd)

<u>Parameter</u>	<u>Original</u> <u>Value</u>	<u>Alternative</u> <u>Value</u>	<u>Source</u>
Diffusion			
coefficients	($\times 10^{-5}$ cm ² /s)		
Fe ²⁺	0.7	0.5	(8)
H ⁺	9.5	8.5	(9)
Cl ⁻	2.0	1.5	(10)
OH ⁻	5.3	5.6	(11)
Fe(OH) ⁺	1.5	1.	
Fe(OH) ₂ (aq)	1.0	0.7	
FeCl ⁺	1.2	1.5	
FeCl ₂ (aq)	1.0	1.5	
Na ⁺	1.3	0.9	
Initial [Fe ²⁺]	10 ⁻¹² M	10 ⁻⁶ M	

Sources (cont'd): (6) - Macdonald (1977)
 (7) - 2 σ in regression calculation
 (8) - Strehblow and Wanners (1977)
 (9) - Stastny and Strafelda (1969)
 (10) - Newman (1973)
 (11) - Breiter and Hoffmann (1960)

(When no source is given, an alternative value was chosen within the expected range.)

modifications are performed for the new calculation. For instance, when the Tafel slope is changed, a new regression calculation is done to determine the modified values of m_1 to m_4 .

The results are presented in Tables 2 and 3. In Table 2, the changes of the input and output parameters are given as:

$$\Delta = \log \frac{p}{p_0}$$

where p : value of the parameter after the modification and
 p_0 : value of the parameter before the modification.

An increase of 6% (diffusion of OH^-) is given as 0.03, while a decrease by 50% (capacity of the double layer) gives $\Delta = -0.30$. Therefore, Δ gives a measure of the uncertainty on each output parameter caused by the estimated uncertainty on the input parameter.

Table 3 uses the values of Table 2 to give an estimate of the effect of each input parameter on each output parameter, as:

$$n = \frac{\Delta(y)}{\Delta(x)}$$

where $\Delta(y)$ and $\Delta(x)$ are the Δ calculated in Table 2 for the output and input parameter, respectively. It can be seen

Table 2

Influence of Input Uncertainties on Output Parameters

<u>Input Parameter</u>	<u>$\Delta(\text{input})$</u>	<u>$\Delta(\text{rp})$</u>	<u>$\Delta(\text{sf})$</u>	<u>$\Delta(\text{ad1})$</u>	<u>$\Delta(\text{ad2})$</u>	<u>$\Delta(\text{cc})$</u>
Depth	0.20	-0.01	0.65	0.18	-0.03	0.22
Radius	-0.30	0.003	-0.05	0.02	0.04	-0.02
Solub. $\text{Fe}(\text{OH})_2$	0.2	-0.2	0	0	0	0
Solub. FeCl_2	0.05	0.	-0.06	0	0	0
(4-7-2) $\left\{ \begin{array}{l} K_1 \\ K_2 \\ K_3 \\ K_4 \\ K_5 \end{array} \right.$	K_1	-0.17	-0.17	0	0	0
	K_2	0.30	-0.32	0	0	0
	K_3	0.19	-0.01	0	0	0
	K_4	2.48	0.25	-0.85	-1.53	-0.27
	K_5	2.04	0.01	-0.09	-0.22	-0.05
Tafel slope (+)	0.07	0.29	-2.0	-0.67	0.09	-0.61
Tafel slope (-)	-0.03	-0.01	1.10	0.21	-0.14	0.37
Cap. 2ble layer	-0.30	0	0	0	0	0
Pot. 0 charge	0.08	0	0	0	0	0
(4-7-1) $\left\{ \begin{array}{l} m_1 \\ m_2 \\ m_3 \\ m_4 \end{array} \right.$	m_1	-0.41	0	0	0	0
	m_2	-0.37	0	0	0	0
	m_3	-0.59	0	0	0	0
	m_4	-0.36	0.06	-1.10	-0.32	0.07
Diffusion coefficients						
Fe^{2+}	-0.15	-0.01	0.46	0.13	-0.02	0.16
H^+	-0.05	-0.05	0	0	0	0

Table 2 (cont'd)

<u>Input Parameter</u>	<u>$\Delta(\text{input})$</u>	<u>$\Delta(\text{rp})$</u>	<u>$\Delta(\text{sf})$</u>	<u>$\Delta(\text{ad1})$</u>	<u>$\Delta(\text{ad2})$</u>	<u>$\Delta(\text{cc})$</u>
Cl^-	-0.12	0.001	-0.05	-0.04	-0.02	-0.02
OH^-	0.03	0.001	0	0	0	0
$\text{Fe}(\text{OH})^+$	-0.17	0.18	0	0	0	0
$\text{Fe}(\text{OH})_2(\text{aq})$	-0.15	0	0	0	0	0
FeCl^+	0.10	0	-0.04	-0.02	-0.001	-0.01
$\text{FeCl}_2(\text{aq})$	0.18	0	-0.004	-0.003	0.001	-0.001
Na^+	-0.16	0	-0.01	-0.01	-0.005	-0.004
Initial $[\text{Fe}^{2+}]$	6.0	0	0	0	0	0

("0" means that the effect of the variation is smaller than the computation error.)

Table 3
Sensitivity of the Output Parameters

<u>Input Parameter</u>	<u>n(rp)</u>	<u>n(sf)</u>	<u>n(ad1)</u>	<u>n(ad2)</u>	<u>n(cc)</u>
Depth	-0.05	3.65	0.90	-0.15	1.10
Radius	-0.01	0.17	-0.07	-0.13	0.07
Solub. $\text{Fe}(\text{OH})_2$	-1.0	0	0	0	0
Solub. FeCl_2	0	-1.2	0	0	0
$\left. \begin{array}{l} K_1 \\ K_2 \\ K_3 \\ K_4 \\ K_5 \end{array} \right\} (4-7-2)$	1.00	0	0	0	0
	-1.07	0	0	0	0
	-0.05	0	0	0	0
	0.10	-0.34	-0.62	-0.11	-0.26
	0.005	-0.04	-0.11	-0.02	-0.08
Tafel slope (+)	4.14	-28.6	-9.57	1.29	-8.71
Tafel slope (-)	0.33	-36.7	-7.00	4.67	-12.3
Cap. 2ble layer	0	0	0	0	0
Pot. 0 charge	0	0	0	0	0
$\left. \begin{array}{l} m_1 \\ m_2 \\ m_3 \\ m_4 \end{array} \right\} (4-7-1)$	0	0	0	0	0
	0	0	0	0	0
	0	0	0	0	0
	-0.17	3.06	0.89	-0.19	1.0
Diffusion coefficients					
Fe^{2+}	0.07	-3.07	-0.87	0.13	-1.07
H^+	1.0	0	0	0	0

Table 3 (cont'd)

<u>Input Parameter</u>	<u>n(rp)</u>	<u>n(sf)</u>	<u>n(ad1)</u>	<u>n(ad2)</u>	<u>n(cc)</u>
Cl ⁻	-0.01	0.42	0.33	0.17	0.17
OH ⁻	0.03	0	0	0	0
Fe(OH) ⁺	-1.06	0	0	0	0
Fe(OH) ₂ (aq.)	0	0	0	0	0
FeCl ⁺	0	-0.40	-0.20	-0.01	-0.1
FeCl ₂ (aq.)	0	-0.02	-0.02	0.01	-0.01
Na ⁺	0	0.06	0.06	0.03	0.02
Initial [Fe ²⁺]	0	0	0	0	0

that n expresses the order of the dependence of y on x as:

$$\frac{y}{y_0} = \left(\frac{x}{x_0}\right)^n$$

Therefore, n is a measure of the sensitivity of the particular output parameter to each input parameter. It is in principle independent of the uncertainty on the parameters.

Table 4 lists the input parameters having the largest influence on the output parameters. Generally, the most critical parameters are the ones related to the iron dissolution current, i.e. the Tafel slope and m_4 (in the solutions considered, the influence of m_1 to m_3 is negligible). This underlines the importance of the assumption that dissolution takes place according to the model of Burstein and Davies.

6-3 Precision

The results obtained by the program will be affected by various errors. The errors introduced by the use of inexact data have just been analyzed.

Errors are also created in the calculations because of the limited number of digits used. These are called round-off errors and are very difficult to quantify. They can only be diminished by judicious programming. This type of error is found to be particularly likely to occur in the

Table 4

Most Influential Parameters

(listed in order of importance)

	<u>Parameters Whose Error</u> <u>is Most Influential</u>	<u>Parameters with</u> <u>Major Sensitivity</u>
K_{rp}	K_2 (FeOH ⁺ equil.) Tafel slope K_4 (FeCl ⁺ equil.) Solubility Fe(OH) ₂ Fe(OH) ⁺ diffusion coeff.	Tafel slope K_2 Fe(OH) ⁺ diffusion coeff. Solubility Fe(OH) ₂ K_1 (H ₂ O decomposition) H ⁺ diffusion coeff.
K_{sf}	Tafel slope m_4 (Cl ⁻ coeff.) K_4 Depth	Tafel slope Depth Fe ²⁺ diffusion coeff. m_4 Solubility FeCl ₂
K_{ad1}	K_4 Tafel slope m_4 K_5 (FeCl ₂)	Tafel slope Depth m_4 Fe ²⁺ diffusion coeff. K_4

Table 4 (cont'd)

	<u>Parameters Whose Error is Most Influential</u>	<u>Parameters with Major Sensitivity</u>
K_{ad2}	K_4 Tafel slope m_4 K_5	Tafel slope m_4 Cl^- diffusion coeff.
K_{cc}	K_4 Tafel slope m_4	Tafel slope Depth Fe^{2+} diffusion coeff. m_4

calculation of the last unknown concentration with the electroneutrality condition (Equation 5-1). It has been avoided by choosing as last unknown a concentration which does not become small compared to any other (see A-7).

Finally, we shall consider the truncation errors. These errors arise from the replacement of the derivatives by approximations at discrete points. The system of equations to be integrated contains both time and space derivatives.

The time integration is done by LSODE and the truncation error on each step is controlled by the input parameters RTOL (relative tolerance) and ATOL (absolute tolerance) in LSODE. The global truncation error is expected to vary smoothly with RTOL and ATOL. In the present case, the concentrations on one side, and the potential at the metal surface on the other side, are attributed different values of RTOL and ATOL as their errors influence the results in a different way. Various runs were made with ATOL and RTOL values for the concentrations from 10^{-4} to 10^{-16} and from 10^{-3} to $3 \cdot 10^{-6}$ respectively. For the potential, only the absolute error has a meaning and therefore RTOL was set to 0 and ATOL was varied between 10^{-14} and 10^{-7} .

The values chosen for most of the calculations are:

	<u>RTOL</u>	<u>ATOL</u>
Concentrations	10^{-4}	10^{-16}
Potential	0	10^{-5}

as the results obtained for smaller values of these parameters vary only by small, random quantities attributable to the round-off error. These errors are much smaller than the errors introduced by the spatial derivatives studied below.

The approximation formulae chosen for the spatial derivatives (see 5-8) all have a truncation error proportional to the square of the interval between nodes. In the first region, the cylindrical hole, this interval is:

$$DX = \frac{DEPTH}{NN1}$$

where DEPTH is the depth of the hole and NN1 is the number of nodes in this region. Similarly, in the transition region, the interval is:

$$DX1 = \frac{A}{NN2}$$

where A is the radius of the pore and NN2 is the number of nodes in this region. The interval between nodes in the third region is dependent on DX1 and cannot be varied independently.

Therefore, it is assumed that the total truncation error E_T on the final result is of the form:

$$E_T = a'(DX)^2 + b'(DX1)^2$$

or:

$$E_T = a \left(\frac{1}{NN1} \right)^2 + b \left(\frac{1}{NN2} \right)^2$$

where a and b are constants.

During the early calculations, this last formula was used to estimate the truncation error and to choose an optimum setting for the parameters NN1 and NN2, taking into account that the computing time increases with the required precision.

A total of 10 runs were made with a 1M NaCl solution and a polarizing potential of +100 mV vs SHE. NN1 was varied from 35 to 60 and NN2 from 4 to 6. Table 5 shows the results obtained for K_{sf} , as well as the computing times. The truncation error is evaluated by least-square curve fitting of the results on K_{sf} with the corresponding values of NN1 and NN2, according to:

$$K_{sf} = (K_{sf})_o + a(1/NN1)^2 + b(1/NN2)^2$$

The value obtained for $(K_{sf})_o$ is 9.897 ± 0.003 (95% confidence interval). The variation of K_{sf} with NN1 and NN2 is illustrated on Figure 13, together with the computing time. In view of these results, the values of NN1 and NN2 chosen are:

Table 5

Variation of K_{sf} and the Computing Time with NN1 and NN2

<u>NN1</u>	<u>NN2</u>	<u>K_{sf}</u>	<u>Time (s)</u>
35	6	989.64	523
39	4	991.70	200
39	5	990.63	237
43	4	991.85	206
43	5	990.79	260
43	6	990.23	605
50	4	991.96	249
50	6	990.35	473
55	6	990.43	330
60	5	991.33	322

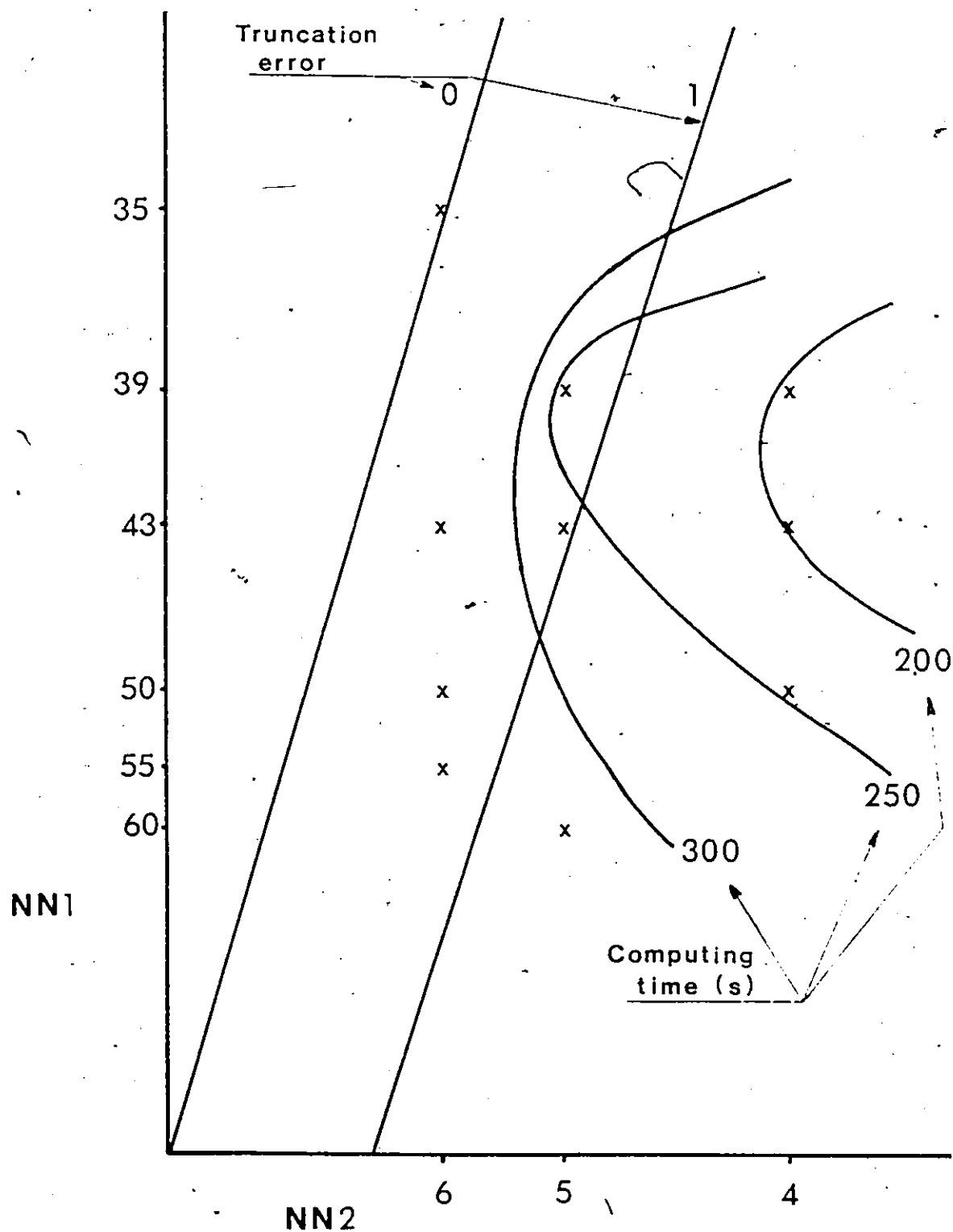


Figure 13 - Variation of the truncation error on K_{sf} and of the computing time with NN1 and NN2

$$NN1 = 39 ; NN2 = 5,$$

as these values give a reasonable accuracy while avoiding a steep rise in computing time. The truncation error is in this case about $8 \cdot 10^{-3}$ or a relative error of 0.1%.

No further test of this type was run for other simulations, but the present results would lead us to the conclusion that the truncation error was probably not larger than 1 or 2% in any other cases.

6-4 Stability

For many of the conditions leading to pitting, no pseudo steady-state can be reached in the NaCl-borate buffer solution. Instead, the various concentrations reach a region of slow and continuous increase. This increase is sufficient to fail the steady-state test outlined in 6-1.

This instability can be explained by considering that in many of the cases leading to pitting, equation (5-10) in 5-7-1, giving the dependence of the current density on the solution composition, reduces to:

$$j = 4.57 \cdot 10^4 [Cl^-] \exp(19.8 E) \quad (6-1)$$

(all the concentrations and potentials mentioned in this paragraph are taken at the metal/solution interface).

The following approximations can also be made, for the sake of developing this qualitative argument:

* The process is controlled by the dissolution and diffusion of iron in the pore, that is:

$$\frac{\delta [\text{Fe}^{2+}]}{\delta t} = D \cdot \frac{\delta [\text{Fe}^{2+}]}{\delta x^2} \quad (6-2)$$

and:

$$N_{\text{Fe}} = -D \frac{\delta [\text{Fe}^{2+}]}{\delta x} \quad (6-3)$$

* The electrolyte in contact with the metal surface is a concentrated solution of ferrous chloride, i.e.:

$$[\text{Cl}^-] = 2[\text{Fe}^{2+}]$$

At the metal surface, from 5-4 and (6-1), we have:

$$\begin{aligned} N_{\text{Fe}} &= \frac{j}{2F} \\ &= \frac{4.57 \cdot 10^4 \cdot \exp(19.8 E)}{2F} [\text{Cl}^-] \end{aligned} \quad (6-4)$$

so that from (6-3) and (6-4):

$$- D \frac{\delta [\text{Fe}^{2+}]}{\delta x} = \frac{4.57 \cdot 10^4 \exp(19.8 E)}{F} [\text{Fe}^{2+}]$$

i.e.:

$$\frac{\delta [\text{Fe}^{2+}]}{\delta x} = -k_1 [\text{Fe}^{2+}]$$

where k_1 is a constant, assuming that the variation of the potential is small compared to the variation of $[\text{Fe}^{2+}]$.

Taking derivatives:

$$\begin{aligned} \frac{\delta^2 [\text{Fe}^{2+}]}{\delta x^2} &= -k_1 \frac{\delta [\text{Fe}^{2+}]}{\delta x} \\ &= k_1^2 [\text{Fe}^{2+}] \end{aligned}$$

Replacing in (6-2):

$$\frac{\delta [\text{Fe}^{2+}]}{\delta x} = D k_1^2 [\text{Fe}^{2+}] \quad (6-5)$$

The solution of this equation is of the type:

$$[\text{Fe}^{2+}] = [\text{Fe}^{2+}]_0 \exp(D k_1^2 t)$$

Since the coefficient inside the exponential is positive, the concentration is growing exponentially and so is the error. Generally, differential equations which can

be approximated by equations like (6-5), where:

$$\frac{\delta (D k_f^2 [\text{Fe}^{2+}])}{\delta [\text{Fe}^{2+}]} = D k_f^2 > 0$$

are unstable (James, Smith and Wolford, 1977).

Obviously, the instability is a numerical artifact caused by the linear dependence of the current density on the chloride concentration. A more realistic approach introducing a saturation of the iron surface by adsorbed chloride would give steady state values.

To circumvent this problem, the values of the parameters are extrapolated. It is felt that such a procedure is justified since in all cases the parameters seemed to reach a plateau at around 10^{-5} s. The extrapolation is performed by fitting the output parameter values for the last four results to a cubic polynomial in:

$$y = \frac{1}{\sqrt{t}}$$

and extrapolating to $y = 0$. This particular form of variable was chosen because preliminary tests showed that it resulted in minimal curvature.

6-5 Testing of the Program

As a verification of the computer program, simulations of the dissolution experiments of Strehblow and Wanners (1977) have been undertaken. These experiments are conducted in a manner somewhat different from the experiments leading to pitting, as described in 5-1. However, it is felt that these simulations provide a worthwhile check on the integrity of the program.

Strehblow and Wanners dissolved iron specimens in HCl-FeCl_2 solutions by applying a galvanostatic step i and measuring the time τ necessary to obtain a jump in potential. They found that the product $i\sqrt{\tau}$ is independent of i , and varies in a quasi-linear fashion with $[\text{Fe}^{2+}]$. These results are shown in Figure 14 and can be rationalized by assuming that at time τ , FeCl_2 precipitates and that therefore Sand's relationship applies (Vetter, 1977):

$$i\sqrt{\tau} = a + b[\text{Fe}^{2+}]$$

The simulations are performed by using only that part of the geometry where the diffusion is planar (the cylindrical hole). The formula involving the resistance of the solution is modified and the current density, instead of being computed as in 5-5, is constant. The value of τ is obtained when K_{sf} is reaching 1, i.e. when the solution at the metal surface is theoretically saturated.

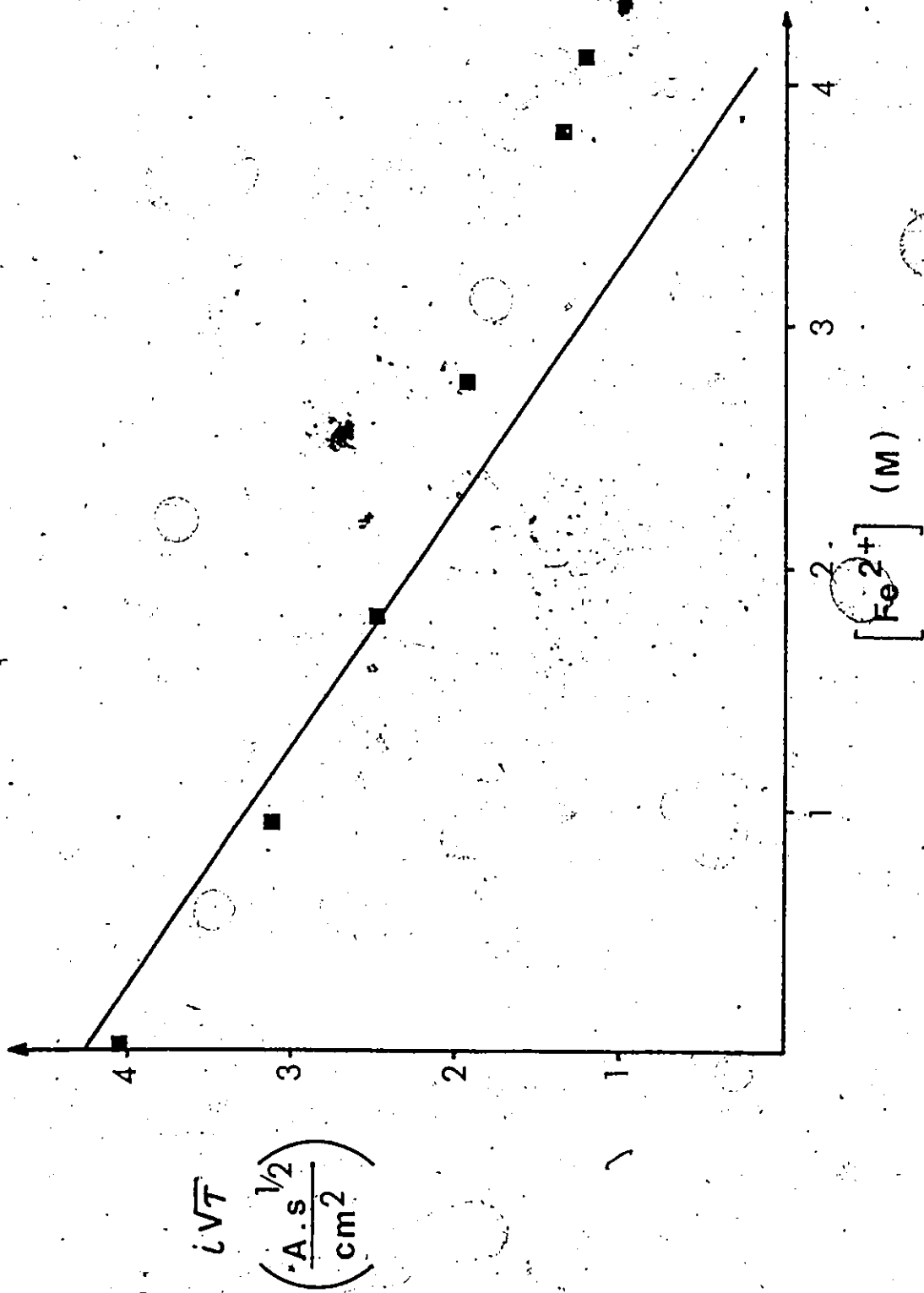


Figure 14 - Comparison between the results of Strehblow and Wemmers (■) and the simulation of this work (line)

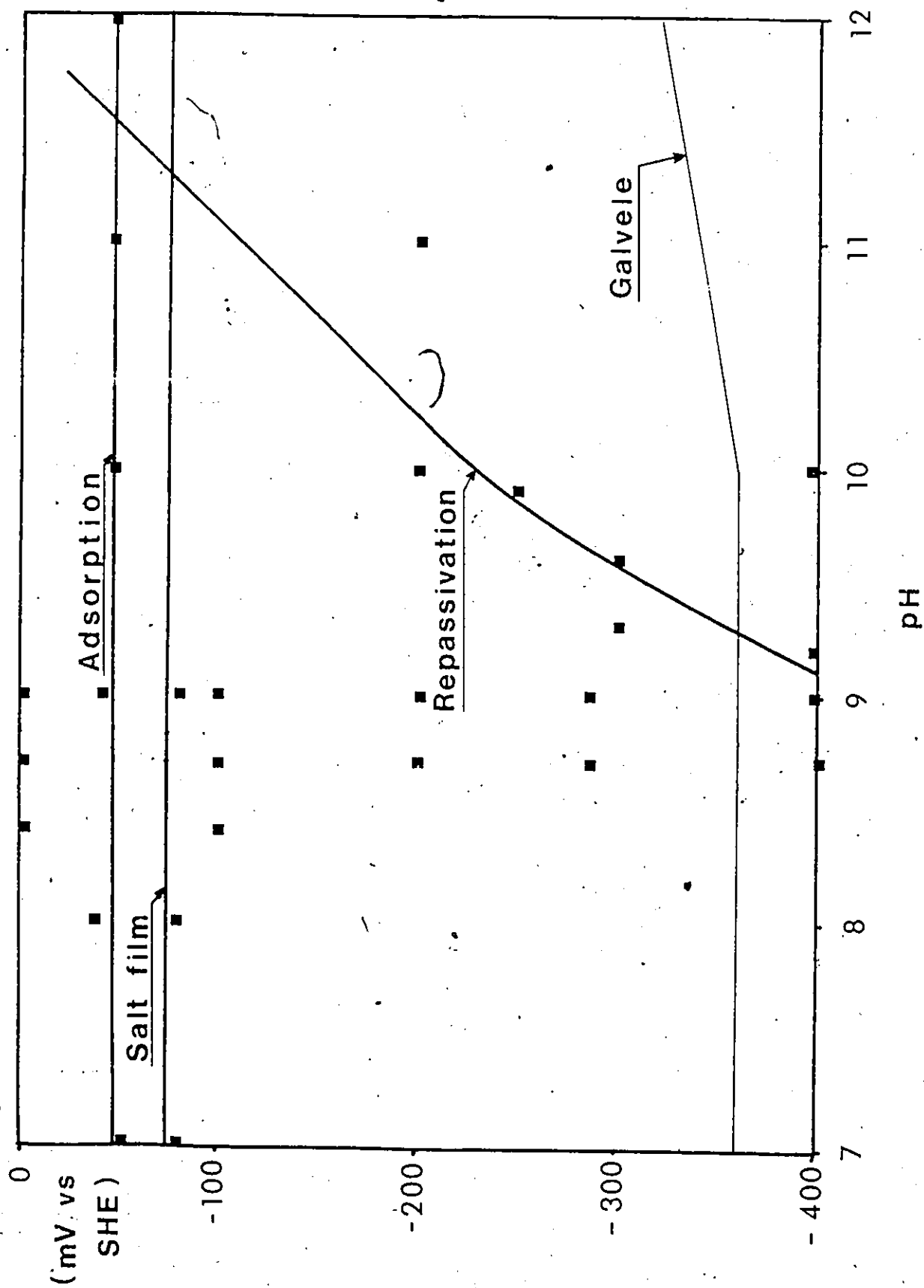
The results of the simulation fall on the straight line shown on Figure 14 and they fit reasonably well with Strehblow and Wanners' results, indicating the absence of gross error in the programming. This also shows that the assumptions leading to the Sand relationship are verified. The deviation between experimental and theoretical values at high concentrations can be explained by the fact that in the simulation, the activity coefficients were supposed to equal 1. This assumption is not valid at high concentrations: the activity coefficient of FeCl_2 at 4M is about 1.8 (McCafferty, 1981).

6-6 Pitting in NaOH-NaCl Solutions

A first series of calculations are performed simulating the dissolution of iron in solutions of different pH containing 1M of NaCl. These solutions are chosen for their relative simplicity, and also because they have been used for pitting experiments by Alvarez and Galvele, as quoted by Galvele (1976 and 1978).

Results are shown in Figure 15. Each line is the locus of the points where one criterion is equal to 1. Only the repassivation criterion K_{rp} is changing with pH. The adsorption criterion K_{ad1} and the salt film criterion K_{sf} , depending on $[\text{Fe}^{2+}]$, $[\text{Cl}^-]$ and the potential at the bottom of the pore, do not vary appreciably with the pH in the range considered. The critical concentration criterion

Figure 15 - Variations of K_{rp} , K_{sf} and K_{adl} with potential and pH



K_{cc} and the other adsorption criterion K_{ad2} , depending also on $[Cl^-]$ and the potential, show the same independence and are not illustrated.

All the criteria apart from the repassivation criterion K_{rp} can describe Galvele's results by adjustment of a constant and therefore the comparison cannot permit a useful discrimination between the criteria. Additionally, the experimental pitting potentials are very close to the equilibrium potential of iron and therefore doubtful. It is known that iron in this type of solution presents only a very small passive region (if any) and it is therefore very difficult to define the pitting potential as pitting starts very close to the active region (Strehblow, 1981). No conclusion can be drawn from these calculations and the results are presented here only as an illustration of the method.

6-7 Pitting in NaOH-NaCl-B(OH)₃ Solutions

6-7-1 Sources of Data

This particular system was chosen because it is simple to simulate and it has been studied experimentally by various investigators. Pitting potentials have been published by Janik-Czachor (1971), Heusler and Fischer (1976) and Strehblow and Titze (1977). As outlined in 5-1, the compositions and potentials corresponding to pit initiation are used as initial conditions. The composition of the

solution has three degrees of freedom. It is defined here by the chloride concentration, the pH and the total borate concentration ($[B(OH)_3] + [B(OH)_4^-]$). The compositions and potentials used are shown on Table 6 together with the results obtained for each of the data points published.

Janik-Czachor reports various values for the pitting potential, depending on the method of determination (galvanostatic, potentiostatic or repassivation). For each concentration of chloride, two calculations are performed here, corresponding to the upper and lower value of the range of pitting potentials reported.

Heusler and Fischer determine the pitting potential potentiostatically. The results are obtained in solutions of three different borate concentrations and the authors report that the pitting potential does not depend on the pH. In the case of their solution (2), the actual pH of the solution used is not indicated. Therefore, two series of calculations are executed, corresponding to the two values of the pH quoted earlier in the article as values used for this solution. No values of the pH were available for their solution (3), so the same two values as for solution (2) are used.

6-7-2 Analysis of the Results

A criterion will fit its purpose if its value is a constant in all the cases considered. To evaluate if this

Table 6
Results Obtained for Different Sets of Data

<u>Strehblow and Titze</u> (pH 8; 0.05 M total borat��)			
Bulk $[Cl^-]$ (M)	0.01	0.029	0.1
Polarization potential (mV vs SHE)	-19	-119	-169
K_{rp}	$8.75 \cdot 10^3$	910	302
K_{sf}	$9.81 \cdot 10^{-6}$	$2.72 \cdot 10^{-6}$	$6.87 \cdot 10^{-6}$
K_{ad1}	$5.60 \cdot 10^{-4}$	$1.56 \cdot 10^{-5}$	$8.66 \cdot 10^{-6}$
K_{ad2}	$2.71 \cdot 10^{-3}$	$2.62 \cdot 10^{-4}$	$1.36 \cdot 10^{-4}$
K_{cc} (= surface $[Cl^-]$ in M)	0.378	0.117	0.180
Surface potential (mV vs SHE)	-126.8	-156.7	-184.6
Surface pH	8.5	8.3	8.0
Potential above H evolution (mV)	376	333	290

Table 6 (cont'd)

Janik-Czachor; upper potential
(pH 8.4; 0.202 M total borate)

Bulk $[Cl^-]$ (M)	0.01	0.05	0.1	0.5
Polarization potential (mV vs SHE)	216	144	122	44
K_{rp}	$3.30 \cdot 10^6$	$4.33 \cdot 10^5$	$7.48 \cdot 10^4$	150.9
K_{sf}	56.0	184	328	326
K_{ad1}	18.8	14.0	19.2	16.8
K_{ad2}	.881 ²⁰	.585	.668	.579
K_{cc} (= surface $[Cl^-]$ in M)	27.7	47.8	58.4	58.1
Surface potential (mV vs SHE)	-88.6	-113.1	-115	-118.4
Surface pH	8.8	8.3	7.9	6.6
Potential above H evolution (mV)	431	378	352	269

Table 6 (cont'd)

Janik-Czachor; lower potential
(pH 8.4; 0.202 M total borate)

Bulk $[Cl^-]$ (M)	0.01	0.05	0.1	0.5
Polarization potential (mV vs SHE)	194	111	66	16
K_{rp}	$2.42 \cdot 10^6$	$2.66 \cdot 10^5$	$4.52 \cdot 10^4$	289
K_{sf}	23.6	49.2	32.4	98.1
K_{ad1}	9.95	4.93	2.90	5.85
K_{ad2}	.664	.320	.214	.301
K_{cc} (= surface $[Cl^-]$ in M)	21.7	31.0	28.0	38.9
Surface potential (mV vs SHE)	-89.5	-117	-125	-124.9
Surface pH	8.8	8.3	8.0	6.8
Potential above H evolution (mV)	430	375	345	276

Table 6 (cont'd)

Heusler and Fischer; Solution 1
(pH 7.3; 0.2 M total borate)

Bulk $[Cl^-]$ (M)	0.005	0.01	0.02
Polarization potential (mV vs SHE)	166	144	121
K_{rp}	$2.63 \cdot 10^5$	$8.82 \cdot 10^4$	$1.67 \cdot 10^4$
K_{sf}	3.60	8.65	17.5
K_{ad1}	0.950	1.28	1.80
K_{ad2}	.142	.150	.165
K_{cc} (= surface $[Cl^-]$ in M)	12.6	17.5	21.9
Surface potential (mV vs SHE)	-115	-122	-126
Surface pH	8.5	8.2	7.8
Potential above H evolution (mV)	386	362	334

Table 6 (cont'd)

Heusler and Fischer; Solution 2; pH 7.2
(0.4 M total borate)

Bulk $[Cl^-]$ (M)	10^{-3}	$2.15 \cdot 10^{-3}$	0.01	0.1	0.5
Polarization potential (mV vs SHE)	188	157	122	44	-10
K_{rp}	$6.11 \cdot 10^5$	$4.66 \cdot 10^5$	$1.95 \cdot 10^5$	$1.45 \cdot 10^3$	37.4
K_{sf}	$1.38 \cdot 10^{-2}$	$4.69 \cdot 10^{-2}$	2.08	12.7	24.1
K_{ad1}	.316	.237	.626	1.32	1.94
K_{ad2}	.152	.105	.112	.135	.157
K_{cc} (= surface [Cl^-] in M)	1.43	2.50	10.6	19.8	24.1
Surface potential (mV vs SHE)	-57.5	-81.3	-117	-128	-129
Surface pH	8.9	8.9	8.5	7.3	6.4
Potential above H evolution (mV)	470	442	384	302	252

Table 6 (cont'd)

Heusler and Fischer; Solution 2; pH 8.3

(0.4 M total borate)

Bulk $[Cl^-]$ (M)	10^{-3}	$2.15 \cdot 10^{-3}$	0.01	0.1	0.5
Polarization potential (mV vs SHE)	188	157	122	44	-10
K_{rp}	$1.12 \cdot 10^6$	$9.23 \cdot 10^5$	$1.17 \cdot 10^6$	$2.05 \cdot 10^5$	$7.63 \cdot 10^3$
K_{sf}	$6.63 \cdot 10^{-4}$	$1.56 \cdot 10^{-3}$.179	7.28	21.7
K_{ad1}	1.29	.780	1.23	1.31	1.90
K_{ad2}	.487	.342	.293	.156	.160
K_{cc} (= surface $[Cl^-]$ in M)	.275	.457	3.59	16.1	23.4
Surface potential (mV vs SHE)	14.7	-7.4	-64.3	-119	-128
Surface ¹ pH	9.0	9.0	8.9	8.4	7.6
Potential above H evolution (mV)	547	524	463	377	321

Table 6 (cont'd)

Heusler and Fischer; Solution 3
(0.55 M total borate)

Bulk pH	7.2	8.3
Bulk $[Cl^-]$ (M)	0.01	0.01
Polarization potential (mV vs SHE)	94	94
K_{rp}	$2.09 \cdot 10^5$	$6.74 \cdot 10^5$
K_{sf}	.174	$5.84 \cdot 10^{-3}$
K_{ad1}	.178	.363
K_{ad2}	$6.72 \cdot 10^{-2}$.181
K_{cc} (= surface [Cl^-] in M)	4.43	.934
Surface potential (mV vs SHE)	-108	-42.1
Surface pH	8.6	8.9
Potential above H evolution (mV)	403	487

is realized, all the data are pooled and studied statistically. If a criterion is valid, the deviations of each individual result around the mean (i.e. the residuals) should be normally distributed and should not vary systematically with any variable.

The statistics are performed on the logarithm (base 10) of the possible criteria, as their variations span several orders of magnitude.

The means and standard deviations of the 26 results are:

	mean	standard deviation
K_{rp}	4.69	1.43
K_{sf}	-0.204	2.46
K_{ad1}	-0.251	1.65
K_{ad2}	-0.930	0.950
K_{cc}	0.816	0.847

The histograms of the corresponding distributions are shown on Figure 16, together with the associated normal curves. The width of the classes for each histogram is equal to 1 s. The height of the bars corresponding to the 3 results of Strehblow and Titze (1977) are cross hatched and it is clear that except for the case of K_{rp} , these results are quite distinct from the remaining 23 results. It must

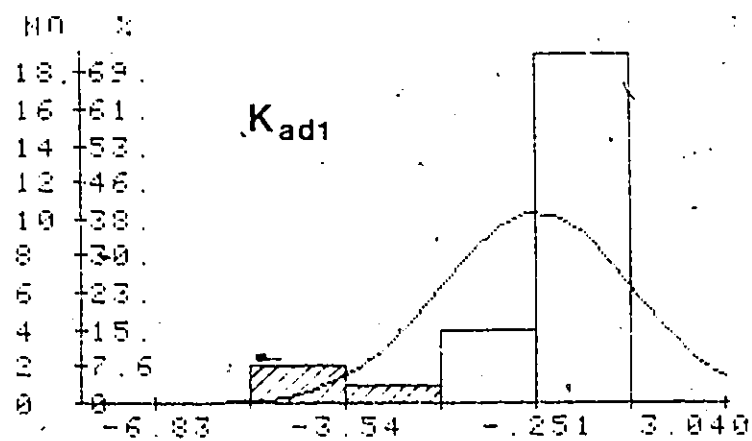
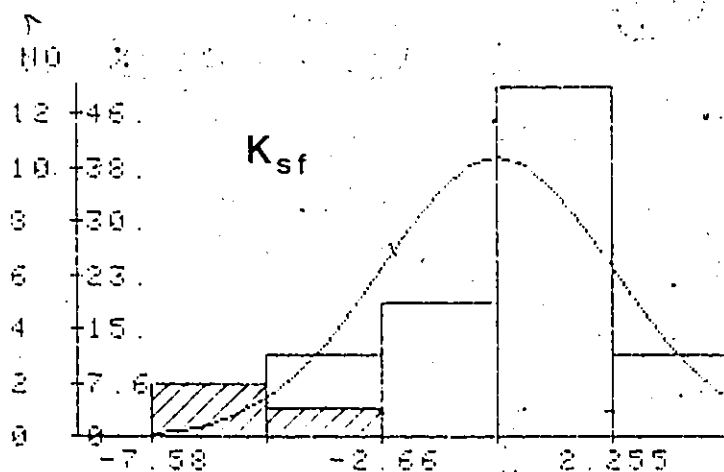
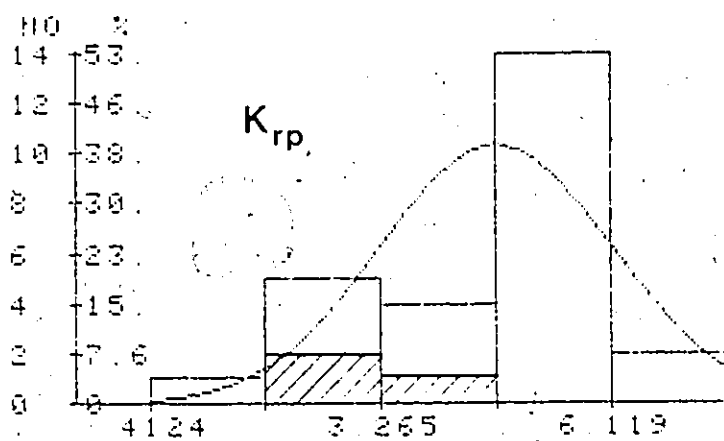


Figure 16 - Histograms of the distributions of criteria; hatched regions correspond to the results from Strehblow and Titze (1977)

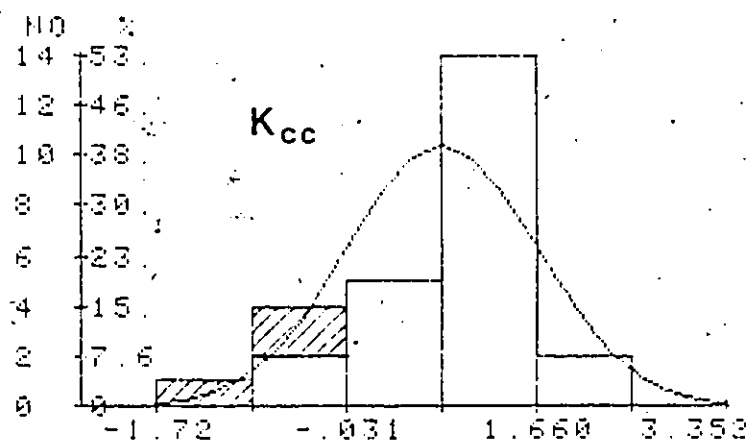
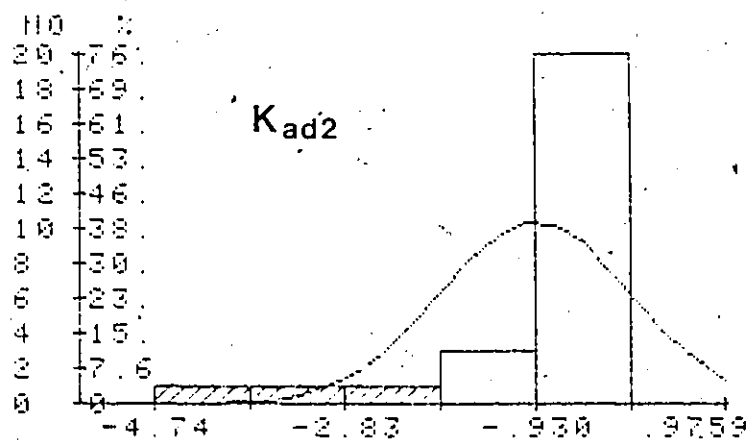


Figure 16 - cont'd

be noted that these results of Strehblow and Titze are close to the ones reported by Kolotyrkin and Freiman (1965).

Janik-Czachor (1971) attributes the difference between her own results and the results of Kolotyrkin and Freiman to the purity of the iron used.

It was decided to examine further the statistics without these three extraneous results. The means and standard deviations of the 23 remaining results are:

	mean	standard deviation
K_{rp}	4.90	1.37
K_{sf}	0.454	1.72
K_{ad1}	0.286	0.611
K_{ad2}	-0.620	0.305
K_{cc}	1.01	0.675

The results corresponding to the data of Janik-Czachor and Heusler and Fischer (solution 2, pH 8.3) are plotted against the chloride concentration on Figures 17 and 18, respectively.

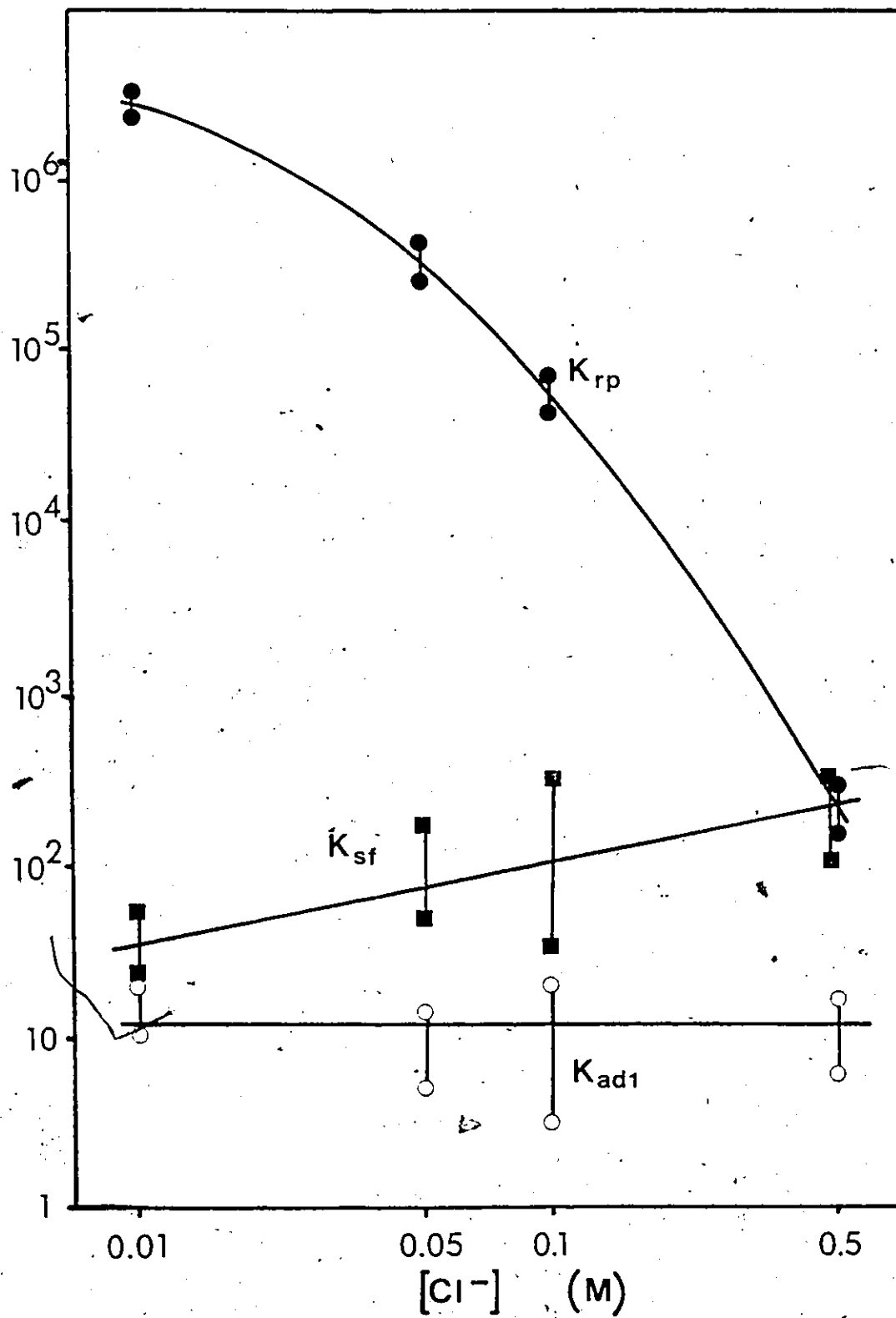


Figure 17 - Criteria computed from the results of Janik-Czachor.

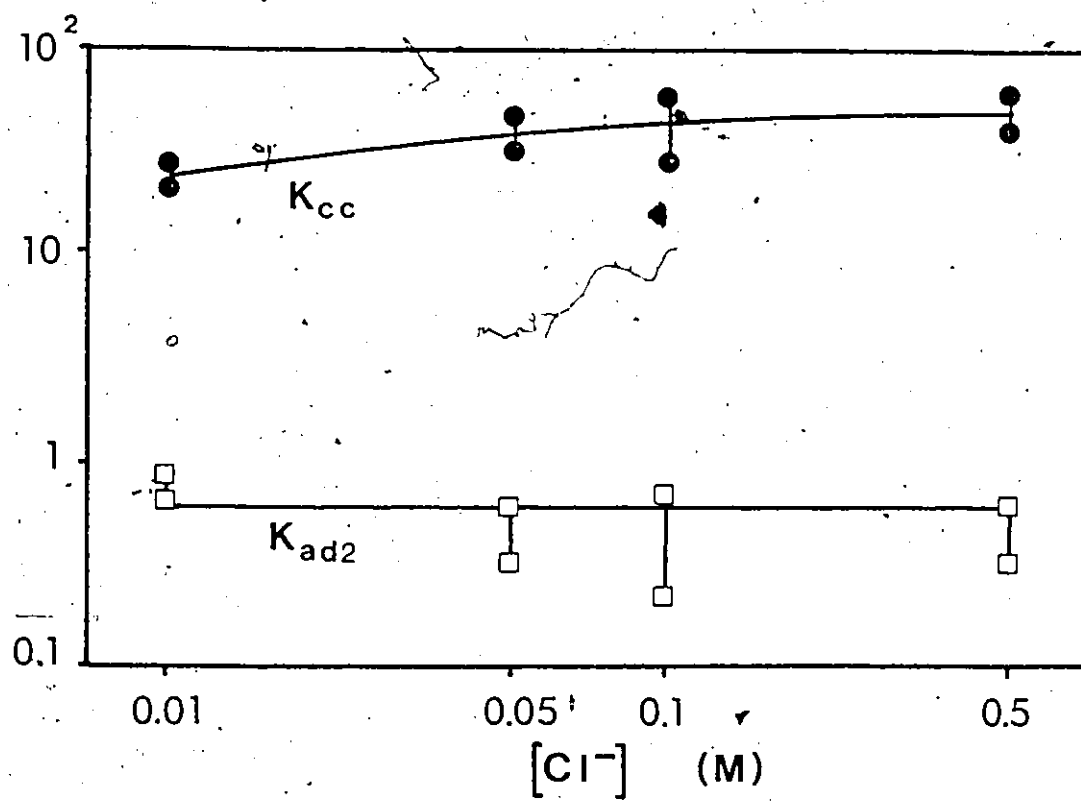


Figure 17 - cont'd

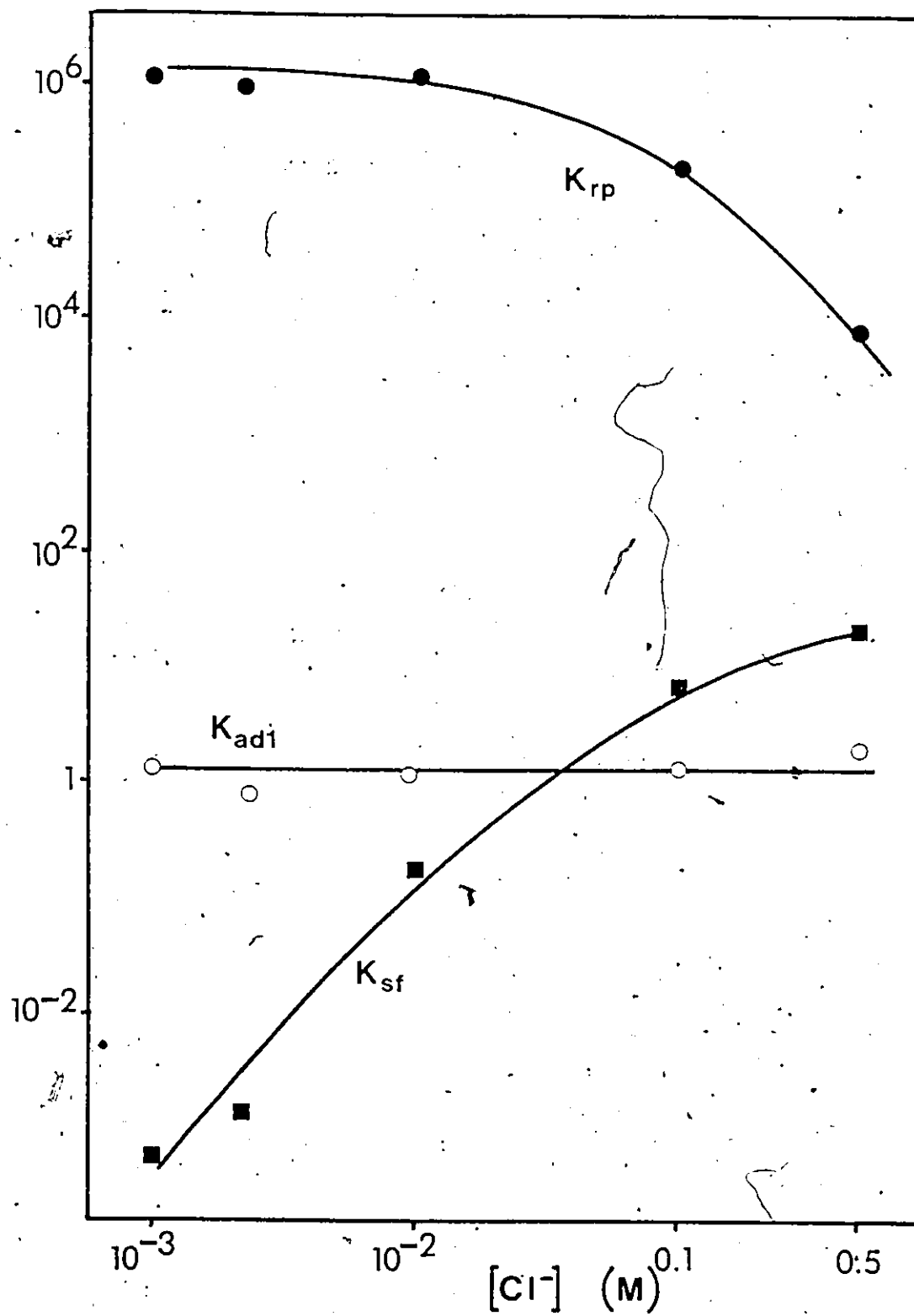


Figure 18 - Criteria computed from the results of Heusler and Fischer (solution 2; pH 8.3)

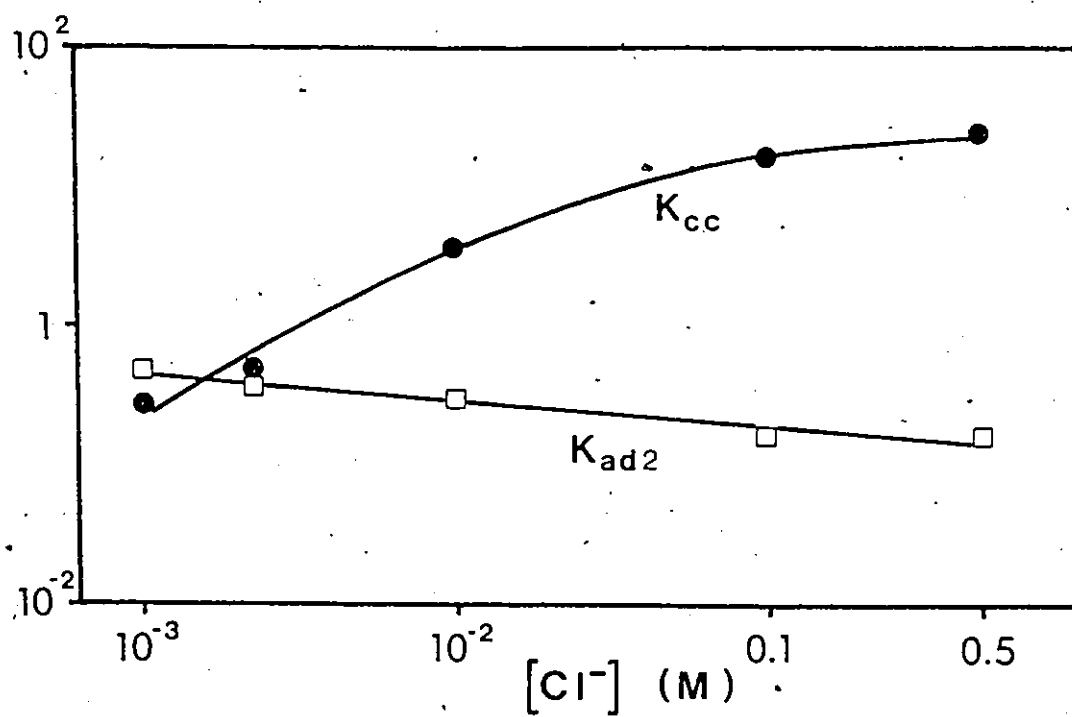


Figure 18 - cont'd

CHAPTER VII

DISCUSSION

The hypotheses introduced in this work will be examined in light of hypotheses assumed by others. The validity of the assumptions will be verified and finally the results of the simulation will be evaluated.

Unless otherwise noted, all the hypotheses discussed in this chapter are also adopted in the models of Pickering and Frankenthal (1972) and Galvele (1976b).

7-1 Ideal Solution

It has been assumed that the solution behaves like an infinitely dilute solution, i.e. the activity coefficients are equal to 1, the Nernst-Einstein relation between diffusion and mobility coefficients (see 5-3) is valid and that the diffusion coefficients are independent of the concentrations.

This assumption is a convenient simplification, which however does not correspond to reality. The mean molar activity coefficient for a solution of ferrous chloride decreases from 1 to about 0.5 between 0 and 0.5 M, then increases up to approximately 2.5 at saturation

(4.25 M) (McCafferty, 1981). Similarly, as we are studying solutions varying from very dilute to saturated, we should expect a whole range of values for the activity coefficients. (7)

7-2 One Dimensional Diffusion

All the calculations have been made with the assumption that the length of the pore in the passive film is much larger than its diameter. In such circumstances, the concentration gradient is uniform across the section and the diffusion is one-dimensional. This would not be true in the case of an exposed patch of metal if the size of the patch is similar or larger than the thickness of the passive film.

Two modes of diffusion have been taken into account: the planar diffusion within the pore and the spherical diffusion from the pore mouth (with a zone of accommodation between the two). Previous models do not include the spherical diffusion zone and assume that the bulk conditions prevail at the pore mouth. Although this simplification probably yields qualitatively similar results, it introduces errors certainly larger than the calculation errors obtained in this study (from Figure 8, approximately 15%).

7-3 Inert Film

In all the models, the passive layer has no other

role than to define the geometry of the flaw. The hypothesis is that there are no chemical or electrochemical reactions and no adsorption occurring on the walls of the pore. In the borate buffer solution under consideration, it is likely that the dissolution of iron oxide will be slow relative to the time scale of the processes considered here. But it is possible that adsorption could take place on the walls of the pore. This would influence the movement of the species present in the pore and also alter the mass balance of the species at a given point in the pore.

7-4 No Convection

It has been assumed in this study that mass transfer takes place only by diffusion and migration, i.e. under the influence of the concentration and potential gradients.

In the idealized model, no massive movement of liquid should take place inside the pore after its volume has been filled with the bulk solution. However, if the pore deepening is appreciable, it may cause an influx of bulk solution in the pore or an egress of concentrated metal solution.

The influence of the processes studied here does not extend far enough in the bulk of the solution for free convection to be a problem.

7-5 No Precipitation

It is assumed that all the species present are dissolved. The only exceptions are $\text{FeCl}_2(\text{s})$ and $\text{Fe}(\text{OH})_2(\text{s})$ which are involved in two of the proposed criteria.

The figures obtained from the simulation indicate a large supersaturation for $\text{Fe}(\text{OH})_2$. This is interpreted as an indication that the corresponding chemical reactions are not in equilibrium (see 7-7) rather than pointing to the precipitation of ferrous hydroxide.

7-6 Supporting Electrolyte

The model of Galvele assumes the presence of an excess of supporting electrolyte leading to a cancellation of the potential difference in the system. As a consequence, the migration of species under the potential gradient can be neglected.

This hypothesis is not necessary here, as migration is fully accounted for in the equations. Furthermore, the calculated potential difference between the reference electrode in the bulk solution and the metal surface is about 200 to 300 mV, which is actually not negligible.

7-7 Chemical Reactions

Pickering and Frankenthal assume that there is no hydrolysis or complexing reactions taking place in solution. This led to a simplification of the equations as the only

species present were H^+ , anion Y^- and the dissolving metal cation M^+ .

Galvele introduces various chemical reactions: the hydrolysis of the metal ions; the decomposition of water; and the buffering reaction. However, as this leads to a complication of the equations, Galvele then introduces the assumption of the supporting electrolyte.

With the method used here, all the necessary chemical reactions can be taken into account (see 5-2 and 5-7-2) without the assumption of the supporting electrolyte.

A limitation still exists because all the reactions are assumed to be at equilibrium. This is probably true for the decomposition of water, but the results show that it is not so in the case of the hydrolysis of Fe^{2+} . The mean value obtained for K_{rp} is approximately 100,000 and values larger than 10^6 have been obtained (Figures 17 and 18). These figures actually correspond to the supersaturation ratio for the precipitation of $Fe(OH)_2$, and such high values are very improbable. It must be noted that the occurrence of precipitation can be excluded, as it would plug the pore and lead to repassivation, while the experimental conditions correspond to pitting. According to current theories of dissolution of iron (see Chapter 4), $FeOH^+$ is described as the first dissolved species formed. Therefore, a possible interpretation of the present results is that the supersaturation ratio is actually much lower than calculated, and

that the uptake of OH^- by FeOH^+ is too slow for the reaction to be considered in equilibrium.

In spite of this inconsistency, the results on the criteria other than K_{rp} are believed to be reasonably correct, as the interaction between Fe^{2+} and OH^- , and the resulting pH seems to have little influence on the interaction between Fe^{2+} and Cl^- (see 6-6 and Figure 15).

7-8 Steady State

Pickering and Frankenthal (1972) and Galvele (1976b) draw conclusions from assuming that the system has reached a steady state.

The method adopted here allows calculations to be made at any moment during the evolution of the system. Although the present results are mainly obtained after reaching a pseudo steady state, the considerations given above (7-7) show that kinetic data could be used to realistically model the evolution of the system.

7-9 Breakdown and Repair

As stated in 5-1, one of the basic assumptions of this work is that pitting corrosion occurs through a breakdown and repair mechanism.

One of the objections raised to this mechanism is that the large current densities it implies should generate observable current peaks every time a pore opens and then

5

repassivates. Taking the figures obtained here, a current density of 10^5 A/cm² through a circular area 1 nm in diameter will generate 3 nA. Considering that it will take about 10 μ s to reach the appropriate criteria for pitting, it is probable that it will take the same time or less to repassivate in other conditions. This objection is therefore not valid, as it would be impossible to reliably detect peaks in current of 3 nA, lasting for less than 10 μ s.

Another objection is that as the breakdown and repair mechanism implies a continuous dissolution of the metallic substrate, the concentration of metallic ions should build up in the solution. Using the same figures as above, one event, i.e. the repassivation of one pore, would generate according to Faraday's law 10^{-17} g. of Fe²⁺. If the solution volume is 100 cm³, this represents 10^{-13} ppm. To reach a level of detection of 0.1 ppm, 10^{12} events need to occur. In a sample of 1 cm², this is an average of 1 event for 100 nm², which would represent a large amount of perturbation and breakdown of the passive layer. Furthermore, the noise analysis studies (see 2-6) suggest that the frequency of the events associated with corrosion (the events whose number increase when chloride is added) is lower than 100 Hz. If all the events occur at this frequency, the limit of detection would be reached in 300 years.

7-10 Temperature

The present calculations assume that the temperature is constant. This is true only if the heat generated by the passage of the current is negligible.

The temperature increase in the pore can be computed in first approximation with a few simplifying assumptions:

* The system is assumed to have reached thermal pseudo steady state. This is probably true, but in any case, represents an overestimation of the temperature increase.

* The heat is generated uniformly inside the pore at a rate:

$$H = \frac{\Delta V \cdot j}{L} = \frac{0.3 \times 10^5}{5 \cdot 10^{-7}} = 6 \cdot 10^{10} \text{ W/cm}^3$$

where ΔV is the potential drop in the pore (about 0.3 V),

j is the current density (10^5 A/cm^2) and

L is the length of the pore ($5 \cdot 10^{-7} \text{ cm}$).

The temperature inside the pore follows the equation:

$$\frac{\delta^2 T}{\delta x^2} = - \frac{H}{K_L} \quad (7-1)$$

where T is the temperature increase above ambient (in Kelvin),

x is the distance along the pore ($0 < x < L$),

K_L is the thermal conductivity of the liquid phase
(W/cm·K).

* At both ends of the pore, the heat flows into the semi-infinite medium with a constant flux F , as from a hemisphere of radius r_o , the radius of the pore ($5 \cdot 10^{-8}$ cm). In this case, the temperature increase on the surface of the hemisphere is (Carslaw and Jaeger, 1959):

$$T = \frac{r_o F}{K}$$

where K is K_M or K_L , the thermal conductivity of the metal or the liquid (670 and 6.1 mW/cm·K respectively),
 F is F_1 or F_2 , the heat flux at either end of the pore.

Equation (7-1) integrates to:

$$T = \frac{-H}{K_L} x^2 + bx + c$$

with the boundary conditions:

$$\begin{aligned} T_1 &= \frac{-r_o F_1}{K_M} & F_1 &= -K_L \left(\frac{\delta T}{\delta x} \right)_1 \\ T_2 &= \frac{-r_o F_2}{K_L} & F_2 &= -K_L \left(\frac{\delta T}{\delta x} \right)_2 \end{aligned}$$

where the suffix 1 refers to the metal side ($x = 0$),
the suffix 2 refers to the bulk solution side

$(x = L),$

and b and c are constants to be determined.

This whole system is easily solved and yields:

$$T_1 = 2 \cdot 10^{-3} \text{ K}$$

$$T_2 = 0.2 \text{ K}$$

$$T_{\text{maximum}} = 0.5 \text{ K}$$

The heating effect is therefore negligible.

7-11 Fixed Geometry

It is assumed that the pore in the passive film has the shape of a cylinder of fixed dimensions.

The actual cross-section of the pore has little influence on the mass transfer process unless, as mentioned in 7-2, the height of the cylinder becomes similar to its cross-section.

However, it may be expected that the length of the pore will increase with time, as the metal is dissolved from the bottom of the pore. This dissolution can be imagined to take place in different ways: forming a pyramid (etch pit), forming a hemisphere (round pit) or continuing the pore (tunnel).

In order to evaluate the order of magnitude of this deepening, the following extreme estimates were made:

* Tunnel:

The dissolution takes place by formation of a tunnel of the same diameter as the pore. The process reaches a

steady state after 3 μ s with a current density of $2 \cdot 10^5$ A/cm². These figures were obtained from the simulation of the results of Janik-Czachor (upper potential, 0.01 [Cl⁻]). Application of Faraday's law, assuming 100% current efficiency, gives an increase in depth of 200 nm, 40 times the original length of the pore assumed in the calculations.

* Hemisphere:

A less drastic result is obtained if one assumes that the dissolution forms a hemisphere. Taking the figures from the simulation of Heusler and Fischer's solution 3 at pH 7.2 (10^{-5} s to reach $2.3 \cdot 10^4$ A/cm²), the radius of the hemisphere reaches only 6.3 nm.

In both cases the change in the geometry of the pore is important and far from negligible. One way to avoid this is to introduce in the calculations a moving boundary at the bottom of the pore. Unfortunately, this leads to a numerically much more complex problem.

7-12 Cathodic Reaction

The location of the cathodic reaction during pitting corrosion is the subject of various studies (Kaesche, 1962; Alkire and Siitari, 1979). As mentioned before (2-9-3), this is important for two reasons. From a quantitative point of view, the cathodic current generated will correspond to an anodic metal dissolution, i.e. to an increase in

corrosion. Also, the cathodic reaction may lead to the evolution of hydrogen, which can completely block the pore and change drastically the mechanisms involved in a qualitative way (Pickering and Frankenthal, 1972).

In the present model, it is assumed that the cathodic reaction takes place only at the counter-electrode, i.e., outside of the pore, as assumed in the previous models.

Table 6 shows the values of the potential as well as the pH at the metal surface. With these two values, it is possible to see if hydrogen evolution is thermodynamically possible at the bottom of the pore. The equilibrium potential for the hydrogen evolution is given by:

$$E_H = -0.059 \text{ pH} - 0.0295 \log p_{H_2}$$

The last line of Table 6 gives the difference between this potential and the actual potential, assuming a hydrogen pressure of one atmosphere. It can be seen that this potential difference is never less than 250 mV. In other terms, the partial pressure of hydrogen is never higher than $3 \cdot 10^{-9}$ atmosphere and therefore hydrogen evolution is impossible.

Of course, the values just mentioned are related to the steady state conditions. The value of the surface potential rises with time from the potential of zero charge (-370 mV) to the values indicated in Table 6. Applying the

same relation as before, the hydrogen pressure would be larger than one atmosphere at -370 mV if the pH was less than 6.26. This is not the case here, even at steady state.

Therefore, within the original assumptions, the evolution of hydrogen cannot take place.

7-13 Comparison of Criteria

The criterion corresponding to the localized acidification theory, K_{rp} , reaches very high values which is interpreted as an indication that the corresponding species are not in equilibrium (see 7-7). Furthermore, K_{rp} is seen to vary systematically with the chloride concentration over various orders of magnitude, explaining the large standard deviation obtained (Figures 17 and 18).

The same type of variation is observed on the same figures for K_{sf} and K_{cc} . The two criteria corresponding to an adsorption mechanism are much closer to being constant, and are nearly independent of the chloride concentration. The values obtained for the standard deviation indicate that K_{ad2} is the best criterion in the sense that it corresponds to the smallest standard deviation, 0.305. This is equivalent to a spread by a factor of 2.

Since the adsorption of the chloride ions seems to be the critical mechanism determining pitting corrosion, it was thought that it might be possible to detect an effect of

the pH, as it is possible that the adsorption of OH^- may here inhibit the pitting process.

The mechanism of pitting and pitting inhibition proposed by Matsuda and Uhlig (1964), Strehblow and Titze (1977) and McCafferty (1979), among others, assume that when an inhibitor is present, there is a critical coverage ratio:

$$\theta_c = \frac{\theta_A}{\theta_I} \quad (7-2)$$

where θ_I is the coverage by the inhibiting ion OH^- and θ_A is the coverage by the aggressive ion Cl^- . Pitting then occurs when and only when this critical coverage ratio is exceeded.

In our case, following McCafferty, one can state:

$$\frac{\theta_A}{1 - \theta_A - \theta_I} = K'_A [\text{Cl}^-] \exp \left[\frac{\Delta H_{\text{ads},A}}{RT} + \gamma_A \frac{FE}{RT} \right]$$

where $\Delta H_{\text{ads},A}$ is the heat of adsorption of Cl^- and γ_A is the electroadsorption valency (Strehblow and Titze, 1977).

If we choose the assumption of the Temkin isotherm:

$$\Delta H_{\text{ads},A} = \Delta H^\circ_A - r_A \theta_A$$

where ΔH_A° is the initial heat of adsorption of Cl^- and

r_A is the Temkin parameter,

this transforms to:

$$\frac{\Theta_A}{1 - \Theta_A - \Theta_I} = K_A [\text{Cl}^-] \exp \left[\frac{\gamma_A \cdot FE - r_A \Theta_A}{RT} \right]$$

by lumping various constants within K_A . Using the usual intermediate coverage assumption, this gives:

$$-\frac{r_A \Theta_A}{RT} = \ln K_A + \ln [\text{Cl}^-] + \gamma_A \frac{FE}{RT}$$

A similar procedure can be followed for OH^- , and it ultimately gives:

$$\frac{r_I \Theta_I}{RT} = \ln K_I + \ln [\text{OH}^-] + \gamma_I \frac{FE}{RT}$$

By regrouping constants, this gives the following general relationship between the variables:

$$\frac{[\text{Cl}^-]}{[\text{OH}^-]^\alpha} \exp [\beta E] = K_{ca}$$

The same values of Table 6 were used to find the parameters α , β and K_{ca} by linear regression, using the relation:

$$E = A + B \log [\text{Cl}^-] + C \log [\text{OH}^-]$$

$$\text{where } A = \frac{\text{Log } K_{ca}}{\beta \text{ Log } e}$$

$$B = - \frac{1}{\beta \text{ Log } e}$$

$$C = \frac{\alpha}{\beta \text{ Log } e}$$

The following values were obtained:

	<u>Mean</u>	<u>Standard Deviation</u>
A.	-14.8	31.52
B	-48.9	7.5
C	5.8	6.4

It can be seen that B and therefore β is relatively well defined:

$$\beta = 4.71 \cdot 10^{-2} \text{ mV}^{-1} \quad (\text{standard deviation: } 7.3 \cdot 10^{-3})$$

but C and α are not significantly different from zero. This can mean that the present data are insufficient to establish a relation between the pitting potential and the pH at the bottom of the pore. It could also mean that this relation does not exist and that, in the range studied, the OH^- ion cannot be considered as an inhibitor for pitting corrosion, in the sense indicated above.

CHAPTER VIII

CONCLUSIONS

The detail of information obtained by using a computer simulation indicates the advantage of this methodology in the study of phenomena related to localized corrosion.

From the values obtained for the parameter K_{rp} at the metal surface, one can conclude that the equilibrium between Fe^{2+} and its complexes with OH^- is not realized during the events which were simulated.

Of the five pitting theories considered, the adsorption of the aggressive ion according to the formulation of Strehblow and Titze (1977) is the most consistent with experimental results published in the literature. A more precise definition of an adsorption criterion, including a value for the critical coverage of Cl^- , must await the acquisition of better kinetic data on the reaction of iron surfaces with water and chloride ions.

The two previous conclusions are used to propose the following combination of the repassivation and adsorption theories as the best theoretical representation of the experimental data. Whenever a breakdown of the passive layer occurs, two processes start competing:

* The build-up of a chemisorbed chloride layer on the iron surface; the kinetics of this process depends upon the kinetics of iron dissolution and upon mass transfer between the metal surface and the bulk solution.

* The precipitation of ferrous hydroxide; the kinetics of this reaction are slower but the thermodynamic conditions are overwhelmingly in its favour.

When a critical minimum coverage of adsorbed Cl^- (e.g. a monolayer) is reached before the precipitation of ferrous hydroxide occurs, then a pit initiates, probably through the formation of a salt layer which prevents further repassivation (Galvele, 1978; Beck and Alkire, 1979). On the other hand, if this minimum coverage is not reached when the precipitation of $\text{Fe}(\text{OH})_2$ is completed, then repassivation is obtained when the precipitation of ferrous hydroxide blocks the pore and so heals the passive film.

CHAPTER IX

FUTURE WORK

The calculations performed in the simulation could be improved in the following manner:

- * The activity coefficient of the ions can be calculated by approximated formulae derived from the Debye-Huckel theory or the semi-empirical formulae derived from it, as in Newman (1973, p. 91) for example. This in turn allows the improvement of the diffusion coefficients, by allowing the introduction of a term correcting for non-ideality.
- * To avoid the instabilities mentioned in 6-4, a saturation of the adsorption sites by the Cl atoms can be taken into account in the expression computing the current density in 5-7-1. This is done by fitting the experimental points to an expression of the type:

$$j = \left(p_1 + \frac{p_2}{p_3 + [H^+]} + \frac{p_4 [Cl^-]}{p_5 - [Cl^-]} \right) \exp (a E)$$

where a and the p_i 's are empirical constants..

The results obtained here rely heavily on the values of the constants computed in 5-7-1: from 6-2, it is seen that the errors on the Tafel slope and m_4 are the most important. Unfortunately, as was already pointed out, the experimental data are very scarce. The prediction capability of the program would benefit from an improved knowledge of the kinetics of dissolution of iron, i.e. the kinetic constants corresponding to the elementary steps, when adsorption of either OH^- or Cl^- is involved.

- * As pointed out in 7-11, the model is limited by the assumption of the fixed geometry. The development of a numerical solution of the differential equations with a moving boundary would represent a great progress. Again, it would have to be decided if the dissolution produces a tunnel or a hemisphere.
- * If this last modification is performed, then it is possible to simulate later stages of pit development. It may be possible to study the effect of hydrogen evolution on pit growth. This local cathodic reaction inside the pit could allow the formation of a close system, nearly independent of the outside electrochemical conditions, and favouring the growth of deep pits.

- * Another possible extension is the study of the repassivation mechanisms through supersaturation of the solution, precipitation of the passivating phase (with or without time delay) and subsequent increase in the electrical resistance of the pore.
- * Increasing still further the complexity of the model, it may be possible to simulate the growth of the salt film layer on the metal at the bottom of the pit. Of course, this can be considered as a solid state process, but it is coupled with the system considered here through the passage of electrical charge and diffusion of species produced by dissolution of the film.
- * There is no limitation in principle to the use of the model with other metals or even alloys. One possible difficulty, in the case of alloys, is the local enrichment of the first few atomic layers of the surface in the more noble metal.

CHAPTER X

REFERENCES

Abd Rabbo, M.F., Richardson, J.A., and Wood, G.C. (1976),
Corros. Sci., 16, 677.

Abd Rabbo, M.F., Wood, G.C., Richardson, J.A., and Jackson,
C.K. (1974), Corros. Sci., 14, 645.

Alkire, R.C., Ernsberger, D., and Beck, T.R. (1978), J.
Electrochem. Soc., 125, 1382.

Alkire, R.C., Ernsberger, D., and Damon, D. (1976), J.
Electrochem. Soc., 123, 458.

Ambrose, J.R., and Kruger, J. (1972), Proc. 4th Cong.
Metallic Corrosion, p. 698, N.A.C.E., Houston.

Ambrose, J.R., and Kruger, J. (1974), Report NBSIR 74-583,
National Bureau of Standards, U.S. Department of
Commerce, Washington, D.C.

Arvia, A.J., and Podesta, J.J. (1968), Corr. Sci., 8, 203.

Asakura, S. and Nobe, K. (1971), J. Electrochem. Soc., 118,
13 and 19.

Ateya, B.G. and Pickering, H.W. (1975), J. Electrochem.
Soc., 122, (8), 1018.

Ateya, B.G. and Pickering, H.W. (1977), in "Stress Corrosion
Cracking and Hydrogen Embrittlement in Iron Base

- Alloys", R.W. Staehle ed., p. 1183, N.A.C.E., Houston.
- Ateya, B.G. and Pickering, H.W. (1978), in "Passivity of Metals", R.P. Frankenthal and J. Kruger ed., The Electrochemical Society, Princeton, New Jersey, p. 350.
- Augustynski, J. (1978), in "Passivity of Metals", R.P. Frankenthal and J. Kruger ed., The Electrochemical Society, Princeton, New Jersey, p. 989.
- Augustynski J., Dalard, F. and Sohm, J.C. (1972), Corros. Sci., 12, 713.
- Aziz, P.M. (1956), Corrosion, 12, 495t.
- Baes, C.F. and Mesmer, R.E. (1976), "The Hydrolysis of Cations", John Wiley, New York.
- Bargeron, C. . and Benson, R.C. (1980), J. Electrochem. Soc., 127, (11), 2528.
- Beck, T.R. (1973), J. Electrochem. Soc., 120, 1310 and 1317.
- Beck, T.R. (1982), J. Electrochem. Soc., 129, 2412.
- Beck, T.R., and Alkire, R.C. (1979), J. Electrochem. Soc., 126, 1662.
- Beck, T.R., and Grens, E.A. (1969), J. Electrochem, Soc., 116, 177.
- Behrens, D. (1975), Br. Corr. J., 10, 122.
- Bertocci, U. (1980), J. Electrochem, Soc., 127, 1931.
- Bertocci, U. (1981), J. Electrochem, Soc., 128, 520.
- Bockris, J.O'M., Drazic, D., and Despic, A.R. (1961), Electrochem. Acta, 4, 325.

- Bockris, J.O'M., and Reddy, A.K.N. (1970), "Modern Electrochemistry", Plenum Pres, New York.
- Bohni, H., and Uhlig, H.H. (1969), J. Electrochem. Soc., 116, 906.
- Bond, A.P. (1972), in "Localized Corrosion - Cause of Metal Failure", p. 250, ASTM STP 516, American Society for Testing Materials.
- Bond, A.P., and Lizlovs, E.A. (1968), J. Electrochem. Soc., 115, 1130.
- Bonhoeffer, K.F., and Heusler, K.E. (1956), Z. Phys. Chem. N.F., 8, 390.
- Bonhoeffer, K.F., and Heusler, K.E. (1957), Z. Elektrochem., 61, 122.
- Boyllis, J.R. (1925), Chem. Metallurg. Eng., 32, 874.
- Brauns, E., and Schwenk, W. (1961), Werkst. Korros., 12, 73.
- Brieter, M., and Hoffmann, K. (1960), Z. Elektrochem., 64, 462.
- Britton, S.C., and Evans, U.R. (1930), J. Chem. Soc., 1773.
- Broll, A., and Holtan, H. (1973), Corros. Sci., 13, 237.
- Broll, A., Holtan, H., and Prestrud, K.I. (1974), Corrosion, 30, 427.
- Brooksbank, D., and Andrews, K.W. (1969), J. Iron and Steel Inst., 207, 474.
- Brooksbank, D., and Andrews, K.W. (1971), J. Iron and Steel Inst., 210, 246.

- Brennert, S. (1937), J. Iron and Steel Inst., 135, 101^V.
- Burstein, G.T., and Davies, D.H. (1980), Corros. Sci., 20, 1143.
- Burstein, G.T., and Davies, D.H. (1981), J. Electrochem. Soc., 128, 33.
- Butler, J.N. (1964), "Ionic Equilibrium, a mathematical approach", Addison-Wesley.
- Carslaw, H.S., and Jaeger, J.C. (1959), "Conduction of Heat in Solids", Oxford, p. 248.
- Chao, C.Y., Lin, L.F., and Macdonald, D.D. (1981), J. Electrochem. Soc., 128, 1187.
- Chao, C.Y., Lin, L.F., and Macdonald, D.D. (1982), J. Electrochem. Soc., 129, 1874.
- Chin, R.J., and Nobe, K. (1972), J. Electrochem. Soc., 119, 1457.
- Collins, J.A., and Monack, M.L. (1973), Mat. Perf., 12, 11 (June 1973).
- Conte, S.D. and de Boor, C. (1980), "Elementary Numerical Analysis, An Algorithmic Approach", McGraw-Hill.
- Darwish, N.A., Hilbert, F., Lorenz, W.J., and Rosswag, H. (1973), Electrochim. Acta, 18, 421.
- Davydov, A.D., and Kamkin, A.N. (1978), Elektrokimiya, 14 (7), 979.
- Davydov, A.D., Mirzoev, R.A., Kamkin, A.N., and Roshchina, T.A., (1978), Elektrokimiya, 14 (6), 901.
- Drazic, D.M., and Hao, C.S. (1982), Electrochim. Acta, 27,

1409.

Edwards, J.D., and Keller, F. (1944), Trans. Amer. Inst. Min. (Metall.) Engrs., 156, 288.

Eichkorn, G., Lorenz, W.J., Albert, L., and Fisher, H. (1968), Electrochim. Acta. 13, 183.

Eldredge, G.G. (1957), Corrosion, 13, 51t.

Engell, H.J. (1977), Electrochim. Acta, 22, 987.

Engell, H.J., and Stolica, N.D. (1959), Arch. Eisenhüttenwes., 30, 239.

Epelboin, I., Gabrielli, C., and Keddam, M. (1975), Corros. Sci., 15, 155.

Epelboin, I., Gabrielli, C., Keddam, M., and Takenouti, H. (1975), Z. Physik. Chemie N.F., 98, 215.

Epelboin, I., and Keddam, M. (1977) in "Stress Corrosion Cracking and Hydrogen Embrittlement in Iron Base Alloys", R.W. Staehle et al ed., p. 21, N.A.C.E., Houston.

Evans, C.A. (1977), paper 14, "Corrosion/77", N.A.C.E., Houston.

Evans, U.R. (1930), Trans. Amer. Electrochem. Soc., 57, 407.

Evans, U.R. Bannister, L.C., and Britton, S.C. (1931), Proc. Roy. Soc., A131, 367.

Faita, G., Mazza, F., and Bianchi, G. (1974), in "Localized Corrosion", B.F. Brown et al ed., N.A.C.E., Houston, Texas, p. 34.

Finley, H.F. (1967), Corrosion, 23, 83.

Finley, H.F., and Toncre, A.C. (1964), Mat. Prot., 3, 29.

Foley, R.T. (1975), J. Electrochem. Soc., 122, 1493.

Forchhammer, P., and Engell, H.J. (1969), Werkst. Korros.,
20 1.

Foroulis, Z.A., and Thubrikar, M.J. (1975), J. Electrochem.
Soc., 122, 1296.

Franck, U.F. (1960), Werkst. Korros., 11, 401.

Franck, U.F. (1961), First Int. Cong. Met. Corr., London, p.
120.

Freiman, I.I., LeMin, L., and Raskin, G.S. (1973), Zashch.
Met., 9, 680.

Frost, R. (1972), "Robert Frost, Poetry and Prose", Holt,
Rinehart and Winston, New York.

Gabrielli, C. (1973), Met. Corrosion Industries, p. 171,
223, 309 and 356.

Galvele, J.R. (1976a), in "Passivity and its Breakdown in
Iron and Iron Base Alloys", R.W. Staehle and H. Okada
ed., N.A.C.E., Houston, Texas, p. 118.

Galvele, J.R. (1967b), J. Electrochem. Soc., 123, 464.


Galvele, J.R. (1978), in "Passivity of Metals", R.P.

Frankenthal and J. Kruger ed., The Electrochemical
Society, Princeton, New Jersey, p. 285.

Galvele, J.R. (1981), Corros. Sci., 21, 551.

Gear, C.W. (1971), Comm. A.C.M., 14, (3), 176.

Golovina, G.V., Florianovich, G.M., and Kolotyřkin, Ya.M.

- (1965), Zashch. Met., 2, (1), 41.
- Greene, N.D., and Fontana, M.G. (1959), Corrosion, 15, (1), 32t and 39t.
- Harned, H.S. and Robinson, R.A., Trans. Faraday Soc., 36 (1940), 973.
- Heimann, R.B., Ives, M.B., and Zaya, P.G.R. (1982), J. Crystal Growth, 57, 48.
- Heine, M.A., Keir, D.S., and Pryor, M.S. (1965), J. Electrochem. Soc., 112, 29.
- Herbsleb, G., and Engell, H.J. (1961), Z. Elektrochemie, 65, 881.
- Heusler, K.E. (1958), Z. Elektrochem., 62, 529.
- Heusler, K.E., and Fischer, L. (1976), Werkst. Korros., 27, 551 and 697.
- Hilbert, F., Miyoshi, Y., Eichkorn G. and Lorenz, W.J. (1971), J. Electrochem. Soc., 118, 1919.
- Hills, G., Pour, A.K., and Scharifker, B. (1983), Electrochim. Acta, 28, (7), 891.
- Hines, J.G. (1961), Corros. Sci., 1, 21.
- Hisamatsu, Y. (1976), in "Passivity and its Breakdown in Iron and Iron Base Alloys", R.W. Staehle and H. Okada ed., N.A.C.E., Houston, Texas, p. 99.
- Hisamatsu, Y., Yoshii, T., and Matsumura, Y. (1974), in "Localized Corrosion", B.F. Brown et al ed., N.A.C.E., Houston, Texas, p. 247.
- Hoar, T.P. (1947), "Electrode Processes", Disc. Far. Soc.,
- 

1, 299.

Hoar, T.P. (1949), Trans. Far. Soc., 45 683.

Hoar, T.P. (1967), Corros. Sci., 7 341.

Hoar, T.P. (1971), (Chairman of the Committee), "Report of the Committee on Corrosion and Protection", Department of Trade and Industry, H.M.S.O., London.

Hoar, T.P., and Foster, D.J., quoted by Hoar, T.P. (1970), J. Electrochem. Soc., 117, (1), 17C.

Hoar, T.P., and Jacob, W.R. (1967), Nature, 216, 1299.

Hoar, T.P., Mears, D.C., and Rothwell, G.P. (1965), Corros. Sci., 5, 279.

Isaacs, H.S. (1973), J. Electrochem. Soc., 120, 1456.

Iverson, W.P. (1968), J. Electrochem. Soc., 115, 617.

James, M.L., Smith, G.M., and Wolford, J.C. (1977), "Applied Numerical Methods for Digital Computation", p. 438, Harper and Row, New York.

Janik-Czachor, M. (1971), Br. Corr. J., 6, 57.

Janik-Czachor, M. (1979), Werkst. Korros., 30, 255.

Janik-Czachor, M. (1980), Zashch. Met., 16, 265.

Janik-Czachor, M. (1981), J. Electrochem. Soc., 128, (12), 513c.

Janik-Czachor, M., and Ives, M.B. (1978), in "Passivity of Metals", R.P. Frankenthal and J. Kruger ed., The Electrochemical Society, Princeton, New Jersey, p. 369.

Janik-Czachor, M., Szummer, A., and Szklarska-Smialowska, Z.

- (1975), Corros. Sci., 15, 775.
- Jones, D.A., and Wilde, B.E. (1978), Corros. Sci., 18, 631.
- Kabanov, B., Burshtein, R. and Frumkin, A. (1947), Disc. Far. Soc., 1, 259.
- Kabanov, B. and Kascheev, V.D. (1963), Dokl. Akad. Nauk. SSSR, 151, 833.
- Kaesche, H. (1962), Z. Phys. Chem. N.F., 34, 87.
- Kasper, C. (1940), Trans. Electrochem. Soc., 77, 353.
- Keller, F., Hunter, M.S., and Robinson, D.L. (1953), J. Electrochem. Soc., 100, 411.
- Kelly, E.J. (1965), J. Electrochem. Soc., 112, 124.
- Kolotyrkin, Ya.M. (1961), J. Electrochem Soc., 108, 209.
- Kolotyrkin, Ya.M. (1963), Corrosion, 19, (8), 261t.
- Kolotyrkin, Ya.M., and Freiman, L.I. (1965), Dokl. Akad. Nauk. SSSR, 162 (2), 376.
- Kolotyrkin, Ya.M., and Gilman, V.A. (1961), Dokl. Akad. Nauk. SSSR, 137, 642.
- Koudelkova, M., and Augustynski, J. (1979), J. Electrochem. Soc., 126, 1659.
- Koudelkova, M., Augustynski, J., and Berthou, H. (1977), J. Electrochem. Soc., 124, 1165.
- Kruger, J. (1976), in "Passivity and its Breakdown in Iron and Iron Base Alloys", R.W. Staehle and H. Okada ed., N.A.C.E., Houston, Texas, p. 91.
- Kuo, H.C., and Landolt, D. (1975), Electrochim. Acta, 20, 393.

- Kuo, H.C., and Nobe, K. (1978), J. Electrochem. Soc., 125, 853.
- Leckie, H.P., and Uhlig, H.H. (1966), J. Electrochem. Soc., 113, 1262.
- Lin, L.F., Chao, C.Y., and Macdonald, D.D. (1981), J. Electrochem. Soc., 128, 1194.
- Lochel, B.P., and Strehblow, H.H. (1980), Werkst. Korros., 31, 353.
- Lochel, B.P., and Strehblow, H.H. (1983), Electrochim. Acta, 28, (4) 565.
- Lorenz, W.J. (1965), Corr. Sci., 5, 121.
- Lorenz, W.J., and Eichkorn, G. (1965), J. Electrochem. Soc., 112, 1225.
- Lorenz, W.J., Yamaoka, H., and Fisher, H. (1963), Ber. Bunsenges. Phys. Chem., 67, 932.
- Lotlikar, M.M., and Davies, D.E. (1966), Proc. 3rd Int. Cong. Met. Corr., vol. 1, p. 167.
- Lumsden, J.B., and Staehle, R.W. (1973), paper 122, "Corrosion/73", N.A.C.E., Houston.
- McBee, C.L., and Kruger, J. (1971), Nature, 230, 194.
- McBee, C.L., and Kruger, J. (1974), in "Localized Corrosion", B.F. Brown et al ed., N.A.C.E., Houston, Texas, p. 252.
- McCafferty, E. (1979), J. Electrochem. Soc., 126, 385.
- McCafferty, E. (1981), J. Electrochem. Soc., 128, 39.
- McCafferty, E., and Hackerman, N. (1972), J. Electrochem.

- Soc., 119, 999.
- McCracken, D.D., and Dorn, W.S. (1964), "Numerical Methods and Fortran Programming", John Wiley.
- Macdonald, D.D. (1977), "Transient Techniques in Electrochemistry", p. 30, Plenum Press, New York.
- MacDougall, B. (1979), J. Electrochem. Soc., 126, 919.
- MacDougall, B. (1982), Communication at the Eastern Canadian Regional Conference, N.A.C.E., November 23, 1982.
- Mankowski, J., and Szklarska-Smialowska, Z. (1977), Corros. Sci., 17, 725.
- Mansfeld, F. (1981), Corrosion, 36, 301.
- Mansfeld, F., Kendig, M.W., and Tsai, S. (1982), Corrosion, 38, 570.
- Masuko, N. (1974), Proc. 5th Int. Cong. Metallic Corrosion, N.A.C.E., Houston, -p. 1051.
- Matsuda, S., and Uhlig, H.H. (1964), J. Electrochem. Soc., 111, 157.
- Mears, R.B., and Brown, R.H. (1937), Ind. and Eng. Chem., 29, 1087.
- Mears, R.B., and Evans, U.R. (1935), Trans. Far. Soc., 31, 527.
- Nagayama, M., and Cohen, M. (1962), J. Electrochem. Soc., 109, 781.
- Newman, J.S. (1973), "Electrochemical systems", p. 217 to 228, Prentice-Hall.
- Newman, J.S., Hanson, D.N., and Vetter, K (1977),

- Electrochim. Acta, 22, 829.
- Novakovski, V.M., and Sorokina, V.M. (1966), Zashch. Met., 2, 416.
- Oldfield, J.W., and Sutton, W.H. (1978), Br. Corros. J., 13, (1), 13.
- Okamoto, G. (1973), Corros. Sci., 13, 471.
- Okamoto, G., Tachibana, K., Nishiyama, S., and Sugita, T. (1976), in "Passivity and its Breakdown in Iron and Iron Base Alloys", R.W. Staehle and H. Okada ed., N.A.C.E., Houston, Texas, p. 106.
- Painot, J., and Augustynski, J. (1975), Electrochim. Acta, 20, 747.
- Painot, J., and Augustynski, J. (1976), J. Electrochem. Soc., 123, 841.
- Parsons, R. (1959), "Handbook of Electrochemical Constants", Butterworths, London.
- Payer, J.H., Boyd, W.K., Dippold, D.G., and Fisher, W.H. (1980), Mat. Perf., 19, (5), 34.
- Pessall, N., and Liu, C. (1971), Electrochim. Acta, 16, 1987.
- Petit, J.A., Kondo, B., and Dabosi, F. (1980), Corrosion, 36, 145.
- Pickering, H.W. (1983), Corros. Sci., 23, 1107.
- Pickering, H.W., and Frankenthal, R.P. (1972), J. Electrochem. Soc., 119, 1297.
- Popov, Yu.A., Alekseev, Yu.V., and Kolotyarkin, Ya.M. (1978),

- Elektrokhimya, 14, 1260 and 1390; (1979), 15, 342, 449, 564, 770 and 926.
- Pourbaix, M., Klimzack-Mathieu, L., Mertens, C., Meunier, J., Vanleughenague, C., de Munck, L., Laureys, J., Neelemans, L., and Warzee, M. (1963), Corros. Sci., 3, 239.
- Pryor, M.J. (1974), in "Localized Corrosion", B.F. Brown et al ed., N.A.C.E., Houston, Texas, p. 2.
- Rene, R.W., and Uhlig, H.H. (1974), J. Inst. Engr. Austral., 46, 3.
- Richardson, J.A., and Wood, G.C. (1970), Corros. Sci., 10, 313.
- Richardson, J.A., and Wood, G.C. (1973), J. Electrochem. Soc., 120, 193.
- Rosenfeld, I., and Maximtschuk, W. (1960), Z. Physik. Chem., 215, 25.
- Saito, H., Shibata, T., and Okamoto, G. (1979), Corros. Sci., 19, 693.
- Sato, N. (1971), Electrochim. Acta, 16, 1683.
- Schwenk, W. (1963), Corros. Sci., 3, 107.
- Schwenk, W. (1964), Corrosion, 20, 129t.
- Shibata, T., and Takeyama, T. (1976), Corrosion, 33, 243; Nature, 260, 315.
- Shibata, T., and Takeyama, T. (1981), 8th Int. Congress on Met. Corr., Mainz, West Germany.
- Shreir, L.L. (1976a), in "Corrosion", vol. 1, p. 1.150, L.L.

- Shreir ed., Butterworths, London.
- Shreir, L.L. (1976b), *ibid.* p. 1.182.
- Shuck, R.R., and Swedlow, J.L. (1974), in "Localized Corrosion", B.R. Brown et al ed., N.A.C.E., Houston, Texas, p. 184 and 190.
- Sillen, L.G., and Martell, A.E. (1964), "Stability Constants of Metal-Ion Complexes", Chemical Society, London.
- Silverman, D.C. (1982), *Corrosion*, 38, 453.
- Smialowski, M., Szklarska-Smialowska, Z., Rychcik, M., and Szummer, A. (1969), *Corros. Sci.*, 9, 123.
- Stastny, M., and Strafelda, F. (1969), *Collect. Czech. Chem. Comm.*, 34, 168.
- Strehblow, H.H. (1976), *Werkst. Korros.*, 27, 792.
- Strehblow, H.H. (1981), private communication.
- Strehblow, H.H., and Lochel, B.P. (1983), 5th. Int. Symp. on Passivity, Bombannes-Bordeaux, France.
- Strehblow, H.H., and Titze, B. (1977), *Corros. Sci.*, 17, 461.
- Strehblow, H.H., Vetter, K.J., and Willgallis, A. (1971), *Ber. Bunsenges. Physik. Chem.*, 75, 822.
- Strehblow, H.H., and Weners, J. (1975), *Z. Physik. Chem. N.F.*, 98, 199.
- Strehblow, H.H., and Weners, J. (1977), *Electrochim. Acta*, 22, 421.
- Suzuki, T., and Kitamura, Y. (1972), *Corrosion*, 28, 1.
- Suzuki, T., Yamabe, M., and Kitamura, Y. (1973), *Corrosion*,

29, 18.

Szklarska-Smialowska, Z. (1971), Corrosion, 27, 223.

Szklarska-Smialowska, Z., Szummer, A., and Janik-Czachor, M.
(1970), Br. Corr. J.; 5, 159.

Szklarska-Smialowska, Z., Viefhaus, H., and Janik-Czachor,
M. (1976), Corros. Sci., 16, 649.

Tajima, S., and Ogata, M. (1968), Electrochim. Acta, 13,
1845.

Tester, J.W., and Isaacs, H.S. (1975), J. Electrochem. Soc.,
122, 1438.

Turnbull, A. (1980), Br. Corr. J.; 15, (4), 162.

Turnbull, A., and Thomas, J.G.N. (1982), J. Electrochem.
Soc., 129, (7), 1412.

Uhlig, H.H. (1946), Chem. Eng. News, 24, 3154.

Uhlig, H.H. (1950), J. Electrochem. Soc., 97, 215c.

Uhlig, H.H. (1967), Corros. Sci., 7, 325.

Uhlig, H.H., and Gilman, J. (1964), Corrosion, 20, 289t.

Uhlig, H.H., and Wulff, J. (1939), Trans. AIME, 135, 494.

Van Muylden, J., Pourbaix, M., and Van Laer, P. (1965),

Report RT.127, CEBELCOR, Brussels, Belgium.

Vermilyea, D.A., and Tedmon, C.S. (1970), J. Electrochem.
Soc., 117, 437.

Vetter, K.J. (1965), Ber. Bunsenges, Phys. Chem., 69, 589
and 683.

Vetter, K.J. (1967), "Electrochemical kinetics", p. 207,
Academic Press, New York.

- Vetter, K.J. (1974), Proc. 5th Int. Cong. Met. Corr.,
N.A.C.E., Houston, p. 332.
- Vetter, K.J., and Strehblow, H.H. (1970), Ber. Bunsenges.
Physik. Chem., 74, 1024.
- Vetter, K.J., and Strehblow, H.H. (1974), in "Localized
Corrosion", B.F. Brown et al ed., N.A.C.E., Houston,
Texas, p. 240.
- Videm, K. (1974), Proc. 5th Int. Cong. Met. Corr., N.A.C.E.,
Houston, p. 264.
- Weil, K.G., and Menzel, D. (1959), Z. Elektrochem., 63,
669.
- West, J.M. (1965), "Electrodeposition and Corrosion
Processes", Van Nostrand.
- Wilde, B.E. (1976), in "Passivity and its Breakdown in Iron
and Iron Base Alloys", R.W. Staehle, and H. Okada ed.,
N.A.C.E., Houston, Texas, p. 129.
- Wilde, B.E., and Williams, E. (1971), Electrochim. Acta, 16,
1971.
- Wood, G.C., Richardson, J.A., Abd Rabbo, M.F., Mapa, L.B.,
and Sutton, W.H. (1978), in "Passivity of Metals", R.P.
Frankenthal and J. Kruger, ed., The Electrochemical
Society, Princeton, New Jersey, p. 973.
- Wood, G.C., Sutton, W.H., Richardson, J.A., Riley, T.N.K.,
and Malherbe, A.G. (1974), in "Localized Corrosion",
B.F. Brown et al ed., N.A.C.E., Houston, Texas, p.
526.

APPENDIX A

DESCRIPTION OF THE COMPUTER PROGRAM

The structure of the program is shown on Figure 19. In this diagram, the hierarchy is indicated by the vertical position and the connecting lines: each subroutine is called by the program or subroutine connected to it and situated above it.

Briefly, MAIN reads the input, prints it and performs all the calculations which have to be performed once. DRIVER does the management of the LSODE package. PRIN prints the results of each output from LSODE. CONC computes the concentrations of all the species present and the current density, given the main concentrations and the potential at the bottom of the pore (see 5-2, 5-3, and 5-6). CALC is the main subroutine called by LSODE to compute the time derivative of the main components, as described in 5-3 and 5-8. JAC is a dummy subroutine provided only for compatibility with the LSODE package. DCDT computes the time derivatives, given the T_i 's (TRANS(I,N)), as described in 5-3 and 5-8. DERIV computes the first and second space derivatives of the concentrations by finite difference. INTEG computes the numerical integral of a given variable

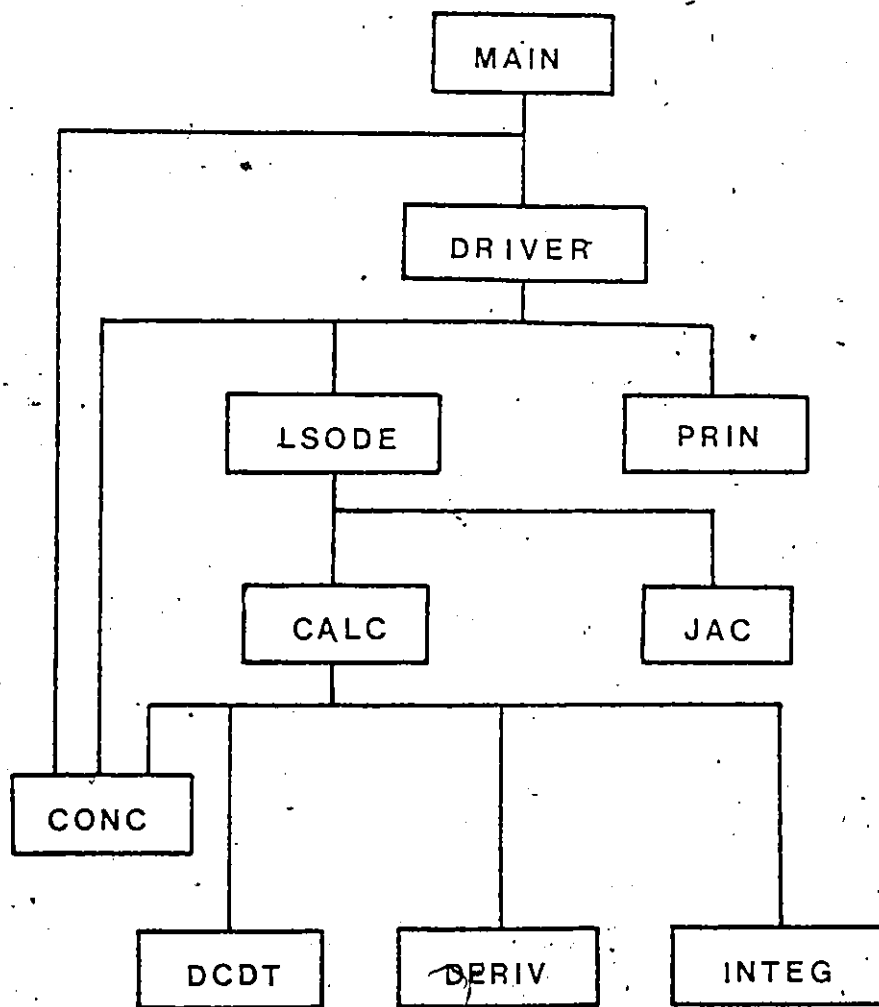


Figure 19 - Diagram of the computer program

over the computed radius grid. The whole program is designed so that only DCDT and CONC have to be modified when a change is introduced in the chemical system.

In the following, the numbers in parenthesis refer to the line numbers of each unit, which are on the left hand side in Figures 20 to 29. Some of the features described here were of interest at one point in the development of the program but their use has been discontinued because of the evolution of the project. As this is a description of the program as it presently stands, they have been described nevertheless.

A-1 Program MAIN (Figure 20)

The program MAIN reads the input, prints it and performs various initializing tasks before calling the subroutine DRIVER. The control returns to MAIN only at the end of the run. All the values computed in MAIN are passed to the various subroutines mainly through common blocks (54-74).

The input data are read from file TAPE1, which can be renamed for convenience in a procedure-command file (91-151) and then the input is printed (152-249). If in some preliminary work on the program, a more detailed print-out is desired in MAIN, the input variable PRTDET is set to TRUE. Examples of input and output are shown on Figures 21 and 22, respectively. The input file is written


```

HEUSLER AND FISCHER ; SOLUTION 10.2 B .PH 7.3 ; 166 MV ; SE-3 CL-
570
* NUMB. SPEC NUMB. MAIN COMF IS IT A RESTART POINTS FIN.DIFF.
  10 4 F 3
* TOTAL NUMB NODES      NODES IN CHANNEL      NODES IN INTERM.ZONE
  100 43 5
* RADIUS DEPTH DIST TO REF. TEMP IS WHOLE ELECT.DISS.7
  1. 5. 2. 20. F.
* KX(1.....) MOL/CM3
  1.78E-20 1E7 1.3E5 100. 8.93E7
* REFASS: SPECIE,SOL.PROD.,SUP.SAT. / SALT FILM: SPECIE,SOL.PROD.,SUP.SAT
  7 2E-11 1E3 8 3E-5 1E6
* TAPEL SLO. CAP.2BLE LAYER FIX.POT OR CUR POTENTIAL STATIC?
  116. 40. 166. T
* POTENTIAL OF ZERO CHARGE NUMB. OF PARAMETERS
  -370. 4.
* PARAMETERS TO COMPUTE CURRENT DENSITY
  76.7E7 1.15E-1 3.67E-15 4.57E14
* LSODE : MF INIT. T. MAX. NUMB. OUTPUT TIME LIM.
  15 -0. 200 1E3
* TOL VALUES FOR CONC. AT NODE 1 REL. ABS.
  1E-4 1E-16
* TOL VALUES FOR OTHER CONC. REL. ABS.
  1E-4 1E-16
* TOL VALUES FOR POTENTIAL REL. ABS.
  0. 1E-5
* PR. DETAILS MAIN NUMB.OF PEAKS OUTPUT/DEC DEC.START DET.CASI-SAT
  F 0 2 1E-11 F
* PEAKS
  1 10 100
* SPECIES CHARGE DIFFUSION COEFFICIENT
  FE1+ 1. 7E-6
  H+ 1. 9.5E-5
  NA+ 1. 1.3E-5
  B(OH)3 0. 1E-5
  OH- -1. 5.3E-5
  FE(OH)2 1. 1.5E-5
  FECL2 0. 1E-5
  FECL2 0. 1E-5
  B(OH)4- -1. 1.5E-5
  CL- -1. 2E-5
* CONCENTRATIONS OF SPECIES 1,2,... NSPEC AT ALL NODES IN MOL/L
  1E-12 5.012E-8 1.1148E-2 0.1939

```

ONLY COPY AVAILABLE
SEULE COPIE DISPONIBLE

Figure 21 - Example of input to the computer program

PITTING CORROSION SIMULATION OF H-TAKOSON AND REPAIR
 HUSSER AND FISCHER SOLUTION 110.2 E .PH 7.31 1 100 MV 1 SE-3 CL-
 570

GEOMETRICAL DATA:
 RADIUS OF PINHOLE 1.100 NANO-M
 DISTANCE TO REFERENCE ELECTRODE 2.00 MM DEPTH 5.00 NANO-M

ELECTROCHEMICAL DATA:
 POLARIZATION
 TAFEL SLOPE 111.00 MV/DECADE
 CAPACITY OF THE DOUBLE LAYER 40. MIC.F/CM2
 CONSTANTS FOR CALCULATION OF CURRENT DENSITY IN SUPR.CMDC:
 1 7.070202E-3
 2 .115000
 3 3.676000E-10
 4 6.576000E-15

EQUILIBRIUM CONSTANTS (ALL CONCENTRATIONS IN MOLE/CM3)
 1 1.70000E-20
 2 2.00000E+07
 3 1.30000E+06
 4 1.00E+00
 5 6.40000E+07

DEPASSIVATING SPECIES IFEC112 SOLUBILITY PRODUCT 12.000E-11 SUPERSTURATION 11.000E+09
 SALT FILM SPECIES IFEC12 SOLUBILITY PRODUCT 13.000E-05 SUPERSTURATION 11.000E+06

IONS ARE PRESENT: THE FIRST 4 OF WHICH ARE MAIN COMPONENTS
 SPECIES DIFFUSION COEFFICIENT (CM2/SEC)
 FE2+ 2 7.000E-05
 H+ 1 1.500E-05
 OH- 1 1.500E-05
 H2O 0 1.000E-05
 H2 1 1.000E-05
 O2 1 1.000E-05
 H2O2 1 1.000E-05
 HCO3- 1 1.000E-05
 CO3- 1 1.000E-05
 H2PO4- 1 1.000E-05
 HPO4- 1 1.000E-05
 PO4- 1 1.000E-05
 SiO4- 1 1.000E-05
 SiO2 1 1.000E-05
 SiH4 1 1.000E-05
 SiH2 1 1.000E-05
 SiH 1 1.000E-05
 Si 1 1.000E-05

Figure 22 - Example of output to the computer program

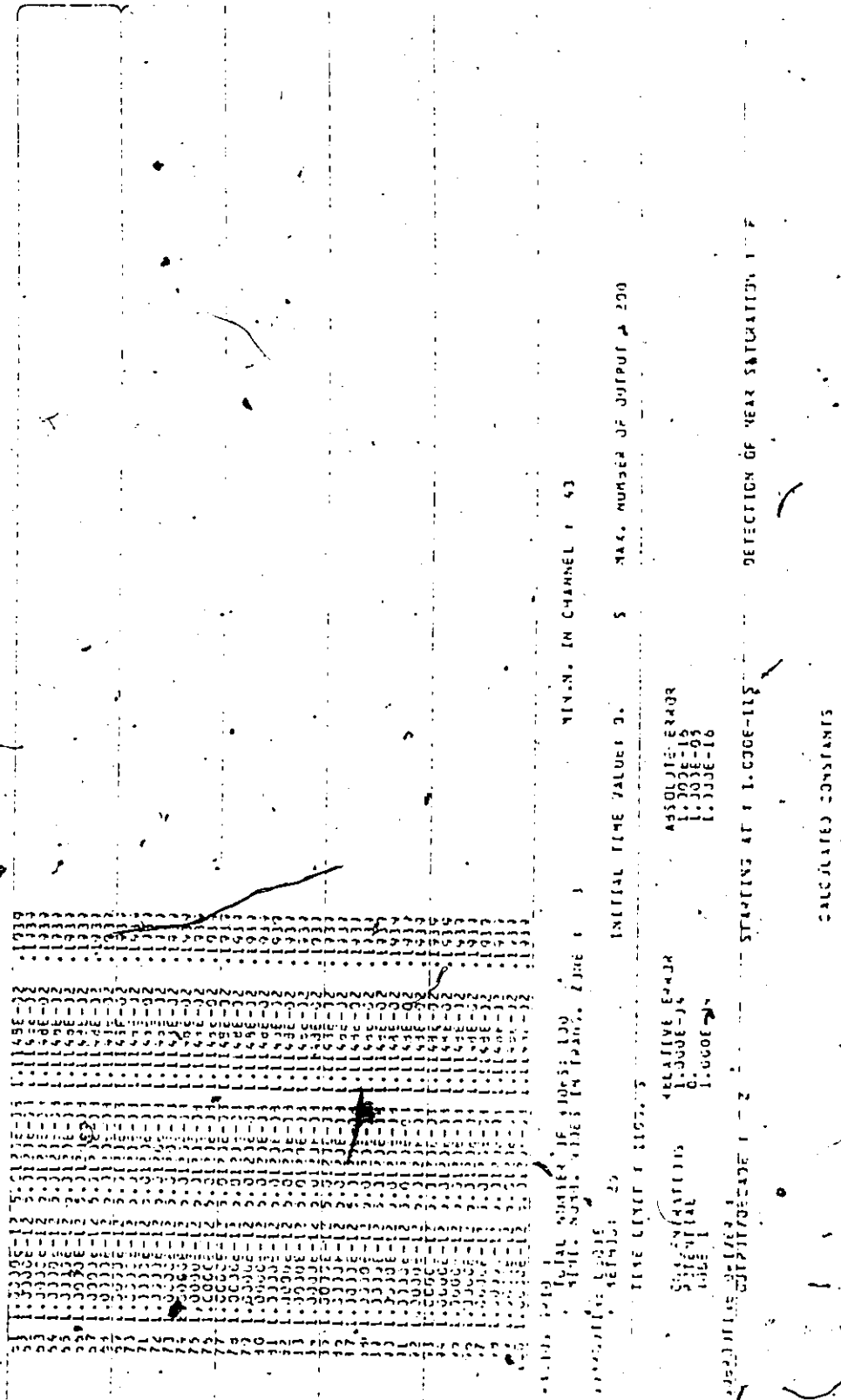


Figure 22 - Cont'd

ONLY COPY AVAILABLE
SEULE COPIE DISPONIBLE

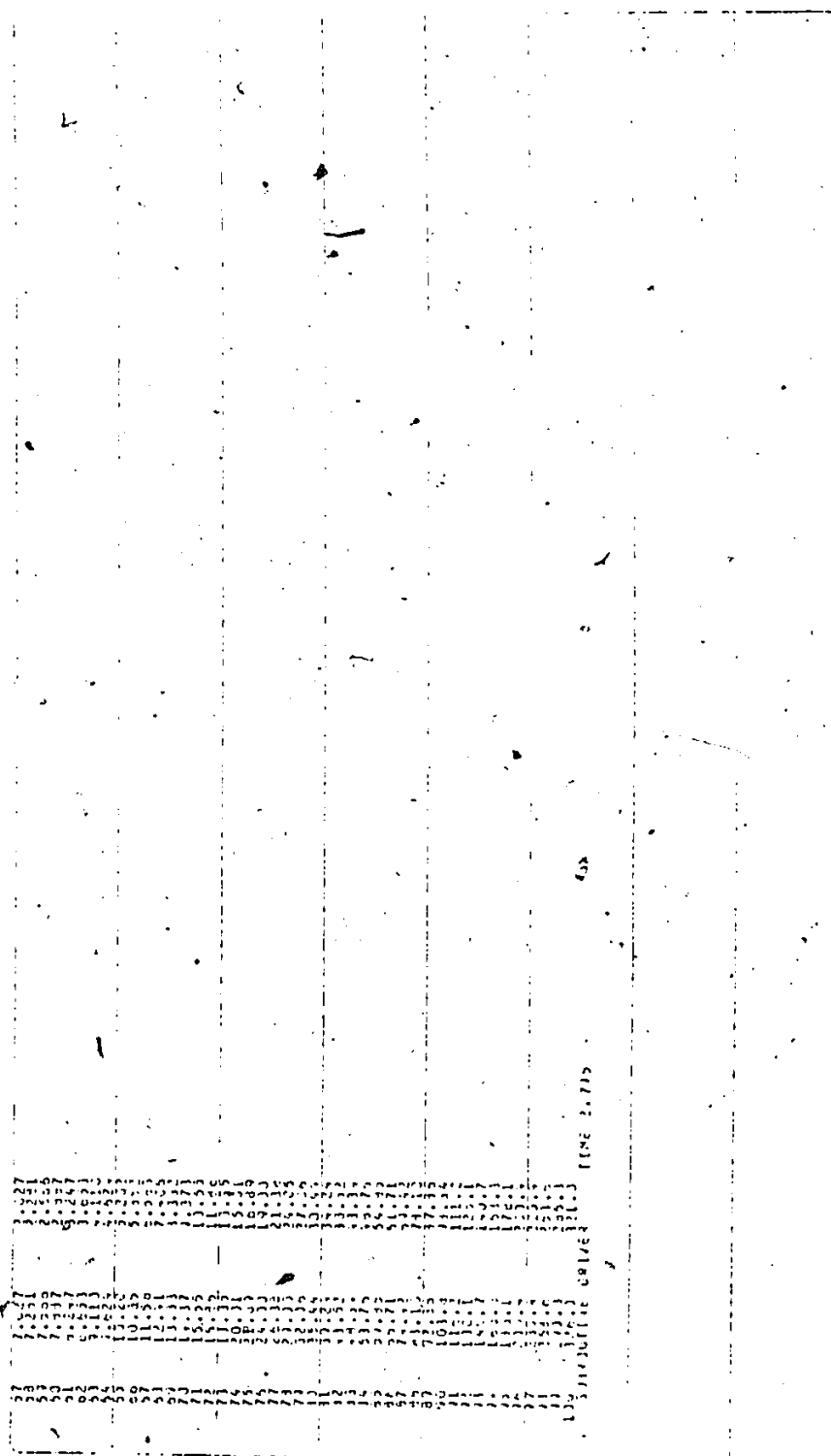


Figure 22 - Cont'd

ONLY COPY AVAILABLE
SEULE COPIE DISPONIBLE

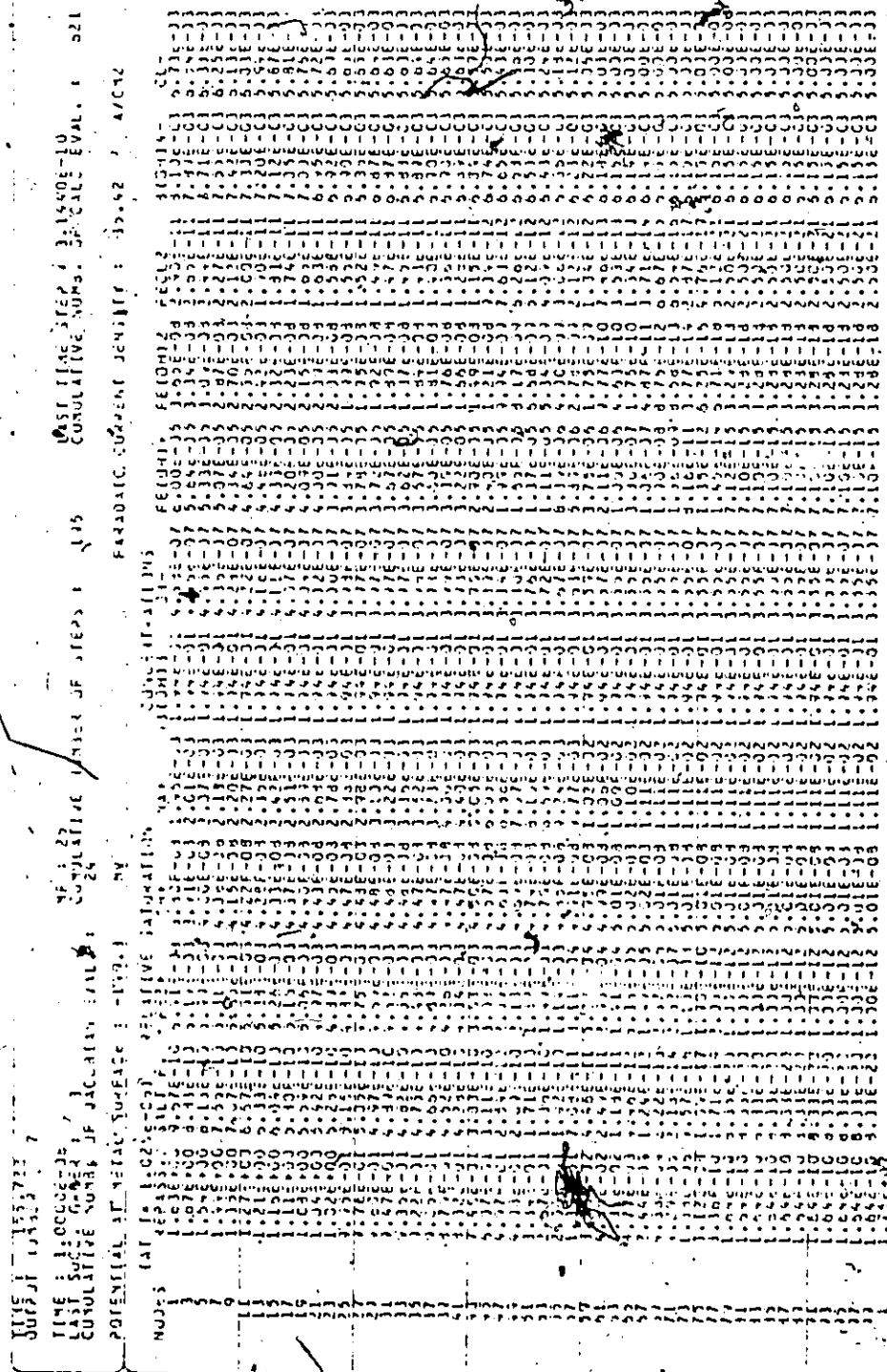


Figure 22 - 1

ONLY COPY AVAILABLE
SEULE COPIE DISPONIBLE

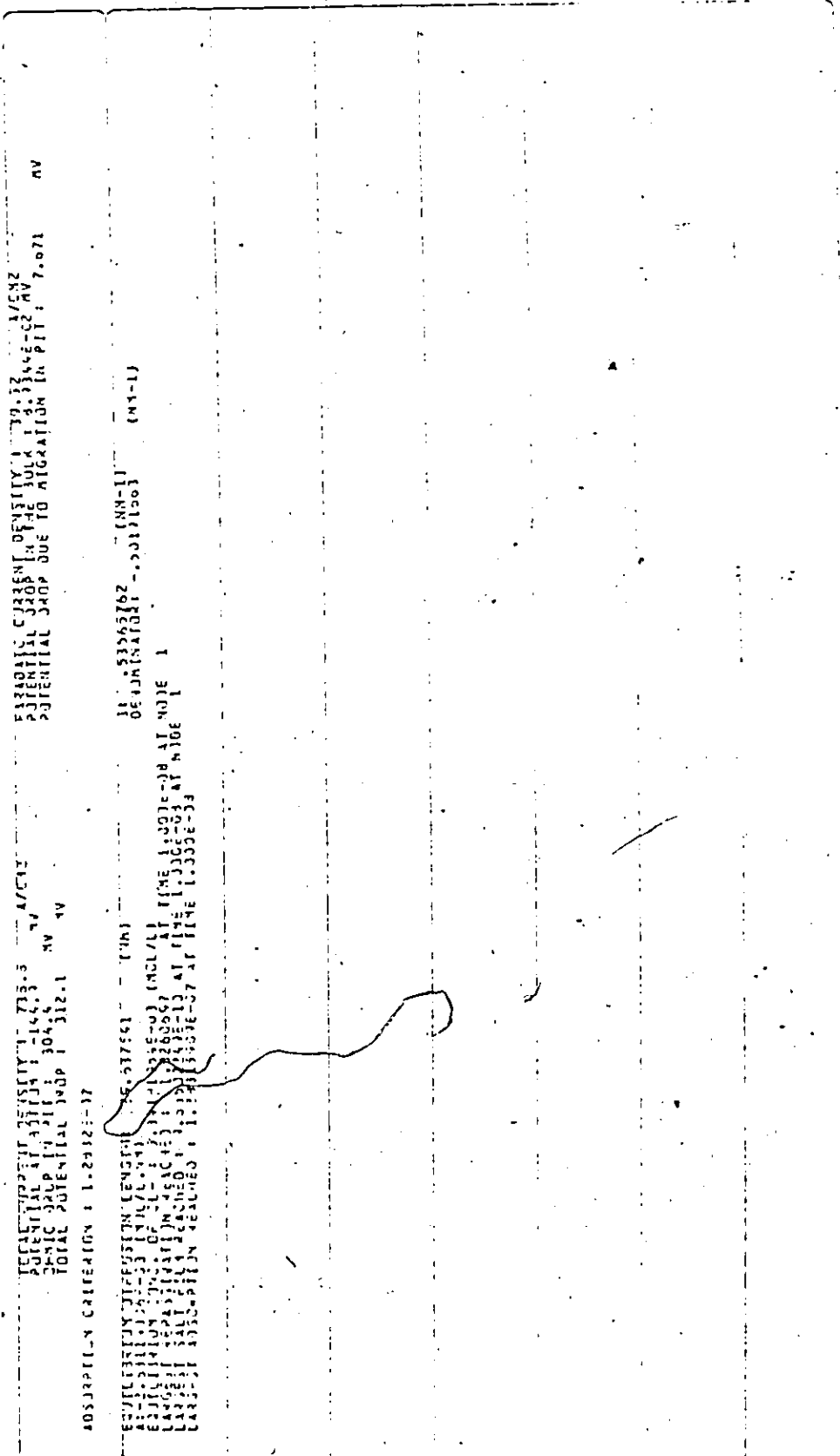


Figure 22 - Cont'd

in free format, which allows for more flexibility and clarity. The meaning of each input variable is indicated in the line of comments immediately above. When, as is often the case, the initial concentrations in the pore are identical everywhere and equal to the bulk concentration, only the first values need be supplied and the same values are placed in the proper arrays (140-151). The same is true for the values of the arrays RTOL and ATOL (113-125) which control the error in LSODE (see 6-3).

Some changes are made from the input and output units to the program units (250-268). For the variables for which this is the case, the two set of units are indicated in the comments at the beginning of the program, together with the units of most of the other variables.

The node grid is established by computing the values for the arrays RA (distance from the metal-surface) and R (radius of curvature), as well as the three step sizes (DR1, DR2 and DR3) corresponding to the three different zones (269-318). Various parameters depending on these step sizes are also computed for the subroutines DERIV and CALC; these are the variables with names starting with DR and the array D3.

Various constants without precise physical meaning are computed in MAIN and transferred to one or various subroutines to avoid repetitions of identical calculations. The meaning of most of these constants is indicated in the

comments at the beginning of MAIN or of the respective sub-routines (319-338).

Since all the calculations are made on the main concentrations and these are the only ones specified in the input, all the others have to be calculated (339-349).

The conductivity and transfer coefficients for the bulk composition are calculated (350-361), as well as the ohmic drop in the bulk of the solution (362-369).

The values of the dimensions of the work arrays of LSODE are computed (370-382) as well as the half-bandwidth of the banded jacobian MB.

The values of the variables necessary to draw the graphs of the results are recorded on file PITGRA (383-388).

Finally, the computed constants are printed (389-405) and subroutine DRIVER is called (414). Immediately before and after the call to DRIVER, the values characterizing the run (406-408) and the last values obtained for the variables (415) are recorded on file MRGOUT, in case it is desired to carry further the calculations at a later date. MRGOUT can then be accessed and the final values obtained previously can be used as the new starting point.

A-2 Subroutine DRIVER (Figure 23)

After computation of all the concentrations (56), the values of some of the variables are stored for printing

```

SUBROUTINE DRIVER (IWORK(1), IWORK(2), IWORK(3), IWORK(4), IWORK(5), ISTATE)
  THIS SUBROUTINE CONTROLS THE CALLS TO LSODE, CHECKS THE
  DEGREE OF SATURATION, PROVIDES THE ERROR S, CHECKS THE RUNNING
  TIME AND PRINTS THE RESULTS.
  PRECISION OF CONCENTRATIONS FOR DECISION ON STEADY STATE IS
  FIXED AT 5E-4
  .....
  PARAMETER (N=10, NSP=10, NMC=1)
  PARAMETER (NMC=10, NMC=10, NMC=1)
  COMMON /DM1/ T, I, IFLIM, IFL, KSP, P, C, SP, ATOL, NEQ, RTOL, NEQ1,
    IFLIM1, MACH, IFL, IFLP, IFLP, IFLP, IFLP, IFLP, IFLP, IFLP, IFLP,
  COMMON /C1/ C1, C2, C3, C4, C5, C6, C7, C8, C9, C10, C11, C12, C13, C14, C15, C16, C17, C18, C19, C20, C21, C22, C23, C24, C25, C26, C27, C28, C29, C30, C31, C32, C33, C34, C35, C36, C37, C38, C39, C40, C41, C42, C43, C44, C45, C46, C47, C48, C49, C50, C51, C52, C53, C54, C55, C56, C57, C58, C59, C60, C61, C62, C63, C64, C65, C66, C67, C68, C69, C70, C71, C72, C73, C74, C75, C76, C77, C78, C79, C80, C81, C82, C83, C84, C85, C86, C87, C88, C89, C90, C91, C92, C93, C94, C95, C96, C97, C98, C99, C100, C101, C102, C103, C104, C105, C106, C107, C108, C109, C110, C111, C112, C113, C114, C115, C116, C117, C118, C119, C120, C121, C122, C123, C124, C125, C126, C127, C128, C129, C130, C131, C132, C133, C134, C135, C136, C137, C138, C139, C140, C141, C142, C143, C144, C145, C146, C147, C148, C149, C150, C151, C152, C153, C154, C155, C156, C157, C158, C159, C160, C161, C162, C163, C164, C165, C166, C167, C168, C169, C170, C171, C172, C173, C174, C175, C176, C177, C178, C179, C180, C181, C182, C183, C184, C185, C186, C187, C188, C189, C190, C191, C192, C193, C194, C195, C196, C197, C198, C199, C200, C201, C202, C203, C204, C205, C206, C207, C208, C209, C210, C211, C212, C213, C214, C215, C216, C217, C218, C219, C220, C221, C222, C223, C224, C225, C226, C227, C228, C229, C230, C231, C232, C233, C234, C235, C236, C237, C238, C239, C240, C241, C242, C243, C244, C245, C246, C247, C248, C249, C250, C251, C252, C253, C254, C255, C256, C257, C258, C259, C260, C261, C262, C263, C264, C265, C266, C267, C268, C269, C270, C271, C272, C273, C274, C275, C276, C277, C278, C279, C280, C281, C282, C283, C284, C285, C286, C287, C288, C289, C290, C291, C292, C293, C294, C295, C296, C297, C298, C299, C300, C301, C302, C303, C304, C305, C306, C307, C308, C309, C310, C311, C312, C313, C314, C315, C316, C317, C318, C319, C320, C321, C322, C323, C324, C325, C326, C327, C328, C329, C330, C331, C332, C333, C334, C335, C336, C337, C338, C339, C340, C341, C342, C343, C344, C345, C346, C347, C348, C349, C350, C351, C352, C353, C354, C355, C356, C357, C358, C359, C360, C361, C362, C363, C364, C365, C366, C367, C368, C369, C370, C371, C372, C373, C374, C375, C376, C377, C378, C379, C380, C381, C382, C383, C384, C385, C386, C387, C388, C389, C390, C391, C392, C393, C394, C395, C396, C397, C398, C399, C400, C401, C402, C403, C404, C405, C406, C407, C408, C409, C410, C411, C412, C413, C414, C415, C416, C417, C418, C419, C420, C421, C422, C423, C424, C425, C426, C427, C428, C429, C430, C431, C432, C433, C434, C435, C436, C437, C438, C439, C440, C441, C442, C443, C444, C445, C446, C447, C448, C449, C450, C451, C452, C453, C454, C455, C456, C457, C458, C459, C460, C461, C462, C463, C464, C465, C466, C467, C468, C469, C470, C471, C472, C473, C474, C475, C476, C477, C478, C479, C480, C481, C482, C483, C484, C485, C486, C487, C488, C489, C490, C491, C492, C493, C494, C495, C496, C497, C498, C499, C500, C501, C502, C503, C504, C505, C506, C507, C508, C509, C510, C511, C512, C513, C514, C515, C516, C517, C518, C519, C520, C521, C522, C523, C524, C525, C526, C527, C528, C529, C530, C531, C532, C533, C534, C535, C536, C537, C538, C539, C540, C541, C542, C543, C544, C545, C546, C547, C548, C549, C550, C551, C552, C553, C554, C555, C556, C557, C558, C559, C560, C561, C562, C563, C564, C565, C566, C567, C568, C569, C570, C571, C572, C573, C574, C575, C576, C577, C578, C579, C580, C581, C582, C583, C584, C585, C586, C587, C588, C589, C590, C591, C592, C593, C594, C595, C596, C597, C598, C599, C600, C601, C602, C603, C604, C605, C606, C607, C608, C609, C610, C611, C612, C613, C614, C615, C616, C617, C618, C619, C620, C621, C622, C623, C624, C625, C626, C627, C628, C629, C630, C631, C632, C633, C634, C635, C636, C637, C638, C639, C640, C641, C642, C643, C644, C645, C646, C647, C648, C649, C650, C651, C652, C653, C654, C655, C656, C657, C658, C659, C660, C661, C662, C663, C664, C665, C666, C667, C668, C669, C670, C671, C672, C673, C674, C675, C676, C677, C678, C679, C680, C681, C682, C683, C684, C685, C686, C687, C688, C689, C690, C691, C692, C693, C694, C695, C696, C697, C698, C699, C700, C701, C702, C703, C704, C705, C706, C707, C708, C709, C710, C711, C712, C713, C714, C715, C716, C717, C718, C719, C720, C721, C722, C723, C724, C725, C726, C727, C728, C729, C730, C731, C732, C733, C734, C735, C736, C737, C738, C739, C740, C741, C742, C743, C744, C745, C746, C747, C748, C749, C750, C751, C752, C753, C754, C755, C756, C757, C758, C759, C760, C761, C762, C763, C764, C765, C766, C767, C768, C769, C770, C771, C772, C773, C774, C775, C776, C777, C778, C779, C780, C781, C782, C783, C784, C785, C786, C787, C788, C789, C790, C791, C79
```

Figure 23 - Subroutine Driver

ONLY COPY AVAILABLE
SEULE COPIE DISPONIBLE

```

107 7 IF (NOT (C(1,1) .GT. 0.04 .AND. C(1,2) .GT. 0.01) GOTO 5
108 IF (C(1,1) .LT. 0.1) GOTO 2
109 PRINT 909,N
110 FORMAT('3***** JITTERS CLOSE TO STATION AT NODE',I3)
111 STPNEX = 0.2 * (1. - C(1,1)) * TINT / (C(1,1) + REPACLI)
112 IF (C(1,1) .LT. 0.1) GOTO 12
113 PRINT 909,N
114 STPNEX = 0.2 * (1. - C(1,1)) * TINT / (C(1,1) + REPACLI)
115 5 CONTINUE
116 IF (NSAT .EQ. 1) S1 = REPACLI
117 IF (NSAT .EQ. 2) S1 = C(1,1)
118 12 CONTINUE
119 CONTINUE
120 .....
121 ..... LOOKING FOR STEADY STATE .....
122 .....
123 TOLD = TOLD + 1E-12
124 IF (C(1,1) .GT. COLD * (T/TOLD)) GOTO 1
125 IF (C(1,1) - COLD * (T/TOLD)) .GT. 0.1 GOTO 1
126 IF (C(1,1) - COLD * (T/TOLD)) .GT. 0.1 GOTO 1
127 IF (C(1,1) - COLD * (T/TOLD)) .GT. 0.1 GOTO 1
128 IF (C(1,1) - COLD * (T/TOLD)) .GT. 0.1 GOTO 1
129 IF (C(1,1) - COLD * (T/TOLD)) .GT. 0.1 GOTO 1
130 PRINT 902,N
131 PRINT 902,N
132 103 FORMAT('3***** STEADY STATE REACHED')
133 CALL PRIN
134 GOTO 899
135 3 CONTINUE
136 TOLD = TOLD + 1E-12
137 .....
138 ..... IS THE PROGRAM PROCESSING TAKING TOO LONG ? .....
139 IF (T .LE. TIMLI) GOTO 1
140 PRINT 906,N
141 FORMAT('3***** TIME 1',F10.3, ': LIMIT EXCEEDED')
142 CALL PRIN
143 GOTO 899
144 CONTINUE
145 .....
146 ..... NORMAL PRINTING .....
147 IF (T .EQ. RWORX(1)) GOTO 6
148 PRINT 902,N
149 402 FORMAT('3***** TIME 1',F10.3)
150 CALL PRIN
151 6 CONTINUE
152 .....
153 ..... FIXING NEXT TIME STEP .....
154 IF (T .LT. T2) GOTO 106
155 IF (NSAT .EQ. 1) THEN
156 IF (MOD(KOUNT, 10) .EQ. 0) THEN
157 T2 = T * 10.
158 T2 = T2
159 ELSE
160 T2 = T * TINC
161 ENDOF
162 ELSE
163 T2 = T * STPNEX
164 ENDOF
165 KOUNT = KOUNT + 1
166 106 CONTINUE
167 IF (TASK .EQ. 4) THEN
168 T1 = MIN(T2, RWORX(1))
169 ELSE
170 T1 = T2
171 ENDOF
172 101 CONTINUE
173 .....
174 ..... LOOP ENDED .....
175 .....
176 PRINT 907, MAXOUT
177 907 FORMAT('3***** SUBROUTINE DRIVER',F10.3, ': MAXIMUM NUMBER OF OUTPUT',F10.3, ' REACHED')
178 899 CONTINUE
179 PRINT 903, C(1,1) * SUPSSF, RLP(1) * SUPSRP
180 910 FORMAT('3***** SALT FILM S.P. 1',F10.3, ': REPASSIVATION S.P. 1',F10.3)
181 RETURN
182 END

```

Figure 23 - Cont'd

ONLY COPY AVAILABLE
SEULE COPIE DISPONIBLE

in common blocks (57-65). If subroutine LSODE indicates an abnormal condition ($ISTATE < 0$), a message is printed, together with the current results, and the run is terminated (66-75).

If precipitation is reached for the species which form either the salt film ($FeCl_2$) or the repassivation of the film ($FeOH_2$), the current results are printed, indicating which process occurred and where it occurred in the pore, and the run is then terminated (76-103). Precipitation is detected when either $REPA(N)$ or $SAFI(N)$ are equal to 1. These quantities represent the concentrations of the passivating and salt film forming species, respectively, divided by the product of the saturation concentration by the supersaturation ratio (see MAIN, 337-338). The time at which the event occurred (TAU) is computed by linear interpolation (98). When this feature is not desirable, the supersaturation ratio SUPSRP and SUPSSF can be increased by a suitable order of magnitude.

In order to improve the precision on the determination of TAU above, the time interval between two outputs can be reduced when the process approaches precipitation (104-121). The time interval starts to decrease when $REPA(N)$ or $SAFI(N)$ reach 0.1. When this feature is not desired, the flag DETSAT is set to FALSE in the input.

The steady state is deemed to be reached when all the conditions listed in 6-1 are met. When this is the

case, a message is printed, together with the current results, and the run is terminated (122-137). Similarly, the program will stop after suitable printing when the running time becomes larger than the limit TIMLIM.

Then the current results are printed through a call to PRIN (148-155) and the next time value is fixed (156-177). Normally, the program is set up so that a fixed number of output NO is obtained per decade of time, i.e. the new time value is the old time value multiplied by the factor TINC (165) where:

$$TINC = (10)^{1/NO} \quad (\text{line 35})$$

Finally, when the maximum number of outputs MAXOUT is reached before any of the above events occur, a message is printed and the program stops.

A-3 Subroutine CALC (Figure 24)

A system was established, which allows the printing of some of the variables computed in CALC when this subroutine is called by LSODE (41-50). The number of calls to CALC is counted, and when a print-out of the detailed calculations performed in CALC is desired, NPEEK in input is set equal to the quantity desired and the array IPEEK is loaded with the values of the call number desired.

After computation of the concentrations (51-68), the

```

.....
THIS SUBROUTINE COMPUTES THE NEW CONCENTRATIONS (OUTPUT)
CORRESPONDING TO THE NEW VALUES OF DEL (INPUT). IT IS CALLED
AT CLOS2.
PARAMETERS COMPUTED IN MAIN
FIX = CURRENT DENSITY COEFF. IN SILVANOSE.
      FIXED POTENTIAL IN POTENTIALS
      DX1 = RT/F
      DX2 = 1/F
      DX3 = RT/F2
      DX4 = A * Z / 2
.....
PARAMETER: R(NNN)=13, NSPM=13, NNCN=1
PARAMETER: Z(NNN)=1, NNCN=1, NNCN=1, NNCN=1, NNCN=1
COMMON /CAL/ Z2(NSPM), Z2(NSPM), Z2(NSPM), Z2(NSPM), Z2(NSPM),
      RESI, CAP, FIX, DX1, DX2, DX3, DX4,
      DRIS2, RRZ(NNN), IPEEK(13), NPEEK, POTSTA
COMMON /C121/ RESOL
COMMON /C123/ Z(NSPM)
COMMON /C1269A/ C(NSPM, NNN), NSPEC, E, CO
COMMON /C1259A/ NN
COMMON /C1277/ R(NNN)
COMMON /C1257/ NN1, NN2
COMMON /C26/ ITP
COMMON /C24/ Q1, Q2, SL, COI, COJ, EQ, DE
COMMON /C24/ TRANS(NSPM, NNN)
DIMENSION BINTEG(NNN), DOC(NSPM, NNN), DELP(NNN), SIG1(NNN),
      AINTEG(NNN), CLEP(NNN), JC(NSPM, NNN), C12(NEQU)
LOGICAL NCPROT, POTSTA
SAVE /C26/, /C24/, /C26A/, ITC, NCPROT
DATA BINTEG(1), ITC, DOC(1,1), J, NNCN(1,1)
NAMELIST /RES2/ DELP, COI, VGM, SL
NAMELIST /RES34/ DC, Q1, BINTEG, Q2, A, E
.....
ITLST = 1
      ADJUST FOR POSSIBLE DETAIL PRINT OUT
ITC = ITC
IF (NPEEK.EQ.0) GOTO 100
IF (ITC.NE.IPEEK(1)) GOTO 100
NCPROT = .FALSE.
ITP = ITP
IF (ITP.GT.NPEEK) NPEEK =
100 CONTINUE
.....
(1) COMPUTATION OF THE CONCENTRATIONS
.....
CALL CONC (C12, NEQU)
COI = CO
IF (NCPROT) GOTO 1
PRINT 900, I, ITC
N = 1
DO 102 N=1, NN
      NE = NE + 1
      PRINT 901, N, (C(I, N), I=1, NSPEC)
100 CONTINUE
PRINT 902, E * E3, CO * 1E-7
CONTINUE
.....
(2) COMPUTATION OF DEL=SUM OF Z2(I)C(I,1) (QUASI-CONDUCTIVITY)
      JELP(N) = 1/DEL AND COEFFICIENTS DESCRIBING SURFACE CONDITIONS
      CO2 = SUM( Z2(I) C(I,1) )
      VGM = 1/F * (C(1,1)/CO2 - D(1))
      SL = 3/2 * RT/F * (1/CO2 * D(1) - 1/DEL(1))
.....
DO 200 N=2, NN-1
      S = 0
      DO 201 I=1, NSPEC
            S = S + Z2(I) * C(I, N)
201 CONTINUE
      JELP(N) = 1/S.
200 CONTINUE
      DELP(NN) = RESI
      DEL1 = 0.
      CO2 = 0.
      DO 202 I=1, NSPEC
            CO2 = CO2 + Z2(I) * C(I, 1)
            DEL1 = DEL1 + Z2(I) * C(I, 1)
202 CONTINUE
      DELP(1) = 1/DEL1
      VGM = DX2 * (DELP(1)/CO2 * D(1) - 1.)
      SL = VGM * DELP(1) + DRIS2 * DX1
      IF (NCPROT) GOTO 12
      PRINT RES2
12 CONTINUE
.....
(3) COMPUTATION OF CONCENTRATION GRADIENTS
.....
CALL DERIV(C, DC, DOC, NSPM, NSPEC - 1)
CONVERSION FROM DC/DLOGR TO DC/DR
DO 302 N=NN1, NN2+1, NN

```

Figure 24 - Subroutine CALC

ONLY COPY AVAILABLE
SEULE COPIE DISPONIBLE


```

      DO 303 I=1, NSPEC-1
      DCC(I,N) = (DCC(I,N) - DCC(I,N)) * RZ(N)
      DCC(I,N) = DCC(I,N)/Z(I)
303 CONTINUE
302 CONTINUE
      DO 300 N=2, NN
      S = 0.
      S1 = 0.
      DO 301 I=1, NSPEC-1
      S = S + Z(I)*DCC(I,N)
      S1 = S1 + Z(I)*DCC(I,N)
301 CONTINUE
      DCC(NSPEC,N) = - S/Z(NSPEC)
      DCC(NSPEC,N) = -S1/Z(NSPEC)
300 CONTINUE
.....
(4) COMPUTES SIG1(N) = SUM OF Z(I)(DCC(I)-C(I))DCC(I,N),
      INTEGRAND = SIG1(N)/DEL(N)
      INTEGRAND
      THE COEFFICIENT OF OHMIC DROP IN THE PIT, AND A FIRST
      APPROXIMATION OF QA, THE COEFFICIENT FOR MIGRATION DROP IN
      THE PIT.
.....
      COMPUTATION OF SIG1 AND INTEGRAND FOR 1
      DO 401 I=2, NSPEC
      S = S + Z(I)*DCC(I,N)
401 CONTINUE
      SIG1(N) = S
      INTEGRAND = S * DEL(N)
400 CONTINUE
.....
      COMPUTATION OF AINTEGRAND IN THE 3 DIFFERENT ZONES
      DO 403 N=1, NN2
      AINTEGRAND = DEL(N)
403 DO 404 I=NN2+1, NN*NN2
      AINTEGRAND = DEL(N)*(1. - FLOAT(N-NN2)*0.5/FLOAT(NN2))
404 DO 405 N=NN2+1, NN
      AINTEGRAND = DEL(N) * DX4 * RZ(N)
405 CONTINUE
      INTEGRATE FOR QA AND Q42.
      CONVERT QA TO OHM.CM3/CM AND Q42 TO V
      CALL INTEG(AINTEGRAND, NN, Q42)
      CALL INTEG(BINTEGRAND, NN, Q42)
      QA = QA * DX1
      Q42 = Q42 * DX1
.....
(5) COMPUTES THE TOTAL CURRENT DENSITY
.....
      IF (POTST) THEN
      F12 = Q42 - SL*CO
      S = RZSOL * QA
      COT = (A - C)/B
      ELSE
      COT = FIX
      ENDIF
      IF (NOPROT) GOTO 3
      PRINT RES14
3 CONTINUE
.....
(6) CONCENTRATION GRADIENTS AT INTERFACE AND SIG1(1)
      XX2 = CO1*CO2URF = COSJRF/D(1)*F*CO2
.....
      IF (NOPROT) GOTO 15
      ORHIC = (Q42 * SL*CO1 * 123
      ORSOL = RESOL * COT * 123
      DROHM = CA * 123 * COT
      DROCT = ORHIC + ORSOL + DROHM
      PRINT 303, COT*1E-7, ORSOL, DROHM, DROCT
10 CONTINUE
      XX2 = CO*DX2 / (CO2*D(1))
      DO 601 I=1, NSPEC
      DCC(I,1) = Z(I) * C(I,N) * XX2
601 CONTINUE
      DCC(1,1) = DCC(1,1) - CO*XX2 / (Z(1)*D(1))
      SIG1(1) = VGH * CO
      IF (NOPROT) GOTO 10
      PRINT 904, CO, COT, XX2
      PRINT 905
      DO 602 N=1, NN
      PRINT 901, N, SIG1(N), (DCC(I,N), I=1, NSPEC)
602 CONTINUE
10 CONTINUE
.....
(7) CORRECTION OF THE SECOND DERIVATIVE AT NODE 1
.....
      S = 0.
      DO 701 I=1, NSPEC-1
      DCC(I,1) = (DCC(I,1) - DCC(I,1))/((2.*D(12)) - DCC(I,1))/D(12)
      S = S + Z(I)*DCC(I,1)
701 CONTINUE
      DCC(NSPEC,1) = - S/Z(NSPEC)
      IF (NOPROT) GOTO 17
      PRINT 906
      DO 702 N=1, NN
      PRINT 901, N, (DCC(I,N), I=1, NSPEC)
702 CONTINUE

```

Figure 24 - Cont'd

ONLY COPY AVAILABLE
SEULE COPIE DISPONIBLE

conductivity is obtained, as well as its ~~reverse~~, and various other variables (69-98).

Then, the first and second derivatives of the concentrations of all species but one are computed by calling DERIV (99-102), the values obtained are corrected in the spherical field (103-111) and the derivatives of the concentration of the last species is computed by difference (112-121).

The integrals necessary to compute the potential differences due to the electric resistance (QA) and to the concentration gradient (QB2) are computed (122-159) as outlined in 5-5.

The total current density (sum of the faradaic current density and of the current necessary to charge the double layer) is computed next (160-174) as outlined in 5-6.

At the metal-solution interface, the flux of all the dissolved species is null and Faraday's Law is obeyed (see 5-4). This implies a relation between the concentrations and their derivatives which forms one boundary condition (175-198). The values of the second derivatives of the concentrations at the metal surface are then corrected for this modification of the first derivatives (199-214):

Finally, the values of T_1 (equation 5-6¹, 5-3) are obtained in the regions of planar diffusion (215-245) and in the region where the diffusion is spherical (246-266) and

these values are used by DCDT (270) to form the array C12PRM of the time derivatives of the concentrations.

A-4 Subroutine PRIN (Figure 25)

Most of the operations performed in this subroutine are self-evident from the listing and consist of the printing of the values just calculated by LSODE. An example of output is shown on Figure 22. Just as in MAIN, when PRTDET is TRUE, a more detailed printout is obtained, displaying the time derivatives of the concentrations.

Additionally, the largest encountered value of the supersaturation ratios is recorded and the corresponding time and location are printed (49-62, 101-104).

The values obtained in the last call to CALC are also saved and used here to compute the various potential drops in the solution (73-81). It must be noted that these values are those obtained at a time TLAST which is in general slightly larger than the time T at which the output of LSODE is obtained. LSODE performs the calculations (through CALC) up to a time TLAST greater than the time T requested for the output and interpolates back to T.

The value of K_{ads1} is also computed here (ADS), as well as its maximum (82-91). Line 86 is the only line of this subroutine which would have to be changed in case of a change of chemical system. This calculation could also be easily transferred to CONC or DCDT which are the only two


```

1-
2-
3-
4-
5-
6-
7-
8-
9-
10-
11-
12-
13-
14-
15-
16-
17-
18-
19-
20-
21-
22-
23-
24-
25-
26-
27-
28-
29-
30-
31-
32-
33-
34-
35-
36-
37-
38-
39-
40-
41-
42-
43-
44-
45-
46-
47-
48-
49-
50-
51-
52-
53-
54-
55-
56-
57-
58-
59-
60-
61-
62-
63-
64-
65-
66-
67-
68-
69-
70-
71-
72-
73-
74-
75-
76-
77-
78-
79-
80-
81-
82-
83-
84-
85-
86-
87-
88-
89-
90-
91-
92-
93-
94-
95-
96-
97-
98-
99-
100-
101-
102-
103-
104-
105-
106-
107-
108-
109-
110-
111-
112-
113-
114-
115-
116-
117-
118-
119-
120-
121-
122-
123-
124-
125-
126-
127-
128-
129-
130-
131-
132-
133-
134-
135-
136-
137-
138-
139-
140-
141-
142-
143-
144-
145-
146-
147-
148-
149-
150-
151-
152-
153-
154-
155-
156-
157-
158-
159-
160-
161-
162-
163-
164-
165-
166-
167-
168-
169-
170-
171-
172-
173-
174-
175-
176-
177-
178-
179-
180-
181-
182-
183-
184-
185-
186-
187-
188-
189-
190-
191-
192-
193-
194-
195-
196-
197-
198-
199-
200-
201-
202-
203-
204-
205-
206-
207-
208-
209-
210-
211-
212-
213-
214-
215-
216-
217-
218-
219-
220-
221-
222-
223-
224-
225-
226-
227-
228-
229-
230-
231-
232-
233-
234-
235-
236-
237-
238-
239-
240-
241-
242-
243-
244-
245-
246-
247-
248-
249-
250-
251-
252-
253-
254-
255-
256-
257-
258-
259-
260-
261-
262-
263-
264-
265-
266-
267-
268-
269-
270-
271-
272-
273-
274-
275-
276-
277-
278-
279-
280-
281-
282-
283-
284-
285-
286-
287-
288-
289-
290-
291-
292-
293-
294-
295-
296-
297-
298-
299-
300-
301-
302-
303-
304-
305-
306-
307-
308-
309-
310-
311-
312-
313-
314-
315-
316-
317-
318-
319-
320-
321-
322-
323-
324-
325-
326-
327-
328-
329-
330-
331-
332-
333-
334-
335-
336-
337-
338-
339-
340-
341-
342-
343-
344-
345-
346-
347-
348-
349-
350-
351-
352-
353-
354-
355-
356-
357-
358-
359-
360-
361-
362-
363-
364-
365-
366-
367-
368-
369-
370-
371-
372-
373-
374-
375-
376-
377-
378-
379-
380-
381-
382-
383-
384-
385-
386-
387-
388-
389-
390-
391-
392-
393-
394-
395-
396-
397-
398-
399-
400-
401-
402-
403-
404-
405-
406-
407-
408-
409-
410-
411-
412-
413-
414-
415-
416-
417-
418-
419-
420-
421-
422-
423-
424-
425-
426-
427-
428-
429-
430-
431-
432-
433-
434-
435-
436-
437-
438-
439-
440-
441-
442-
443-
444-
445-
446-
447-
448-
449-
450-
451-
452-
453-
454-
455-
456-
457-
458-
459-
460-
461-
462-
463-
464-
465-
466-
467-
468-
469-
470-
471-
472-
473-
474-
475-
476-
477-
478-
479-
480-
481-
482-
483-
484-
485-
486-
487-
488-
489-
490-
491-
492-
493-
494-
495-
496-
497-
498-
499-
500-
501-
502-
503-
504-
505-
506-
507-
508-
509-
510-
511-
512-
513-
514-
515-
516-
517-
518-
519-
520-
521-
522-
523-
524-
525-
526-
527-
528-
529-
530-
531-
532-
533-
534-
535-
536-
537-
538-
539-
540-
541-
542-
543-
544-
545-
546-
547-
548-
549-
550-
551-
552-
553-
554-
555-
556-
557-
558-
559-
560-
561-
562-
563-
564-
565-
566-
567-
568-
569-
570-
571-
572-
573-
574-
575-
576-
577-
578-
579-
580-
581-
582-
583-
584-
585-
586-
587-
588-
589-
590-
591-
592-
593-
594-
595-
596-
597-
598-
599-
600-
601-
602-
603-
604-
605-
606-
607-
608-
609-
610-
611-
612-
613-
614-
615-
616-
617-
618-
619-
620-
621-
622-
623-
624-
625-
626-
627-
628-
629-
630-
631-
632-
633-
634-
635-
636-
637-
638-
639-
640-
641-
642-
643-
644-
645-
646-
647-
648-
649-
650-
651-
652-
653-
654-
655-
656-
657-
658-
659-
660-
661-
662-
663-
664-
665-
666-
667-
668-
669-
670-
671-
672-
673-
674-
675-
676-
677-
678-
679-
680-
681-
682-
683-
684-
685-
686-
687-
688-
689-
690-
691-
692-
693-
694-
695-
696-
697-
698-
699-
700-
701-
702-
703-
704-
705-
706-
707-
708-
709-
710-
711-
712-
713-
714-
715-
716-
717-
718-
719-
720-
721-
722-
723-
724-
725-
726-
727-
728-
729-
730-
731-
732-
733-
734-
735-
736-
737-
738-
739-
740-
741-
742-
743-
744-
745-
746-
747-
748-
749-
750-
751-
752-
753-
754-
755-
756-
757-
758-
759-
760-
761-
762-
763-
764-
765-
766-
767-
768-
769-
770-
771-
772-
773-
774-
775-
776-
777-
778-
779-
780-
781-
782-
783-
784-
785-
786-
787-
788-
789-
790-
791-
792-
793-
794-
795-
796-
797-
798-
799-
800-
801-
802-
803-
804-
805-
806-
807-
808-
809-
810-
811-
812-
813-
814-
815-
816-
817-
818-
819-
820-
821-
822-
823-
824-
825-
826-
827-
828-
829-
830-
831-
832-
833-
834-
835-
836-
837-
838-
839-
840-
841-
842-
843-
844-
845-
846-
847-
848-
849-
850-
851-
852-
853-
854-
855-
856-
857-
858-
859-
860-
861-
862-
863-
864-
865-
866-
867-
868-
869-
870-
871-
872-
873-
874-
875-
876-
877-
878-
879-
880-
881-
882-
883-
884-
885-
886-
887-
888-
889-
890-
891-
892-
893-
894-
895-
896-
897-
898-
899-
900-
901-
902-
903-
904-
905-
906-
907-
908-
909-
910-
911-
912-
913-
914-
915-
916-
917-
918-
919-
920-
921-
922-
923-
924-
925-
926-
927-
928-
929-
930-
931-
932-
933-
934-
935-
936-
937-
938-
939-
940-
941-
942-
943-
944-
945-
946-
947-
948-
949-
950-
951-
952-
953-
954-
955-
956-
957-
958-
959-
960-
961-
962-
963-
964-
965-
966-
967-
968-
969-
970-
971-
972-
973-
974-
975-
976-
977-
978-
979-
980-
981-
982-
983-
984-
985-
986-
987-
988-
989-
990-
991-
992-
993-
994-
995-
996-
997-
998-
999-
1000-

```

Figure 25 - Cont'd

subroutines which are system dependent.

Finally, output is made to file PITGRA which stores data useful for graphic representation (107-110).

A-5 Subroutine DERIV (Figure 26)

The formulae used for most of the points are the usual finite different formulae for the derivatives (20-21) (for instance James et al, 1977). All the errors due to the neglected terms in the formulae chosen are proportional to the square of the grid step. In the cases where no formulae could be found because the intervals were unequal, the relevant formulae were derived according to the method of Conte and de Boor (1980, p. 295) and introduced (50, 51). The respective coefficients were computed in MAIN and passed through the common block /DER/ in array D3.

A-6 Subroutine INTEG (Figure 2.7)

This subroutine computes the integral of a function Y defined as an array, over the NN intervals of the spatial grid, taking into account the three different regions (see 5-8). The formulae used are the simple trapezoidal formulae (Conte and de Boor, 1980, p. 305). Although there are much more sophisticated ways to integrate numerically, these formulae are reasonably fast and they give an error which is of the same order as the error on the derivation formulae.

[illegible]

5.


```

SUBROUTINE INTEG(Y,NN,C)
.....
COMPUTES SUP(Y,DR) = C
.....
PARAMETER(NNN=100)
COMMON /C127/ F(NNN)
COMMON /C125/ NN1,NN2
COMMON /INT/ DR1,DR2,DR3
DIMENSION Y(NNN)
.....
      TRAPEZOIDAL MODIFIED
      ERROR PROP. TO DR**2
.....
      S = 0
      DO 200 N=2,NN1-1
        S = S + Y(N)
200 CONTINUE
      Q1 = DR1*(Y(1) + Y(NN1) + 2.*S)

      S = 0
      DO 201 N=NN1+1,NN1+NN2-1
        S = S + Y(N)
201 CONTINUE
      Q2 = DR2*(Y(NN1) + Y(NN1+NN2) + 2.*S)

      S = 0
      DO 202 N=NN1+NN2+1,NN-1
        S = S + Y(N)*R(N)
202 CONTINUE
      Q3 = DR3*(Y(NN1+NN2)*S(NN1+NN2) + Y(NN)*S(NN) + 2.*S)
      C = (Q1 + Q2 + Q3)*0.5
      RETURN
      END

```

Figure 27 - Subroutine INTEG

ONLY COPY AVAILABLE
SEULE COPIE DISPONIBLE

A-7 Subroutine CONC (Figure 28)

Lines 34-37, 46-52 and 55 of this subroutine may have to be changed whenever a change in the chemical system is introduced.

The array C12 of dimension NEQU is passed as argument of the subroutine. It contains the solution of the NEQU equations solved simultaneously by LSODE. The NEQU variables computed are the concentrations of the NMC (= 4) main components at the NN nodes and the potential at node 1 ($NEQU = NN * NMC + 1$). Therefore, the content of C12 is the following:

C12(1): Potential at metal/solution interface (E).

C12(2) to C12(5): Concentrations of the NMC main components at node 1.

C12(6) to C12(9): Concentrations of the NMC main components at node 2.

.....

C12($NEQU - NMC + 1$) to C12(NEQU): Concentrations of the NMC main components at node NN.

The concentration of species I at node N is stored in the array C(I,N). The transfer of the values from C12 to C(I,N) (34-37), as well as the computation of the remaining concentrations (46-52), is done for each node in a DO loop (32-53).

```

SUBROUTINE CONC (C12,N,N1)
.....
      FE IN BORATE BUFFER + CHLORIDE
.....
      COMPUTATION OF THE CONCENTRATIONS FROM THE C12 ARRAY.
      N120 = N120 + N120 * N120, MAIN COMPONENTS * 1
      C12(1) = POTENTIAL AT NOTCH.
      OTHER C12 = CONCENTRATIONS OF THE MAIN COMPONENTS AT NODES
      UNITS :
      C AND C12 : MOLE/CM3 = 1E-5 MOL/L
      CD : A*MM/CM3 = 1E-7 A/CM2
.....
      CAUTION
      THE VALUES OF XK AND CK MUST BE CONSISTENT WITH UNITS OF MOL/CM3
      AND A*MM/CM3 FOR CONCENTRATIONS AND CURRENT DENSITY (RESP.)
.....
      PARAMETER (N120=10, NSPH=10, NMCH=4)
      PARAMETER (NMCH=NSPH-3)
      COMMON /C126-9/ C(NSPH,N120), NSPEC, CO
      COMMON /C123/ Z(NSPH)
      COMMON /C124-9/ NMC
      COMMON /C124/ XK(NMCH), CK(7), XX1
      COMMON /C124/ IYST(N120)
      DIMENSION C12(N120)
      SAVE /C124/

      N = 0
      DO 1 NE = 2, N120 - NMC + 1, N120
        N = N + 1
        C12(N) = C12(N)
        C12(N) = C12(N) + 1
        C12(N) = C12(N) + 2
        C12(N) = C12(N) + 3
        DO 3 J = 1, NMC
          IF (C12(N).GT.0.1) GO TO 3
          C12(N) = 1E-18
          PRINT 900,J,N
          FORMAT(1H, 'C12(12) = 1E-18', 12)
          ..... (SUBROUTINE CONC)
        3 CONTINUE
        C12(N) = XK(1) / C12(N)
        C12(N) = C12(N) * C12(N) * XK(2)
        C12(N) = XK(3) * C12(N) * C12(N)
        C12(N) = XK(5) * C12(N) * C12(N)
        C12(N) = 2. * C12(N) * C12(N) * C12(N) * C12(N)
        C12(N) = C12(N) - C12(N)
        C12(N) = XK(4) * C12(N) * C12(N) * C12(N)
        1 CONTINUE
      C = C12(1)
      A = CK(1) + CK(2) / (CK(3) * C12(1)) + CK(4) * C12(1)
      CD = A * EXP(XX1 * E)
      K12 = N
      END

```

Figure 28 - Subroutine CONC

Wranglen, G. (1969), Corros. Sci., 9, 585.

Wranglen, G. (1974), Corros. Sci., 14, 33.1

Yoshii, T., and Hisamatsu, Y. (1972), J. Japan. Inst.
Metals, 36, 750.

A possible source of error is the calculation of the remaining concentrations (46-52). Since the concentration of one species has to be computed by difference to satisfy the electro-neutrality condition (5-2, equation 5-1), it is important to choose this species so that its concentration is never small compared to the largest of the other concentrations. Otherwise, the calculation will involve at some point the subtraction of two nearly equal numbers and this operation introduces large errors (McCracken and Dorn, 1964, p. 64). When a new chemical system is introduced, these numerical errors may occur and cause some of the computed main components to have negative values. As a diagnostic tool, this condition is detected at line 39, the negative value is replaced by an arbitrary small value 10^{-18} and a message is printed.

In the present case, the main components are (in this order) Fe^{2+} , H^+ , Na^+ and $\text{B}(\text{OH})_3$, as these are the first NMC species listed in the input (Figure 21). $[\text{OH}^-]$, $[\text{Fe}(\text{OH})^+]$, $[\text{Fe}(\text{OH})_2]$ and $[\text{B}(\text{OH})_4^-]$ are computed using the equilibrium formulae mentioned in 5-2 and 5-7-2. $[\text{Cl}^-]$ is computed by difference and then $[\text{FeCl}_2]$ is obtained using the equilibrium between Fe^{2+} and Cl^- . This is possible because FeCl^+ has not been taken into account and also because FeCl_2 being neutral, it is not necessary for the computation of $[\text{Cl}^-]$. Earlier attempts at compute $[\text{Na}^+]$ by difference led to large errors and negative $[\text{Na}^+]$ values, as

$[\text{Na}^+]$ can be as low as 10^{-6} M, while $[\text{Fe}^{2+}]$ and $[\text{Cl}^-]$ are about 10 M.

The potential E is used together with the concentrations to obtain the faradaic current density CD through the chosen formula (55-56) using the constants CK passed in the common block /C134/- for that purpose.

A-8 Subroutine DCDT (Figure 29)

The values of $\text{TRANS}(I,N)$ ($= T_1$) corresponding to each species at each node are passed in the common block /C24/ and used in this subroutine to compute the values of the array C12PRM of dimension NEQU in the argument. The computation is done for each node in a manner similar to that done in CONC. The content of C12PRM is distributed identically to the content of C12 in CONC, with the difference that it now contains the time derivatives of the variables contained in C12.

We use here the following subscripts to designate the different species (these numbers also correspond to the order of the species in the input and in $C(I,N)$):

Fe^{2+}	: 1	FeOH^+	: 6
H^+	: 2	$\text{Fe}(\text{OH})_2$: 7
Na^+	: 3	FeCl_2	: 8
$\text{B}(\text{OH})_3$: 4	$\text{B}(\text{OH})_4^-$: 9
OH^-	: 5	Cl^-	: 10

```

.....
SUBROUTINE DCDT (C12PRM, NEQU)
.....
      GIVEN TRANS(I,N) COMPUTES DC/DT
      DEPENDS ON THE CHEMICAL SYSTEM.
.....
      PA=4 C12PRM(NM)=131, NSPM=10, NMCH=1
      PA=4 C12PRM(NM)=131, NSPM=10, NMCH=1
      COMMON /C12PRM/ C12PRM(NM), NSPM, NMCH, NSP=1-31
      COMMON /C12PRM/ X(INDCM), CK(7),XX1
      COMMON /C12PRM/ HMC
      COMMON /C12PRM/ TRANS(NSPM,NM)
      COMMON /C12PRM/ ISYST(NM)
      COMMON /C12PRM/ CP(NM)
      DIMENSION C12PRM(NM)
      SAVE /C12PRM/
      DATA CP/NMCH*0./

      N=6
      DC 1 NE=2, NEQU-2*NMC + 1, NMC
      N = N+1
      YP1 = TRANS(1,N) + TRANS(3,N) + TRANS(5,N) + TRANS(7,N)
      YP2 = TRANS(6,N) + TRANS(8,N) + 2.*TRANS(7,N) - TRANS(2,N) +
      TRANS(9,N)
      YP10 = TRANS(10,N) + 2.*TRANS(11,N)
      YP4 = TRANS(4,N) + TRANS(9,N)
      C12PRM(NE+2) = CP(NE+2) = YP2 + YP10 - 2.*YP1
      A2 = C(6,N) + 2.*C(7,N)
      A3 = 2.*C(8,N)
      A4 = -(C(2,N) + C(5,N) + C(6,N) + 4.*C(7,N) + C(9,N))
      A5 = C(9,N)
      A7 = C(12,N) + C(3,N)
      A9 = -A3/C(13,N) + 2.*C(11,N)
      A3 = C(1,N) + C(6,N) + C(7,N) + C(8,N) + A3*A5
      A1 = A5/A7
      A4 = A4 + A5*A1
      A10 = A2/A4
      YP2 = YP2 - YP4*A1
      YP1 = YP1 + A4*YP10
      X1 = (YP1 + YP2*A10)/(A9 + A2*A10)
      X2 = (YP2 - A2*X1)/A4
      C12PRM(NE) = CP(NE) = C(1,N) * X1
      C12PRM(NE+1) = CP(NE+1) = C(2,N) * X2
      C12PRM(NE+3) = CP(NE+3) = C(4,N) * (YP4 + A5*X2)/A7
1 CONTINUE
      DC 2 NE = NEQU-NMC + 1, NEQU
      C12PRM(NE) = 0.
      N1=N
      END

```

Figure 29 - Subroutine DCDT

and we shall write the time derivatives as ' (prime), so that:

$$[\text{Fe}^{2+}] \equiv c_1 \quad \frac{\delta [\text{Fe}^{2+}]}{\delta t} \equiv c'_1$$

The relations we have are:

$$c'_1 + c'_6 + c'_7 + c'_8 = T_1 + T_6 + T_7 + T_8 \equiv Y1 \quad (\text{A-1})$$

$$c'_5 + c'_6 + 2c'_7 + c'_9 - c'_2 = T_5 + T_6 + 2T_7 + T_9 - T_2 \equiv Y2 \quad (\text{A-2})$$

$$c'_4 + c'_9 = T_4 + T_9 \equiv Y4 \quad (\text{A-3})$$

$$c'_{10} + 2c'_8 = T_{10} + 2T_8 \equiv Y10 \quad (\text{A-4})$$

These are identical or similar to the relations (5-7) in 5-3 and express the conservation through chemical equilibria of the element in the subscript of Y. The calculation of the Y's is made at lines 23-27.

We can also use the chemical equilibria given in 5-2:

$$\begin{aligned} c_2 \cdot c_5 &= K_5 \\ c_6 &= c_1 \cdot c_5 \cdot K_2 \\ c_7 &= c_6 \cdot c_5 \cdot K_3 \end{aligned}$$

$$c_8 = c_1 \cdot c_{10}^2 \cdot K_4$$

$$c_9 = c_4 \cdot c_5 \cdot K_5$$

and the electroneutrality expressed as:

$$c_{10} = 2c_1 + c_2 + c_3 + c_6 - c_5 - c_9$$

Taking the time derivative of the equilibrium relations, we get:

$$\frac{c'_2}{c_2} = - \frac{c'_5}{c_5} \quad (A-5)$$

$$\frac{c'_6}{c_6} = \frac{c'_1}{c_1} + \frac{c'_5}{c_5} \quad (A-6)$$

$$\frac{c'_7}{c_7} = \frac{c'_6}{c_6} + \frac{c'_5}{c_5} \quad (A-7)$$

$$\frac{c'_8}{c_8} = \frac{c'_1}{c_1} + \frac{2c'_{10}}{c_{10}} \quad (A-8)$$

$$\frac{c'_9}{c_9} = \frac{c'_4}{c_4} + \frac{c'_5}{c_5} \quad (A-9)$$

$$c'_{10} = 2c'_1 + c'_2 + c'_3 + c'_6 - c'_5 - c'_9 \quad (A-10)$$

By combining A-1, A-2, A-4 and A-10, one can obtain directly (28):

$$c'_3 = Y2 - 2Y1 + Y10$$

We shall use the relations A-5 to A-9 to eliminate c'_5 to c'_9 in A-1 to A-4. We now note:

$$x_1 = \frac{c'_1}{c_1}$$

For A-1, we get successively:

$$\begin{aligned} Y1 &= c_1 \left(\frac{c'_1}{c_1} \right) + c_6 \left(\frac{c'_1}{c_1} + \frac{c'_5}{c_5} \right) + c_7 \left(\frac{c'_6}{c_6} + \frac{c'_5}{c_5} \right) + c_8 \left(\frac{c'_1}{c_1} + 2 \frac{c'_{10}}{c_{10}} \right) \\ &= c_1 \left(\frac{c'_1}{c_1} \right) + c_6 \left(\frac{c'_1}{c_1} - \frac{c'_2}{c_2} \right) + c_7 \left(\frac{c'_1}{c_1} - 2 \frac{c'_2}{c_2} \right) + c_8 \left(\frac{c'_1}{c_1} + 2 \frac{c'_{10}}{c_{10}} \right) \\ &= x_1 \cdot (c_1 + c_6 + c_7 + c_8) + x_2 \cdot (-c_6 - 2c_7) + x_{10} \cdot (2c_8) \end{aligned} \quad (A-11)$$

For A-2 to A-4, we get:

$$\begin{aligned} Y2 &= x_1 \cdot (c_6 + 2c_7) + x_2 \cdot -(c_2 + c_5 + c_6 + 4c_7 + c_9) + \\ &\quad x_4 \cdot c_9 \end{aligned} \quad (A-12)$$

$$Y4 = x_2 \cdot -c_9 + x_4 \cdot (c_4 + c_9) \quad (A-13)$$

$$Y10 = x_1 \cdot (2c_8) + x_{10} \cdot (c_{10} + 4c_8) \quad (A-14)$$

We can eliminate x_{10} between A-11 and A-14, obtaining:

$$\begin{aligned}
 x_1 \cdot (c_1 + c_6 + c_7 + c_8 - \frac{4c_8^2}{c_{10} + 4c_8}) + x_2 \cdot (-c_6 - 2c_7) \\
 = Y_1 + Y_{10} \left(\frac{-2c_8}{c_{10} + 4c_8} \right) \quad (A-15)
 \end{aligned}$$

We now have a system of three equations (A-12, A-13 and A-15) with 3 unknowns (x_1 , x_2 and x_4). The coefficients of these equations are computed in lines 29 to 35. using the same notations as in the program, the system is:

$$\begin{aligned}
 A2 \cdot x_1 + A4 \cdot x_2 + A5 \cdot x_4 &= Y2 \\
 - A5 \cdot x_2 + A7 \cdot x_4 &= Y4 \\
 A9 \cdot x_1 - A2 \cdot x_2 &= Y1 + A8 \cdot Y10
 \end{aligned}$$

The solution of this system is mathematically trivial, but may introduce large errors in the results if proper care is not taken. To proceed with the classical elimination, the equations and variables have to be ordered so that the largest coefficients will be on the diagonal of the matrix, in order to be used as a pivot in the elimination (Conte and de Boor, 1980, p. 157).

The coefficients of the matrix were therefore evaluated at different stages of the evolution of the system and it was found that the best arrangement was, in our particular case:

$$A7 \cdot x_4 - A5 \cdot x_2 = Y4$$

$$A5 \cdot x_4 + A4 \cdot x_2 + A2 \cdot x_1 = Y2$$

$$- A2 \cdot x_2 + A9 \cdot x_1 = Y1 + A8 \cdot Y10$$

This system was solved manually and the solution is shown on line 36 to 42. The x_1 's are then transformed in c'_1 's which are put in the array C12PRM (43 to 45).

Finally, the time derivative of the last point (bulk solution) is set to zero, as this is the second boundary condition (47-48).

APPENDIX B

LIST OF SYMBOLS

a	empirical constants (see 6-3, 6-5)
A	empirical constant (7-13)
b	empirical constants (see 6-3, 6-5, 7-10)
b _a	experimental anodic Tafel slope
B	empirical constant (7-13)
c	empirical constants (see 7-10)
c _i	concentration of species i
C	empirical constant (7-13)
C	capacity of the double layer (5-6)
C ₁	= F/RT (7-1)
D	diffusion coefficient of Fe ²⁺ (6-4)

D_i	diffusion coefficient of species i
E	potential at the metal surface (at the outer Helmholtz plane)
E_b	breakdown potential
E_H	equilibrium potential for hydrogen evolution
E_r	repassivation potential
E_T	total truncation error
E_z	minimum potential necessary to obtain current noise (Forchhammer and Engell, 1963)
E_{11}	standard potential for (5-11)
E_{14}	standard potential of (4-14)
F	the Faraday (96,487 C/equiv.)
F_1, F_2	heat flux at either end of the pore (suffix 1 refers to the metal side ($x=0$), suffix 2 refers to the bulk solution side ($x=L$))

H rate of heat generation (7-10)

\vec{j} current density

j_T total current density flowing from the surface
(including charging current for the double layer)

j_o coefficient determined experimentally (see 4-7)

K conductivity of the solution

k_i kinetic constant associated with equation 4-1

k_1 constant (6-4)

$K_{ad1} = \theta_1 \exp \left[\frac{E_{11} F}{RT} \right]$

K_{ad1}^0 pitting criterion for the first adsorption
mechanism

$K_{ad2} = \theta_2 \exp \left[\frac{E_{11} F}{RT} \right]$

K_{ad2}^0 pitting criterion for the second adsorption
mechanism

K_A, K'_A constants (7-13)

- K_{ca} empirical constant (7-13)
- K_{cc}^0 pitting criterion for the critical chloride concentration mechanism
- K_i equilibrium constant; for $i=1$ to 6, see 5-2 and 5-7-2; for $i=11$, see 4-3
- K_L thermal conductivity of the liquid phase
- K_M thermal conductivity of the metal
- K_{rp} supersaturation ratio of $Fe(OH)_2(aq)$
- K_{rp}^0 pitting criterion for the repassivation mechanism
- K_{sf} supersaturation ratio of $FeCl_2$
- K_{sf}^0 pitting criterion for the salt film precipitation mechanism
- $(K_{sf})_o$ value of K_{sf} corrected for the truncation error
- K_W equilibrium constant for water decomposition
- L length of the pore

m	number of equilibrium considered (5-3)
m_i	empirical coefficients
n	number of species considered
$n(p)$	order of the dependence of an output parameter p on an input parameter (see 6-2)
\vec{N}_i	flux of species i
p	value of a parameter after the modification (6-2)
p_o	value of a parameter before the modification (6-2)
P_s	probability of survival
r	distance from the pore opening
r_A	Temkin parameter
r_o	radius of pore
R	gas content (8.316 J/mole.K)
R_B	resistance of the bulk solution

R_i	production rate of species i by chemical reaction
S_1	concentration of $\text{Fe}(\text{OH})_{2(\text{aq})}$ at saturation
S_2	concentration of FeCl_2 at saturation
t	time
t_i	transport number of species i
t_o	incubation time
T	temperature
T_i	see equations 5-6 and 5-6'
T_1, T_2	temperature increase at either end of the pore (see F_1, F_2)
u_i	mobility of species i
x	distance from the bottom of the pore
z_i	charge of species i
α	empirical constant (7-13)

β symmetry factor

γ_A electrosorption valency of Cl (Strehblow and Titze, 1977)

$\Delta(p)$ measure of the variation of parameter p (6-2)

ΔH_A° initial heat of adsorption of Cl

$\Delta H_{ads,A}$ heat of adsorption of Cl

ΔV_1 ohmic drop in the bulk

ΔV_2 ohmic drop in that part of the solution where there is a variation in composition

ΔV_3 potential difference due to the concentration gradient

$\Delta V = \Delta V_1 + \Delta V_2$

θ_1 coverage of $FeCl_{ads}$ (5-9-3)

θ_2 coverage of Cl_{ads} (5-9-3)

θ_A coverage of Cl^- ions (7-13)

θ_c critical coverage ratio (7-13)

θ_{c1} critical coverage of FeCl_{ads}

θ_{c2} critical coverage of Cl_{ads}

θ_I coverage of OH^- ions

λ pit generation rate

μ pit repassivation rate

τ induction time

ϕ electrochemical potential at the point of the solution considered

Computer program variables referred to in the text

A radius of the pore

ATOL absolute tolerance on truncation error in time integration

C(I,N) concentration of species I at node N

DC(I,N) first spatial derivative of the concentration of
species I at node N

DDC(I,N) second spatial derivative of the concentration of
species I at node N

DEPTH depth of the pore

DLR $= \log(RR)$

DX distance between nodes in the region of planar dif-
fusion

DX1 distance between nodes in the transition region

NN total number of nodes

NN1 number of nodes in the region of planar diffusion

NN2 number of nodes in the transition region

R(N) radius at node N

RR ratio of the radii at two successive points

RTOL relative tolerance on truncation error in time
integration